REMARKS

Claims 5, 9-10, 12-14, 30, 33, and 44-46 will be pending before the Examiner upon entry of the above amendments. Claim 14 has been amended. Support for the amendment to claim 14 may be found, *e.g.*, at page 81, line 9, of the instant specification. Thus, the amended claim is fully supported by the instant specification and no new matter has been introduced.

1. The Rejections Under 35 U.S.C. § 102 Should Be Withdrawn

Claims 5, 10, 12-14, 30 and 33 are rejected under 35 U.S.C. § 102(b), as being anticipated by NCBI online, Accession No. AC008687 (hereinafter "AC008687"). Particularly, it is alleged in the Office Action dated January 16, 2004 ("Office Action") that the portion of chromosome 19 comprised in the BAC clone is the gene encoding the polypeptide set forth as SEQ ID NO: 8. It is contended in the Office Action that alignment of portions of SEQ ID NO: 7 with AC008687 sequence indicates that AC008687 comprises the 5′ coding sequence (in the region of 84300 – 84100 of AC008687) and the 3′ coding sequence (in the region of 81500 – 81300 of AC008687) of SEQ ID NO: 7, and absent evidence to the contrary, a skilled artisan would expect that AC008687 encodes the amino acid sequence of SEQ ID NO: 8.

Applicants respectfully disagree. Applicants assert that AC008687 does not encode a polypeptide having the amino acid sequence of SEQ ID NO: 8. The alignment of amino acid sequence encoded by AC008687 and the amino acid sequence of SEQ ID NO: 8 over the length of SEQ ID NO: 8 is provided in attached Exhibit 1 as a CLUSTALW alignment. Exhibit 1 clearly demonstrates that the polypeptide of SEQ ID NO: 8 is different from the polypeptide encoded by AC008687. The polypeptide encoded by AC008687 consists of 261 amino acids, while the polypeptide of SEQ ID NO: 8 consists of 559 amino acids, *i.e.*, the polypeptide encoded by AC008687 is 298 amino acids shorter (at the 5′ end) than the polypeptide of SEQ ID NO: 8. Moreover, the amino acids at positions 552 and 553 of SEQ ID NO: 8 are different from the amino acids at the corresponding positions of the polypeptide encoded by AC008687 (see Exhibit 1).

Therefore, the AC008687 does not encode a polypeptide having the amino acid sequence of SEQ ID NO: 8. As such, claim 5 is not anticipated by AC008687. Since claims 12-14, 30 and

33 depend from claim 5, and claim 10 is directed to a nucleic acid that hybridizes under stringent conditions to the nucleotide sequence of SEQ ID NO: 7 (encoding the polypeptide of SEQ ID NO: 8) or a complement thereof, AC008687 does not anticipate these claims for the same reason.

In view of foregoing, Applicants request that the rejection under 35 U.S.C. § 102 be withdrawn.

2. The Rejection Under 35 U.S.C. § 101 Should Be Withdrawn

Claim 14 is rejected under 35 U.S.C. § 101 for being directed to non-statutory subject matter. The Examiner states that the claimed subject matter encompasses a genetically modified human because host cells of the invention include progeny or potential progeny of the cell, and a human being is not excluded from the potential progeny.

Claim 14 has been amended to recite "an isolated host cell," as suggested by the Examiner. As such, the subject matter of claim 14 does not encompass a genetically modified human. Therefore, the objection has been obviated and should be withdrawn.

3. The Rejections Under 35 U.S.C. § 112, First Paragraph, Should Be Withdrawn

Claims 31, 33-38, 40 and 44 have been rejected under 35 U.S.C. §112, first paragraph, as failing to comply with the enablement requirement. Specifically, it is indicated in the Office Action that the claims contain subject matter which are not described in the specification in such a way as to enable one skilled in the art to make and/or use the invention. In particular, the Office Action indicates that the specification fails to teach a skilled artisan how to use a nucleic acid encoding the polypeptide comprising SEQ ID NO: 8 for the specific and substantial credible utilities set forth in the specification without undue experimentation. Claims 31, 34-38 and 40 have been cancelled. This rejection is therefore moot in regard to these claims. Applicants respectfully submit that the claims, as amended, are fully enabled by the specification as described in detail below.

THE LEGAL STANDARD FOR ENABLEMENT

The test for enablement is whether one reasonably skilled in the art, following the teaching of the patent specification coupled with information known in the art at the time the

patent application was filed, could make or use the invention without undue experimentation. *U.S. v. Telectronics Inc.*, 857 F.2d 778, 8 U.S.P.Q.2d 1217 (Fed. Cir. 1988). Undue experimentation is experimentation that would require a level of ingenuity beyond what is expected from one of ordinary skill in the field. *Fields v. Conover*, 170 U.S.P.Q. 276, 279 (C.C.P.A. 1971). The factors to be considered in determining whether an amount of experimentation is undue are, *e.g.*, the amount of effort involved, the guidance provided by the specification, the presence of working examples, the amount of pertinent literature, and the level of skill in the art. See *In re Wands*, 8 U.S.P.Q.2d 1400, 1404 (Fed. Cir. 1988). It is <u>not</u> undue experimentation just because a considerable amount of experimentation need to be done, so long as the experimentation is merely routine or the specification provides reasonable amount of guidance and direction to the experimentation. See *In re Wands* at 1404; see also, *In re Jackson*, 217 U.S.P.Q. 804, 807 (1982).

Working examples are not necessary to meet enablement requirements, and lacking of examples should not be equated with lack of direction. "Nothing more than objective enablement is required, and therefore it is irrelevant whether the teaching is provided through broad terminology or illustrative examples." *In re Marzocchi*, 169 U.S.P.Q. 367 (C.C.P.A. 1971).

The specification preferably omits well known subject matter. *See Hybritech v. Monoclonal Antibodies, Inc.*, 802 F.2d 1367, 1384 (Fed. Cir. 1986). One skilled in the art is presumed to use the information available to him in attempting to make or use the claimed invention. See *Northern Telecom, Inc. v. Datapoint Corp.*, 908 F.2d 931, 941 (Fed. Cir. 1990). These enablement rules preclude the need for the patent applicant to "set forth every minute detail regarding the invention." *Phillips Petroleum Co. v. United States Steel Corp.*, 673 F. Supp. 1278, 1291 (D. Del. 1991); see also, *DeGeorge v. Bernier*, 768 F.2d 1318, 1323 (Fed. Cir. 1985).

Accordingly, the law does not require the scope of enablement provided by the specification to mirror precisely the scope of protection sought by the claims. *See In re Fisher*, 166 USPQ 18, 24 (C.C.P.A. 1970); see also, *In re Wright*, 27 USPQ2d 1510 (Fed. Cir. 1993). To be enabled, all the law requires is that the scope of enablement provided by the specification bear a "reasonable correlation" to the scope of the claims. *Id.* Moreover, even if evidence to

doubt the proposed correlation exists, "the examiner must weigh the evidence for and against correlation and decide whether one skilled in the art would accept the model as reasonably correlating to the condition." *In re Brana*, 51 F.3d 1560, 1566, 34 USPQ2d 1436, 1441 (Fed. Cir. 1995). Thus, to support a non-enablement rejection, the Examiner must evaluate all the facts and evidence and state why one would not expect to be able to extrapolate the teaching in the specification across the entire scope of the claims. *Id.*

In cases where a compound or composition claim is not limited by a recited use, "<u>any</u> enabled use that would reasonably correlate with the entire scope of that claim is sufficient to preclude a rejection for nonenablement based on how to use." M.P.E.P. § 2164.01(c) (Eighth Edition, August 2001, revised February 2003, emphasis added). See also, *Engel Industries, Inc. v. Lockformer Co.*, 946 F.2d 1528 (Fed. Cir. 1991) ("The enablement requirement is met if the description enables any mode of making and using the claimed invention.")

In addition, the Patent and Trademark Office bears the initial burden of establishing a *prima facie* case of non-enablement. *In re Marzocchi*, 169 U.S.P.Q. 367, 369 (C.C.P.A. 1971); MPEP § 2164.02. A patent applicant's specification that contains a teaching of how to make and use the invention must be taken as enabling unless there is reason to doubt the objective truth of the teachings which must be relied on for enabling support. *Id.*

THE CLAIMS ARE FULLY ENABLED BY THE INSTANT SPECIFICATION

In light of the legal standard discussed *supra*, Applicants submit that (1) the rejection under 35 U.S.C. § 112, first paragraph, is improper; and (2) the claims, as amended, are enabled by the instant specification.

In the Office Action, it is indicated that the specification does not teach a skilled artisan how to use the claimed nucleic acid molecules for the identified utilities without undue experimentation essentially because: (1) the art teaches that the voltage-gated potassium ("Kv") channel family is functionally diverse and there is no utility that is common to all members of the family, therefore, a skilled artisan would not know what conditions contemplated in the specification might be amenable to treatment or diagnosis according to the teachings of the specification; and (2) all the teachings in the specification related to therapy are general in nature and based on circumstantial evidence, therefore, a skilled artisan has to engage in undue

experimentation to first identify a disease that could be treated, develop an effective therapeutic agent and an effective treatment regimen, which is beyond what is considered routine in the art.

Although couched in the language of 35 U.S.C. § 112, first paragraph, the Examiner is in reality making a *de facto* utility rejection (under 35 U.S.C. § 101), that is, that the claimed nucleic acid molecules of the present invention do not have a "specific and credible" use. The reasons provided by the Examiner for rejecting the pending claims as described above all relate back to whether the asserted utilities of the nucleic acid molecules of the present invention are proven to be specific and credible. Since the Examiner in fact admitted the claimed nucleic acid molecules have specific, substantial, and credible utilities (see, *e.g.*, Office Action, page 5, bottom line), a rejection under 35 U.S.C. § 112, first paragraph, should not be imposed. M.P.E.P. § 2107.01 (IV), page 2100-36 (Eighth Edition, August 2001, revised February 2003).

Nonetheless, in order to be fully responsive, Applicants address the issue of enablement of the claimed invention raised by the Examiner as follows.

Since the rejection is only directed to claims encompassing nucleic acid molecules encoding the polypeptide of SEQ ID NO: 8, *i.e.*, the claims are not limited by a recited use, <u>any</u> enabled use, among all the asserted uses disclosed in the specification, is sufficient to preclude a nonenablement rejection based on how to use. See, M.P.E.P. § 2164.01(c) (Eighth Edition, August 2001, revised February 2003); see also, *Engel Industries, Inc. v. Lockformer Co.*, 946 F.2d 1528 (Fed. Cir. 1991).

Applicants submit that the teaching of the instant application enables at least one of the asserted uses of the claimed invention - for use to identify compounds that modulate the Kv channel (*i.e.*, the function of the polypeptide of SEQ ID NO: 8).

The instant specification at, *e.g*, page 89, line 23, to page 96, line 2, describes screening assays that can be used to identify molecules that modulate the functions of the polypeptides of the invention, one of which is the polypeptide having the amino acid sequence of SEQ ID NO: 8. Moreover, at the time of the application was filed, methods of identifying molecules that can modulate functions of an identified ion-channel, such as a potassium channel, were well-known and routine in the art. See *e.g.*, Gonzalez *et al.*, Cell-based Assays and Instrumentation for Screening Ion-channel targets, Drug Discov. Today 4(9):431-439 (1999) (attached hereto as Exhibit 2, "Gonzalez"); and U. S. Pat. No. 6,087,488 (Ganetzky *et al.*, 2000) (attached hereto as

8

Exhibit 3, "Ganetzky"). A person skilled in the art can readily perform a cell-based assay, as taught in the specification at, *e.g.*, the paragraph bridging pages 91-92, in view of Gonzalez and Ganetzky, to identify molecules that can modify the functions of the potassium channel of the invention. No experimentations requiring a level of ingenuity beyond what is expected from a skilled artisan are needed. Therefore, the instant specification enables this asserted use. See, *e.g., U.S. v. Telectronics Inc.*, 857 F.2d 778, 8 U.S.P.Q.2d 1217 (Fed. Cir. 1988); *In re Wands*, 8 U.S.P.Q.2d 1400, 1404 (Fed. Cir. 1988); and *In re Jackson*, 217 U.S.P.Q. 804, 807 (1982).

Moreover, contrary to the statement in the Office Action that there is no utility that is common to all members of the Kv family (see Office Action, page 7, lines 1-3), members of the Kv family all share a common utility – transporting potassium ions. Furthermore, the instant specification not only teaches that the NOV4 polypeptide (the polypeptide having the amino acid sequence of SEQ ID NO: 8) is a new member of a subclass of Kv channels that includes members from several species (see specification, page 18, last paragraph), but also specifically teaches that NOV4 has high homology (83% identity, and 85% similarity) to a mouse Kv channel protein (AAC23664), and a human Kv channel protein (P22001, 69% identity, and 81% similarity). At the time of filing of the instant application, the mouse protein AAC23664 had been shown to be expressed in heart and skeletal muscle (with high expression levels), as well as in pancreatic islet cells. See Kalman *et al.*, J. Biol. Chem. 273:5851-5857 (1998) (attached hereto as Exhibit 4, "Kalman"). It is well-known in the art at the time that potassium channels are involved in neuromsclular disorders such as acquired neuromyotonia. (See Vincent, Eur. J. Biochem. 267:6717-6728 (2000), attached hereto as Exhibit 5, "Vincent"). Kalman also teaches AAC23664 is mapped to human chromosome 19q13.3 (the region that SEQ ID NO: 7, which encodes the polypeptide of SEQ ID NO: 8, is mapped to), a region thought to contain a diabetic susceptibility gene. (See Kalman, page 5856, col. 1, second paragraph). Further, the human protein P22001 has been shown to be expressed in pancreatic islets and insulinomas. See Philipson *et al.*, Proc. Natl. Acad. Sci. USA 88:53-57 (1991) (attached hereto as Exhibit 6, "Philipson").

Therefore, it is clear to a person skilled in the art that the NOV4 polypeptide is involved in the transport of potassium ions. Moreover, the NOV4 potassium channel protein is associatd with pathologies including diabetes mellitus and neuromuscular disorders such as acquired

neuromyotonia.

In view of the foregoing, Applicants assert that the claimed invention is enabled. Thus, the rejection under 35 U.S.C. §112, first paragraph, as failing to comply with the enablement requirement, should be withdrawn.

CONCLUSION

Applicants respectfully request that the amendments and remarks made herein be entered and made of record in the file history of the present application. Applicants respectfully submit that the pending claims are in condition for allowance. If there are any questions regarding these amendments and remarks, the Examiner is encouraged to contact the undersigned at the telephone number provided below.

Respectfully submitted,

Ivor R. Elrifi, Reg. No. 39,529
Attorney for Applicant
c/o Mintz, Levin
One Financial Center
Boston, MA 02111
Telephone: (617) 542 6000
Fax: (617) 542 2241
Customer No. 30623

Dated: June 16, 2004

TRA 1929684v1

Exhibit 1: CLUSTALW Alignment

```
AC008687.5   ***  -------------------------------------------------------------  ***
CG53216-01    1   MERRRTGSRRQKDGEKGDPGTGKAQSRRGRRRRRGRAGRASRQRARGRPVALRPAGVTVP   60

AC008687.5   ***  -------------------------------------------------------------  ***
CG53216-01   61   PPSRPSRPAGLFYARTPDTGHRAGAAVGATRRFAGRRGCARHGAAVPAAPCGCCERLVLN  120

AC008687.5   ***  -------------------------------------------------------------  ***
CG53216-01  121   VAGLRFETRARTLGRFPDTLLGDPARRGRFYDDARREYFFDRHRPSFDAVLYYYQSGGRL  180

AC008687.5   ***  -------------------------------------------------------------  ***
CG53216-01  181   RRPAHVPLDVFLEEVAFYGLGAAALARLREDEGCPVPPERPLPRRAFARQLWLLFEFPES  240

AC008687.5    1   ---------------------------------------------------------MP    2
CG53216-01  241   SQAARVLAVVSVLVILVSIVVFCLETLPDFRDDRDGTGLAAAAAAGPVFPAPLNGSSQMP  300

AC008687.5    3   GNPPRLPFNDPFFVVETLCICWFSFELLVRLLVCPSKAIFFKNVMNLIDFVAILPYFVAL   62
CG53216-01  301   GNPPRLPFNDPFFVVETLCICWFSFELLVRLLVCPSKAIFFKNVMNLIDFVAILPYFVAL  360

AC008687.5   63   GTELARQRGVGQQAMSLAILRVIRLVRVFRIFKLSRHSKGLQILGQTLRASMRELGLLIF  122
CG53216-01  361   GTELARQRGVGQQAMSLAILRVIRLVRVFRIFKLSRHSKGLQILGQTLRASMRELGLLIF  420

AC008687.5  123   FLFIGVVLFSSAVYFAEVDRVDSHFTSIPESFWWAVVTMTTVGYGDMAPVTVGGKIVGSL  182
CG53216-01  421   FLFIGVVLFSSAVYFAEVDRVDSHFTSIPESFWWAVVTMTTVGYGDMAPVTVGGKIVGSL  480

AC008687.5  183   CAIAGVLTISLPVPVIVSNFSYFYHRETEGEEAGMFSHVDMQPCGPLEGKANGGLVDGEV  242
CG53216-01  481   CAIAGVLTISLPVPVIVSNFSYFYHRETEGEEAGMFSHVDMQPCGPLEGKANGGLVDGEV  540

AC008687.5  243   PELPPPLWAPPGKHLVTEV                                           261
CG53216-01  541   PELPPPLWAPPREHLVTEV                                           559
```

TRA 1929687v1

REVIEWS

Cell-based assays and instrumentation for screening ion-channel targets

Jesús E. González, Kahuku Oades, Yan Leychkis, Alec Harootunian and Paul A. Negulescu

Ion channels are an important class of drug targets. They comprise the molecular basis for essential physiological functions including fluid secretion, electrolyte balance, bioenergetics and membrane excitability. High-throughput screening for ion-channel function requires sensitive, simple assays and instrumentation that will report ion channel activity in living cells. This article will review relevant assay technologies for ion channels and describe voltage-sensitive probes and instruments based on fluorescence resonance energy transfer (FRET) that enable ion-channel drug discovery.

Ion channels make good drug targets because they are physiologically essential, are pharmacologically accessible, are encoded by a variety of genes and usually operate as multimeric protein assemblies, resulting in a high degree of functional and anatomical specificity[1,2]. Through molecular cloning, heterologous expression and electrophysiological characterization by patch-clamping, it is clear that the complexity of ion-channel biology also offers multiple opportunities for small-molecule drugs to achieve a specific, desired functional effect. For example, small molecules might influence a variety of biophysical properties of ion channels, such as voltage-dependence, permeability, use-dependence, activation and inactivation. In contrast to simple blockers or openers, the discovery of modulatory compounds could allow the development of drugs that specifically act on cells or tissues exhibiting aberrant levels of ion-channel activity.

To screen compounds against functional ion channels or assemblies, it is necessary to reconstitute and measure channel function in a relevant biological context, such as in a cell. It is also preferable for the assay to be compatible with automated high-throughput screening (HTS) of large compound libraries. These assays would ideally be sensitive and fast, allow probing of various functional states and be amenable to miniaturization to 96-well plates and beyond. The importance of, and requirements for, assay miniaturization in drug discovery have been previously discussed[3,4]. Current formats for ion-channel assays have been recently summarized in an excellent review[5] and will only be discussed briefly here.

The purpose of this article is to discuss the implementation of ion-channel assay technologies that combine high-screening throughput with high-information content. Although there are a variety of approaches being explored, including automated patch-clamping, ion-channel measurements in lipid bilayers and viability assays based on the toxicity of constitutively opened channels[6], it is not currently possible to use these methods for ion-channel HTS. Therefore, the article will focus on platform technologies that have a broad application to HTS, and in particular, will discuss the efforts of Aurora Biosciences Corporation (San Diego, CA, USA) to apply FRET-based voltage sensing to ion-channel HTS.

Jesús E. González, Kahuku Oades, Yan Leychkis, Alec Harootunian and **Paul A. Negulescu***, Aurora Biosciences Corp, 11010 Torreyana Road, San Diego, CA 92121, USA. *tel: +1 619 452 5000, fax: +1 619 404 6719, e-mail: NegulescuP@aurorabio.com

Established assay methods

Ion-channel assay methods can be classified as either high-throughput, low-information assays based on ligand displacement or radiotracer flux, or low-throughput, high-information content electrophysiological assays. Assay and screening methods for ion channels are summarized in Table 1. Ligand-displacement assays require the synthesis of a labeled compound (usually a peptide or small molecule) that has a known pharmacological activity. Because the probe occupies a known binding site, the technique is most effective when detecting molecules that bind to the same site. Although other sites are often allosterically coupled to the ligand site, these assays are not ideal for probing weakly coupled allosteric sites that might go undetected. For compounds that are detected, the functional effect (e.g. agonist or antagonist) is unknown and must be followed up with low-throughput secondary assays.

Radioactive flux assays are also commonly used for HTS screening of ion channels. An important example is $^{86}Rb^+$, which permeates through K^+ channels with similar properties to K^+. Protocols generally require long incubation with the radioactive tracer to load the cells, followed by removal of the excess tracer, and then the channels are kept in an open conformation for long periods (minutes to hours), often with pharmacological modifiers. Non-specific background fluxes are often present and must be subtracted from the data in a similar way as the non-specific binding being taken into account for binding assays. Flux assays also require different radioactive ions for channels with different ion permeabilities, and present the inconvenience associated with radioactive waste. Neither ligand binding nor flux assays are particularly well suited for miniaturization.

Patch-clamp recording represents the gold standard for biophysical evaluation of compound action. The ability to clamp either voltage or current across a cell membrane, in addition to manipulating the ionic composition on either side of the membrane, enables a detailed characterization of ion-channel gating, permeability, and drug interactions. In addition, the technique is so sensitive that single ion channels can be studied. Although patch-clamping is unparalleled for detailed investigation of ion channel function,

Table 1. Comparison of ion-channel assay methods

Method	Information content	Throughput	Typical channels assayed	Sensitivity	Temporal response	Comments
Electrophysiology (patch-clamp)	Very high	Low	All	High	Sub-millisecond	Dialyses cell contents
Binding assays	Low	High	All	Medium	N/A	Requires synthesis of radiolabeled probe that binds to target
Radioactive flux assays	Medium	Medium to high	K^+, Na^+, Cl^-	Medium	Seconds to minutes	Radioactive assay Often requires high-channel expression
Redistribution Membrane-potential dyes	Medium	Medium	K^+	Medium	Slow response time	Prone to dye artifacts
Ca^{2+} dyes	Medium	Medium to high	Ca^{2+}, Na^+	Medium to high	Several seconds to minutes	Na^+-channel assays require co-expression of Ca^{2+} voltage-dependent ion channels Limited for rapidly inactivating channels
FRET-based voltage sensors	High	High	All	High	Sub-second responses to voltage changes	Generic high-throughput method Potential for modifier-free assays Can measure hyperpolarizations Ratiometric

Throughput (compounds per day): low ⩽ 100, medium = 100–2000, high ⩾ 2000; sensitivity means the relative number of channels per cell needed for good signal-to-noise ratio.

it is a cell-by-cell assay technology that is difficult to automate for HTS. Without the development of automated methodology, its role in ion-channel drug discovery will continue as a secondary or tertiary method to provide unequivocal biophysical data regarding the activity and action of hits from primary screens.

Optical readouts of channel function

Recently, optical methods for assaying ion-channel activity have begun to bridge the gap between the high-capacity, low-information assays and low-throughput, high-information assays. These assays utilize fluorescent probes to measure ion-channel-dependent changes to either intracellular ion concentration or membrane potential and are desirable because they are sensitive, can report channel activity in real-time, do not involve radioactivity, and are amenable to miniaturization and automation. Most importantly, these assays can report the activities of all pharmacologically active functional sites on the target.

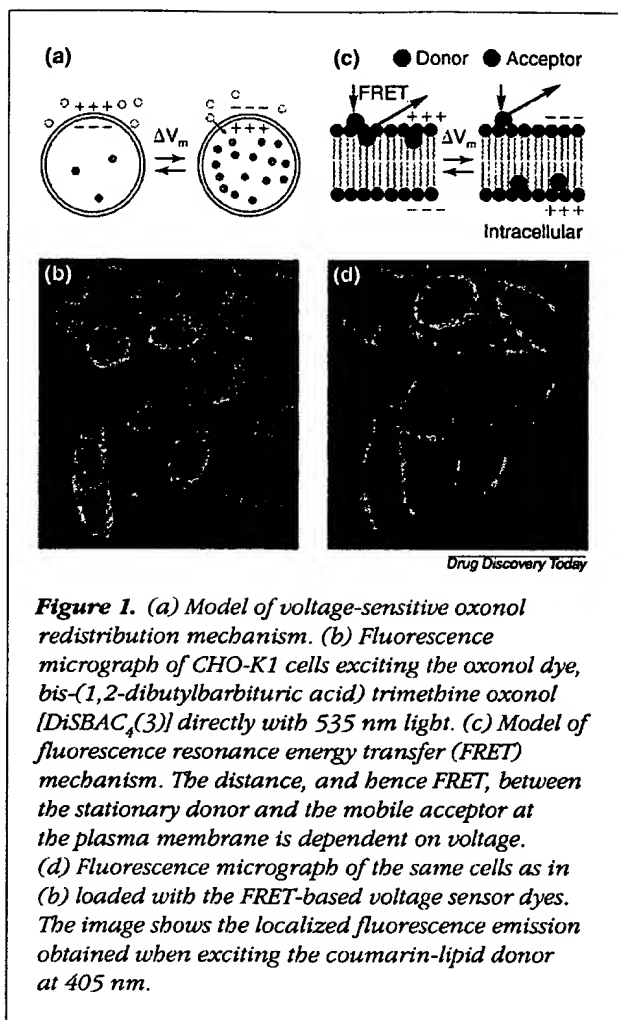## Intracellular Ca^{2+} measurements

Because the Ca^{2+} concentration inside cells can increase dramatically when Ca^{2+} channels are opened, one particularly successful and sensitive approach has been the measurement of intracellular Ca^{2+} with fluorescent indicators. A breakthrough for the application of fluorescent dyes to HTS occurred with the introduction of sophisticated plate readers, such as the Fluorescence Imaging Plate Reader (FLIPR), (Molecular Devices, Sunnyvale, CA, USA), which have integrated liquid handling (used to elicit a response) and kinetic detection (used to record the response)[7]. FLIPR uses an argon laser to rapidly scan a microtiter plate containing dye-loaded cells and a semi-confocal detection method, resulting in excellent sensitivity and a high signal-to-noise ratio. Ca^{2+} levels are measured using indicators such as fluo-3 or Calcium Green, which are efficiently excited at the 488 nm wavelength of the argon ion laser. The system can scan and read a plate every few seconds using a charge-coupled device (CCD) camera, quickly enough to detect most Ca^{2+} responses. The success of this approach has led to the design of assays that couple the activity of a target channel, such as a Na^+ channel, to activation of a voltage-gated Ca^{2+} channel (i.e. conversion to a Ca^{2+} readout)[8]. Although this approach does work, the reporter cell needs to contain relevant endogenous or engineered Ca^{2+} channels. Furthermore, the assay can only detect activity that the Ca^{2+} channel can detect (e.g. a specific voltage range, and in the case of voltage-activated Ca^{2+} channels, only depolarizations) and compounds that interact with the Ca^{2+} chan

nel can interfere with target detection to produce false positive results.

Membrane potential measurements

An indicator of membrane potential is an attractive alternative to Ca^{2+} for ion-channel assays because it is sensitive and versatile. This sensitivity is because of the high electrical resistance of biological membranes, which allows small ionic currents across the plasma membrane to cause large changes in membrane potential. This allows voltage assays to be at least as sensitive as isotopic flux assays while being more convenient. By contrast to Ca^{2+} measurements, voltage assays are generic because changes in membrane potential can be generated by any ionic flux across the membrane. One caution with membrane-potential assays is that, because many cells express endogenous ion channels, care must be taken in the choice of cell lines and assay formats to maximize the voltage response from the target channel.

Membrane potential indicator dyes have historically been divided into slow dyes (response time in minutes) with high sensitivity, and fast dyes (sub-millisecond response times) that have poor voltage sensitivities. The fast dyes generally operate via an electrochromic mechanism in which the transmembrane electric field directly interacts with the excited state of the dye. These 'styryl' dyes have sensitivities of 1–10% per 100 mV and their use has been restricted to basic research using highly optimized, low-noise equipment specially built for neurobiological problems requiring a high temporal resolution[9,10]. The slow dyes are comprised of lipophilic, negatively-charged oxonol dyes, such as bis-(1,2-dibutylbarbituric acid) trimethine oxonol [DiBAC$_4$(3)], which have very low fluorescence in aqueous extracellular solution and greatly increase their quantum yield upon binding to hydrophobic cellular sites[11–13]. The basis of the assay is that depolarized cells accumulate the negatively charged dyes and increase their fluorescence to a greater extent than hyperpolarized cells (Fig. 1a,b). Only the slow dyes, with their relatively good sensitivity, have been applied to HTS. Indeed, the earliest application of a FLIPR-type system was for membrane potential assays using DiBAC$_4$(3). Redistribution dyes can work well for assays configured to detect steady-state changes in membrane potential. However, many ion channels, including Na^+, K^+ and Ca^{2+} channels, rapidly inactivate or desensitize after opening, and hence, these channels must be pharmacologically modified to hold them open for the duration of these slow assays[14,15]. From an HTS perspective, slow redistribution assays also limit throughput. In addition, the dyes are prone to experimental

Figure 1. (a) Model of voltage-sensitive oxonol redistribution mechanism. (b) Fluorescence micrograph of CHO-K1 cells exciting the oxonol dye, bis-(1,2-dibutylbarbituric acid) trimethine oxonol [DiSBAC$_4$(3)] directly with 535 nm light. (c) Model of fluorescence resonance energy transfer (FRET) mechanism. The distance, and hence FRET, between the stationary donor and the mobile acceptor at the plasma membrane is dependent on voltage. (d) Fluorescence micrograph of the same cells as in (b) loaded with the FRET-based voltage sensor dyes. The image shows the localized fluorescence emission obtained when exciting the coumarin-lipid donor at 405 nm.

artifacts including temperature fluctuations and fluorescence artifacts from test compounds.

FRET-based voltage sensor dyes

Improved membrane-potential sensors based on FRET between voltage-sensing oxonol dyes and voltage-insensitive donor fluorophores associated with cell membranes have been demonstrated to retain the voltage sensitivity of the oxonol probes while reporting real-time kinetics of the membrane potential[16-18]. The mechanism of voltage-sensitive FRET is shown in Fig. 1c. In the configuration currently used at Aurora Biosciences, two dye molecules, a coumarin-linked phospholipid (CC2-DMPE) and an oxonol dye, are loaded into the plasma membrane of cells. CC2-DMPE partitions into the outer leaflet of the plasma membrane where it acts as a fixed FRET donor to the mobile,

voltage-sensitive oxonol acceptor. Cells with relatively negative potentials inside will push the negatively charged oxonol to the outer leaflet of the plasma membrane, resulting in efficient FRET (i.e. quenching of the coumarin donor and excitation of the oxonol acceptor). Depolarization results in rapid translocation of the oxonol to the inner surface of the plasma membrane, decreasing FRET. Because FRET can only occur over distances of less than 100 nm, excitation of the coumarin results in specific monitoring of oxonol movements within the plasma membrane. This is shown in Fig. 1d by the appearance of a ring of fluorescence when the coumarin donor is excited with violet light and this contrasts with the non-specific intracellular oxonol distribution revealed when the oxonol is excited directly (Fig. 1b).

Figure 2 uses simultaneous patch-clamping and rapid optical recording to demonstrate the speed, sensitivity and ratiometric nature of the FRET assay in a rat basophilic leukemia (RBL) cell. The responses of the both donor and acceptor fluorophores to depolarizing pulses can be observed in Fig. 2a. By dividing the signals from the coumarin donor and oxonol acceptor, a ratio is obtained (Fig. 2b) that is independent of the excitation intensity, the number of cells being detected and the optical path length. Analysis of these data (Fig. 2c) and similar experiments in other cell types, indicates a sensitivity of about 1% ratio per mV for DiSBAC$_2$(3) over the relevant physiological range. These dyes load quickly and effectively (in approximately 20 min.), appear to be non-toxic, and cells can be maintained with the dyes for hours without degrading the cell response. The dye loading and the assays are usually conducted at room temperature, whilst the FRET signal is minimally affected by normal ambient temperature fluctuations, therefore not requiring special care to control the temperature.

With a response time of a few seconds, the FRET assay using DiSBAC$_2$(3) as an acceptor is 100-times faster than oxonol redistribution assays, and is appropriate for liquid addition protocols which are often used to trigger membrane-potential changes in HTS assays (e.g. Fig 3). Even faster FRET assays are possible because the time constant of the response can be shortened by increasing the oxonol hydrophobicity. For example, Fig. 3a compares the response times of the FRET probes DiSBAC$_2$(3)–CC2-DMPE, DiSBAC$_4$(3)–CC2-DMPE and the slow redistribution dye DiBAC$_4$(3), in patch-clamped cells. The more hydrophobic butyl oxonol, DiSBAC$_4$(3), is clearly the quickest of the three compounds, with a time constant of approximately 10 ms. FRET dyes using DiSBAC$_4$(3) or other more hydrophobic oxonols are therefore quick

(a)

(b)

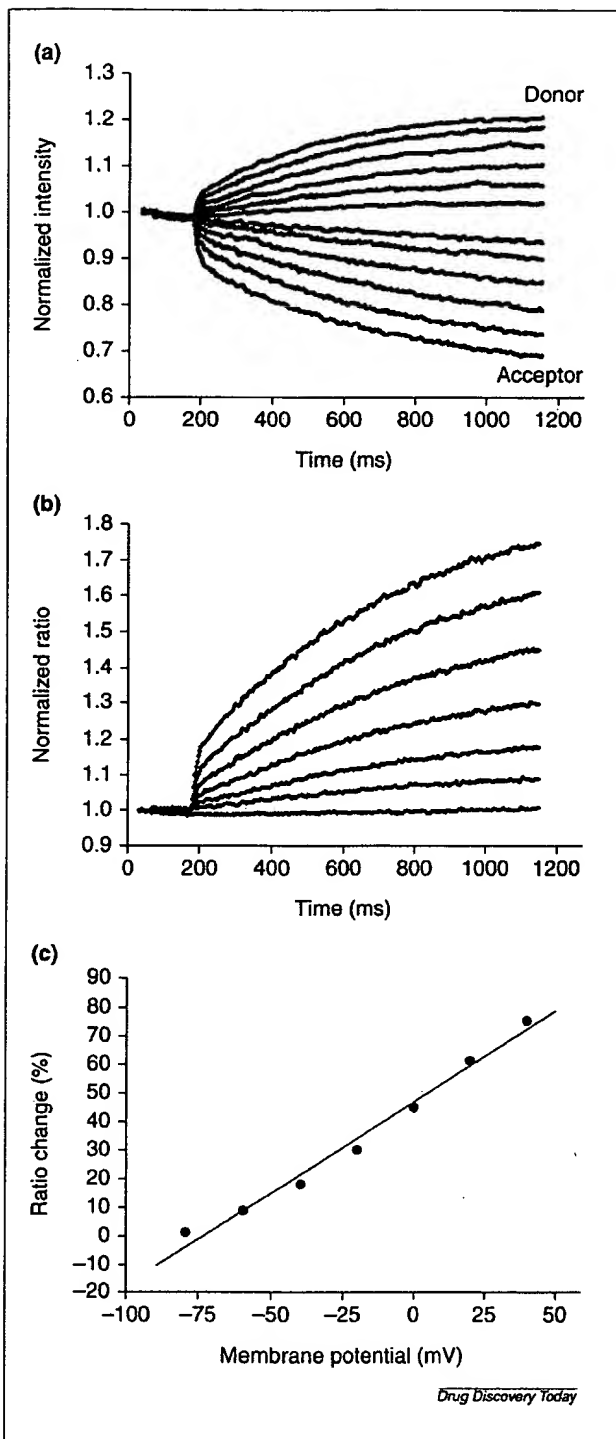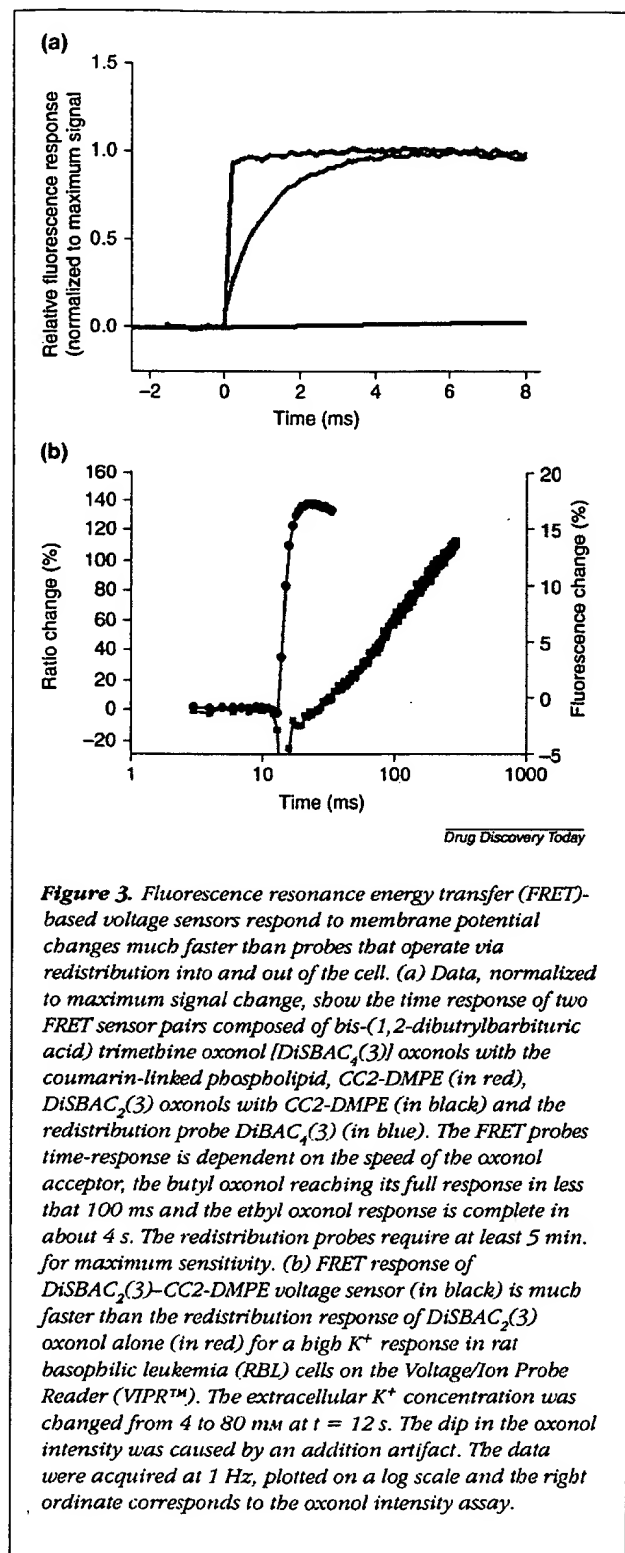**(c)**

Drug Discovery Today

Figure 2. Voltage-sensitive fluorescence resonance energy transfer (FRET) probes provide a sensitive, ratiometric readout of membrane potential in mammalian cells. (a) Single-sweep fluorescence changes in a single voltage-clamped rat basophilic leukemia (RBL) cell stained with the coumarin-linked phospholipid, 15 μM CC2-DMPE (donor) and the oxonol dye, 6 μM bis-(1,2-dibutrylbarbituric acid) trimethine oxonol [DiSBAC$_4$(3)] (acceptor) on the microscope. The individual FRET donor and acceptor intensities synchronously move in opposite directions in response to the voltage changes. For depolarizations, the donor intensities (blue traces) increase and the acceptor oxonol intensities (red traces) decrease. The cell was held at −80 mV and the voltage was stepped up to +40 mV in 20 mV steps. The data were collected at 300 Hz and normalized to a starting ratio of 1. (b) The normalized ratio is sensitive to voltage. (c) The percentage ratio change in cells as a function of membrane potential is approximately linear in the physiological relevant range from −80 mV to +40 mV.

development of more rapid stimulation methods for HTS. Figure 3b compares DiSBAC$_2$(3)–CC2-DMPE and DiSBAC$_2$(3) responses to a depolarizing stimulus in a kinetic plate reader.

Instrumentation for measuring ion-channel activity

A kinetic plate reader has been developed by Aurora that is compatible with the speed, sensitivity and ratiometric output of the FRET-based voltage sensors (and rapid kinetic assays in general). The first-generation instrument (the Voltage/Ion Probe Reader or VIPR™) is an integrated liquid handler and kinetic fluorescence reader for 96-well microtiter plates. The VIPR reader integrates an eight-channel liquid handler, a microplate positioning stage and a fiber-optic illumination and detection system (see Fig. 4). The system was designed to simultaneously measure fluorescence from a column of eight wells before, during and after the introduction of a liquid sample obtained from another microplate or trough. Liquid addition can be used to trigger a response from cells and the protocols used typically work by changing ionic conditions or adding a ligand. A xenon arc lamp provides excitation light, which allows the reader to be used with most fluorescent dyes. The VIPR reader excites and detects emission signals from the bottom of a microtiter plate by a novel design employing eight trifurcated optical fiber bundles (one bundle for each well). One leg of the trifurcated fiber is used as an

enough to measure action potentials. The high sensitivity and rapid temporal response, in conjunction with cell lines with rapid membrane-potential responses will drive the

(a)

(b)

Drug Discovery Today

Figure 3. Fluorescence resonance energy transfer (FRET)-based voltage sensors respond to membrane potential changes much faster than probes that operate via redistribution into and out of the cell. (a) Data, normalized to maximum signal change, show the time response of two FRET sensor pairs composed of bis-(1,2-dibutrylbarbituric acid) trimethine oxonol [DiSBAC$_4$(3)] oxonols with the coumarin-linked phospholipid, CC2-DMPE (in red), DiSBAC$_2$(3) oxonols with CC2-DMPE (in black) and the redistribution probe DiBAC$_4$(3) (in blue). The FRET probes time-response is dependent on the speed of the oxonol acceptor, the butyl oxonol reaching its full response in less that 100 ms and the ethyl oxonol response is complete in about 4 s. The redistribution probes require at least 5 min. for maximum sensitivity. (b) FRET response of DiSBAC$_2$(3)-CC2-DMPE voltage sensor (in black) is much faster than the redistribution response of DiSBAC$_2$(3) oxonol alone (in red) for a high K$^+$ response in rat basophilic leukemia (RBL) cells on the Voltage/Ion Probe Reader (VIPR™). The extracellular K$^+$ concentration was changed from 4 to 80 mM at t = 12 s. The dip in the oxonol intensity was caused by an addition artifact. The data were acquired at 1 Hz, plotted on a log scale and the right ordinate corresponds to the oxonol intensity assay.
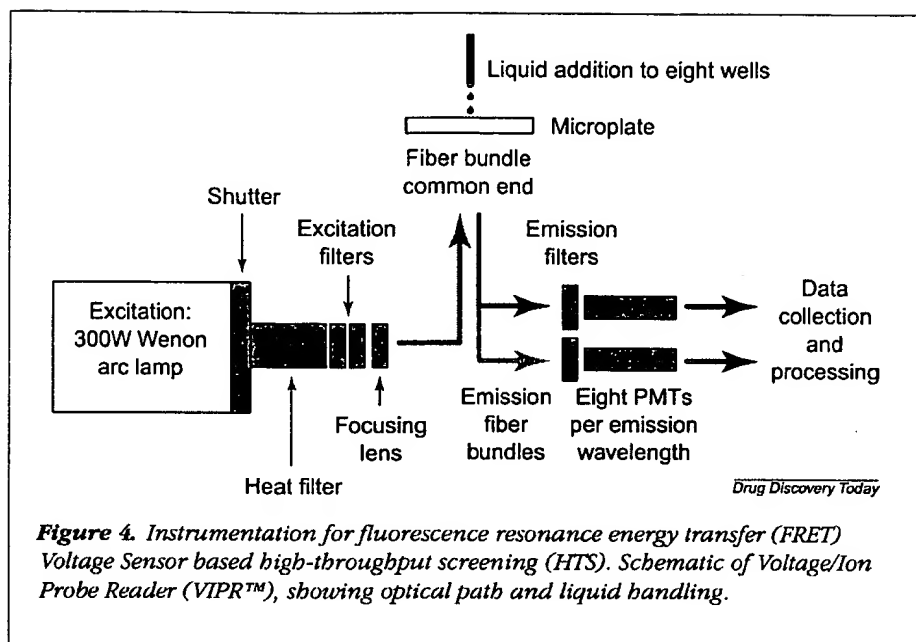
excitation source, the other two legs of the trifurcated fiber being used to detect fluorescence emission. A lens on the end of the fiber increases the efficiency of light excitation and collection. The bifurcated emission fibers allow the reader to detect two emission signals simultaneously and are compatible with rapid signals generated by the FRET-based voltage dyes. Photomultiplier tubes then detect emission fluorescence, enabling sub-second emission ratio detection for advanced applications.

The VIPR reader can be operated in either manual or automated formats. A Windows-based graphical user interface allows the user to customize assay routines, such as how long the data are acquired, how compound additions are performed and when the test compound is added. This allows rapid and flexible assay development. Manual operation is extremely useful for research, pharmacology and screen development purposes. Examples of typical reader data and assays are shown in Fig. 5, which demonstrates assay protocols and pharmacology for a voltage-dependent Na$^+$ channel and a Ba^{2+}-sensitive inward-rectifier K$^+$ channel, respectively. The Na$^+$ channel was heterologously expressed in CHO-K1 cells while the K$^+$ channel was endogenously expressed in RBL cells. As seen from the examples above, these assays typically take 20 to 30 seconds per columns of eight wells, which includes the time for the liquid handler to supply each of the columns. By reading one column at a time, an entire 96-well plate is assayed in approximately 5 min.

The VIPR reader was specifically designed to be compatible with automated HTS and uses washable tips, has a robust robotic interface and a low-profile plate tray to allow robotic access. The reader has been successfully integrated into several automated systems and can typically perform 5000–7000 assays per day. For assays generating 15 mV changes or greater, compounds can be screened in single wells. An example of screening data is shown in Fig. 6, where 560 pharmacophores were assayed at a concentration of 10 μM in an assay for inhibitors of the RBL inward-rectifier ion channel. Figure 6a shows a scatter plot of the data, including both positive and negative controls used to calculate statistical windows, and the data are then shown as a histogram in Fig. 6b. Aurora and its partners have screened over a million data points against at least 12 targets in all major ion-channel classes and the results shown here are fairly typical.

Future enhancements

The development of sensitive, real-time, automation-compatible assays for Ca^{2+} levels and membrane potential has made ion-channel targets more accessible for cell-based

Figure 4. *Instrumentation for fluorescence resonance energy transfer (FRET) Voltage Sensor based high-throughput screening (HTS). Schematic of Voltage/Ion Probe Reader (VIPR™), showing optical path and liquid handling.*

HTS. Further enhancements will allow more rapid and precise stimulation of cells, more sensitive signal detection and more sophistication in the application of molecular and cell biology to assay development.

Techniques for rapid stimulation of cellular membrane potential in microtiter plates would further bridge the gap between patch clamping results and optical assays while maintaining HTS compatibility. Approaches towards achieving this goal include rapid photolysis of chemically caged ligands[19,20] that can rapidly activate channels that in turn induce membrane-potential changes. In this way, light is used to both elicit and measure changes in membrane potential. Alternatively, electrical stimulation can be used for rapid and repetitive stimulation in microtiter plates. For example, electrode arrays have been successfully used for large excitable cells in native tissue or primary cultures[21,22]. Repetitive and rapid stimulation in combination with fast FRET probes and VIPR would potentially enable HTS assays in formats previously restricted to electrophysiology assays. For example, state-dependent blockers of Na^+ or K^+ channels could be screened as therapies for epilepsy, pain or cardiac arrhythmia.

Hypothetically, the maximum response possible using a distributed charge method such as the membrane-bound singly-charged oxonol is predicted by the Nernst potential to be 10-fold per 60 mV. Thus the dye sensitivity could still be improved. Probe performance might be improved by shifting the fluorescence to the red wavelength (to reduce

cell and system autofluorescence), using different classes of fluorophores and increasing the efficiency of voltage-sensitive energy transfer.

The use of genetically encoded fluorescent molecules such as green fluorescent protein (GFP), raises the prospect of engineering all or part of the FRET voltage sensor as a molecular construct. Recently, genetically targeted probes of Ca^{2+} and pH have been described[23-25] and similar approaches could be applied to voltage probes. Such sensors could be expressed in specific subpopulations of cells or even targeted to specific intracellular organelles. Interest in mitochondrial function and its role in disease and metabolism has revealed the importance of intracellular ion channels[26]. However, because intracellular membranes are not easily accessible to patch electrodes and because isolated mitochondria lack cell-based regulatory factors, optical interrogation might be the only prospect for exploring the roles of ion channels inside cells.

Conclusions and perspectives

The rapid evolution of sensitive, function-based assays and related instrumentation is transforming the way the pharmaceutical industry is approaching both research and drug discovery. Assays using cloned molecular targets heterologously expressed in host cells are now standard for drug discovery. However, as cell-based screens begin to provide more biological information per well and screening-based research enables systematic biological exploration, it is likely that compound screening in native cell systems will be used to identify ion channel targets involved in more complex cellular processing, particularly in excitable cells. Responses of primary cultures or differentiated cells displaying complex behavior (e.g. action potentials, repetitive firing, synaptic transmission) are amenable to a miniaturizable, ensemble read-out such as membrane potential. In this way, the discovery tools described here will be used to both screen established targets in heterologous systems and to discover new targets in native cell lines.
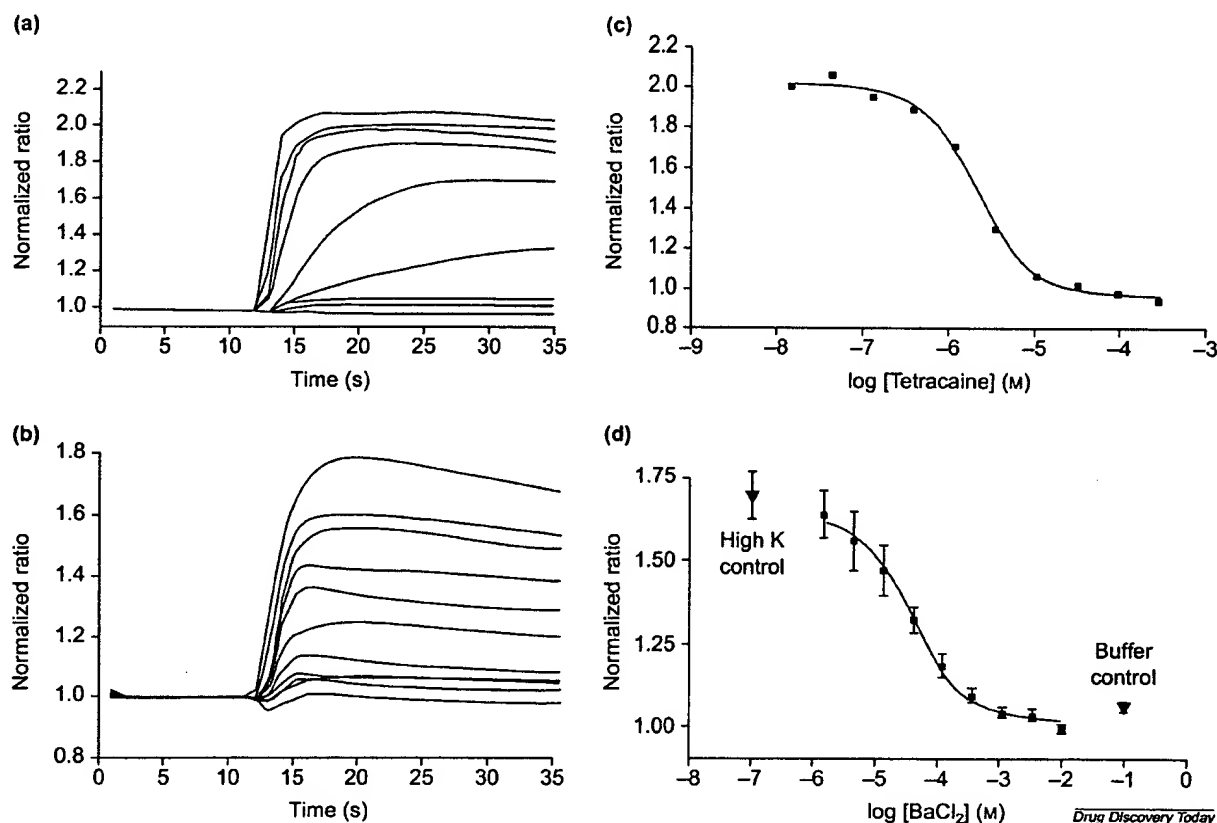
Figure 5. *Examples of ion-channel pharmacology detected on a Voltage/Ion Probe Reader (VIPR™). (a) Na⁺-channel assay in CHO-K1 cells is shown. The cells are kept in a solution in which Na⁺ has been substituted with tetramethyl ammonium, a monovalent cation that does not permeate through Na⁺ channels. The assay uses veratridine to keep the channel partially open and a large depolarization is initiated with the addition of a Na⁺-containing solution. Single-well ratio traces with increasing concentrations of the antagonist tetracaine are shown (a). Single-well dose-response curve of the antagonist tertracaine is shown (c). The IC_{50} is 2 μM, which is similar to the value of 0.7 μM measured electrophysiologically. (b) Assay for endogenous inward-rectifier K^+ channel in rat basophilic leukemia (RBL) cells. The inward-rectifier sets the membrane potential to approximately the K^+-equilibrium potential and addition of a high-K^+ solution causes a channel-dependent depolarization. Single-well ratio traces with increasing concentrations of the antagonist Ba^{2+} are shown (b). Dose-response of the Ba^{2+} blockade of the inward-rectifier and K^+-channel-dependent depolarization is shown. High K^+ and control data are shown on the left and right of the dose-response curve respectively (d). Normalized ratio refers to the final ratio divided by the pre-stimulus ratio, error bars are $\pm$SD of five wells.*

Acknowledgements

We would like to thank Tom Knapp, Mike Maher and Janeen Norberg for their help in the preparation of the figures for this manuscript.

REFERENCES

1 Ackerman, M. and Clapham, D. (1997) *New Engl. J. Med.* 336, 1575–1586

2 Curran, M.E. (1998) *Curr. Opin. Biotechnol.* 9, 565–572
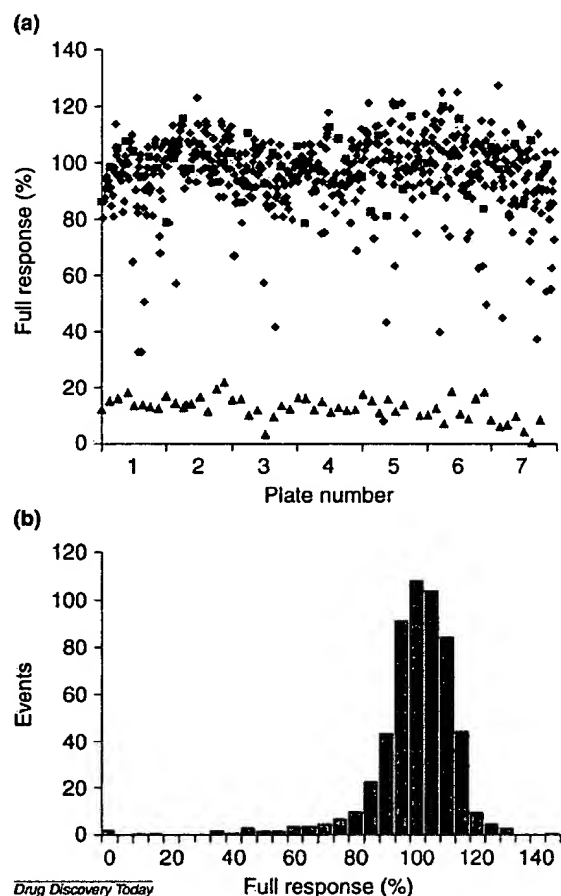
(a)

(b)

Figure 6. Sample screening data from a membrane potential assay using fluorescence resonance energy transfer (FRET) voltage probes. (a) Scatter plot of data from seven 96-well plates. Test compounds were screened at 10 μM (in black diamonds), negative controls (in red squares) and positive Ba^{2+} controls (in blue triangles). 10 μM of each of the compounds were obtained from Microsource Discovery Systems Inc. (Gaylordsville, CT, USA) and LOPAC library at the RBI (Natick, MA, USA). (b) A histogram of the data shows a desirable distribution with the majority of the compounds tightly clustered around 100% full response and a 2% hit rate (defined as more than 50% block). The screening window was X = 3.5 calculated according to the following equation:

$$X = [(mean_{(max)} - 3SD_{(max)}) - (mean_{(min)} + 3SD_{(min)})] / SD_{(max)}.$$

A window >1 means confidence for single-well screening[27].

3 Burbaum, J.J. (1998) *Drug Discovery Today* 3, 313–322

4 Gonzalez, J.E. and Negulescu, P.A. (1998) *Curr. Opin. Biotechnol.* 9, 624–631

5 Denyer, J. *et al.* (1998) *Drug Discovery Today* 3, 323–332

6 Manger, R.L. *et al.* (1993) *Anal. Biochem.* 214, 190–194

7 Shroeder, K.S. and Neagle, B.D. (1996) *J. Biomol. Screen.* 1, 75–80

8 Velicelebi, G. *et al.* (1999) *Methods Enzymol.* 294, 20–47

9 Loew, L.M. (1993) in *Fluorescent and Luminescent Probes for Biological Activity* (Mason, W.T., ed.), pp. 150–160, Academic Press

10 Grinvald, A. *et al.* (1998) *Physiol. Rev.* 68, 1285–1366

11 Epps, D.E., Wolfe, M.L. and Groppi, V. (1994) *Chem. Phys. Lipids* 69, 137–150

12 Rink, T.J. *et al.* (1980) *Biochim. Biophys. Acta* 595, 15–30

13 Holevinsky, K.O. *et al.* (1994) *J. Membr. Biol.* 137, 59–70

14 Narahashi, T. and Herman, M.D. (1992) *Methods Enzymol.* 207, 620–643

15 Strichartz, G., Rando, T. and Wang, G.K. (1987) *Annu. Rev. Neurosci.* 10, 237–267

16 Gonzalez, J.E. and Tsien, R.Y. (1997) *Chem. Biol.* 4, 269–277

17 Gonzalez, J.E. and Tsien, R.Y. (1995) *Biophys. J.* 69, 1272–1280

18 Tsien, R.Y. and Gonzalez, J.E. (1997) US Patent 5661035

19 Nerbonne, J.M. (1996) *Curr. Opin. Neurobiol.* 6, 379–386

20 Adams, S.R. and Tsien, R.Y. (1993) *Annu. Rev. Physiol.* 55, 755–784

21 Breckenridge, L.J. *et al.* (1995) *J. Neurosci. Res.* 42, 266–276

22 Wilson, R.J. *et al.* (1994) *J. Neurosci. Methods* 53, 101–110

23 Miyawaki, A. *et al.* (1997) *Nature* 388, 882–887

24 Llopis, J. *et al.* (1998) *Proc. Natl. Acad. Sci. U. S. A.* 95, 6803–6808

25 Miesenbock, G., De Angelis, D.A. and Rothman, J.E. (1998) *Nature* 394, 192–195

26 Szewczyk, A. and Marban, E. (1999) *Trends Pharmacol. Sci.* 20, 157–161

27 Sittampalam, G.S. *et al.* (1997) *J. Biomol. Screen.* 2, 159–169

In short...

A two-year agreement has been finalized between **Scotia Holdings plc** (Stirling, UK) and **Bristol-Myers Squibb** (BMS; Princeton, NJ, USA) in which Scotia are to develop prototype formulations, utilizing their Galactosome technology, for a number of molecules produced by BMS. BMS are to fund the initial feasibility studies, after which time they can develop any of the prototype formulations for registration and marketing. Under the terms of the agreement, Scotia will be entitled to milestone payments and royalties based on worldwide sales of the formulations.

Genomic Organization, Chromosomal Localization, Tissue Distribution, and Biophysical Characterization of a Novel Mammalian *Shaker*-related Voltage-gated Potassium Channel, Kv1.7*

Katalin Kalman, Angela Nguyen, Julie Tseng-Crank‡§, Iain D. Dukes‡, Grischa Chandy, Carolyn M. Hustad¶, Neal G. Copeland¶, Nancy A. Jenkins¶, Harvey Mohrenweiser‖, Brigitte Brandriff‖, Michael Cahalan, George A. Gutman**, and K. George Chandy‡‡

*From the Departments of Physiology and Biophysics, and **Microbiology and Molecular Genetics, University of California Irvine, Irvine, California 92697; ‡Glaxo-Wellcome Research Institute, Research Triangle Park, North Carolina 27709; ¶Mammalian Genetics Laboratory, ABL-Basic Research Program, NCI-Frederick Cancer Research and Development Center, Frederick, Maryland 21702; and ‖Human Genome Center, Lawrence Livermore National Laboratory, Livermore, California 94550*

We report the isolation of a novel mouse voltage-gated *Shaker*-related K⁺ channel gene, *Kv1.7 (Kcna7/KCNA7)*. Unlike other known Kv1 family genes that have intronless coding regions, the protein-coding region of *Kv1.7* is interrupted by a 1.9-kilobase pair intron. The *Kv1.7* gene and the related *Kv3.3 (Kcnc3/KCNC3)* gene map to mouse chromosome 7 and human chromosome 19q13.3, a region that has been suggested to contain a diabetic susceptibility locus. The mouse Kv1.7 channel is voltage-dependent and rapidly inactivating, exhibits cumulative inactivation, and has a single channel conductance of 21 pS. It is potently blocked by noxiustoxin and stichodactyla-toxin, and is insensitive to tetraethylammonium, kaliotoxin, and charybdotoxin. Northern blot analysis reveals ~3-kilobase pair *Kv1.7* transcripts in mouse heart and skeletal muscle. *In situ* hybridization demonstrates the presence of *Kv1.7* in mouse pancreatic islet cells. *Kv1.7* was also isolated from mouse brain and hamster insulinoma cells by polymerase chain reaction.

Ion channels that exhibit a variety of gating patterns and ion selectivity are critical elements that transduce signals in diverse cell types (1). Voltage-gated potassium-selective (Kv)¹ channels represent the largest family within this class of proteins (2), and perform many vital functions in both electrically excitable and nonexcitable cells. Following initiation of an ac-

tion potential in nerve and muscle cells, Kv channels play the important role of repolarizing the cell membrane (1). Kv channels can also modulate hormone secretion, for example insulin release from pancreatic islet cells (3–6), and regulate calcium signaling during mitogen-stimulated activation of lymphocytes (7).

Kv channels in mammalian cells are encoded by an extended family of at least nineteen genes (2). The largest subfamily, Kv1, is related to the fly *Shaker* gene and contains six members, *Kv1.1–Kv1.6* (2). The *Shaker* gene has 21 exons, which can be alternatively spliced to generate at least five functionally distinct transcripts (8, 9). In contrast, the protein-coding regions of each of the six known mammalian *Kv1* genes and the three known *Xenopus* homologues are contained in a single exon (2, 10), precluding alternative splicing as a means of generating functionally different proteins. The evolutionary significance of this pattern of organization remains a puzzle.

Here we report the identification of a novel mammalian gene, *Kv1.7 (Kcna7/KCNA7)*, that has a genomic organization distinct from the other members of the vertebrate *Kv1* subfamily. We have defined the chromosomal location of this gene in the mouse and human genome, determined its tissue distribution, and characterized the biophysical and pharmacological properties of the cloned channel.

EXPERIMENTAL PROCEDURES

Isolation and Characterization of mKv1.7, hKv1.7, hKv3.3, and hKv3.4 DNA Clones—Three overlapping genomic clones (KC225, KC254, and KC256) were isolated from an AKR/J mouse genomic library screened with a mixture of *mKv1.1* and *rKv1.5* cDNA probes, as described previously (10), and mapped by multiple and partial restriction endonuclease digests, and by dideoxy sequencing. *Kv1.7* cDNAs were amplified by the polymerase chain reaction (PCR) from mouse brain and from the hamster insulinoma cell line, HIT-T1S, using intron-flanking primers (5'-TCTCCGTACTCGTCATCCTGG-3' within S1 and 5'-AAATGGGTGTCCACCCGGTC-3' on the 3' side of S5). The resulting 588-bp PCR fragments were sequenced.

Cosmid clones encoding hKv1.7 and hKv3.3 (11) were isolated from a human chromosome 19-enriched library, Library F (12), screened with mKv1.7 and mKv3.3 probes. A 1.9-kb cDNA fragment of the *Shaw* family gene, hKv3.4, was isolated from a human pancreatic library (13) screened with a mixture of *hKv3.1* (0.9-kb *XbaI/HindIII*), *hKv3.3* (1.4-kb *PstI/EcoRI*), and *mKv3.4* (0.9-kb *HindIII/EcoRI*) probes at a final stringency of 0.5 × SSC and 0.1% SDS at 55 °C (8 × 10⁶ phage screened). The isolated clone spans the region from S1 through the 3' end of the coding region (0.6 kb), and 1.3 kb of the 3'-noncoding region.

Mice—Pancreatic tissue sections were obtained from 9–16-week-old diabetic-prone (*db/db*) and healthy (*db/+*) C57BL/KsJ mice. Mice ho-

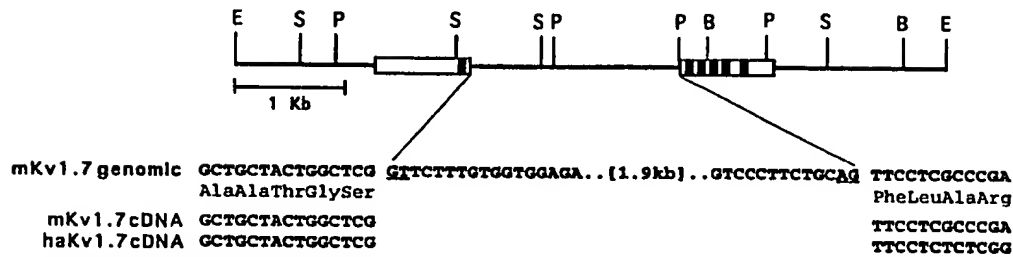*Kv1.7, a Novel Voltage-gated Potassium Channel Gene*

FIG. 1. **Genomic organization of mouse** *Kv1.7*. *Top*, the *mKv1.7* coding sequence is indicated by the two *stippled boxes*, and the six *bars* within these regions indicate the putative membrane-spanning domains S1 through S6. Restriction sites are indicated as follows: *B, BglII*; *E, EcoRI*; *P, PstI*; *S, SacI*. *Bottom*, comparison of the genomic sequence of *mKv1.7* with that of mouse and hamster (*haKv1.7*) cDNAs shows the splice donor and acceptor sites which form the boundaries of the single intervening sequence.

mozygous for the autosomal recessive diabetic susceptibility gene *db*, a mutated form of the leptin receptor (14, 15) on chromosome 4, develop diabetes beginning at about 6 weeks of age (16).

Mapping Mouse and Human Chromosomal Locations of Kv1.7 and Kv3.3—Interspecific backcross progeny were generated by mating (C57BL/6J × *Mus spretus*)F$_1$ females and (C57BL/6J) males, and a total of 205 N$_2$ mice were used to map the two mouse genes, *mKv1.7/Kcna7* and *mKv3.3/Kcnc3*, as described previously (11, 17–20). The probe for *mKv1.7* was the entire 6.4-kb *EcoRI* fragment shown in Fig. 1, and that for mouse *Kv3.3* was a 4-kb genomic *HindIII* fragment containing the entire 3′-exon (11). Although 155 mice were analyzed for all markers and are shown in this segregation analysis, up to 188 mice were typed for some pairs of markers. Recombination frequencies were calculated as described (11, 17–20) using the computer program SPRETUS MADNESS. Gene order was determined by minimizing the number of recombination events required to account for the allele distribution patterns. Fluorescent *in situ* hybridization of cosmids to metaphase human chromosomes was carried out as described previously (21, 22).

Northern Blot Assays—A Northern blot of poly(A)$^+$ RNA from mouse heart, brain, spleen, lung, liver, skeletal muscle, kidney, and testis (CLONTECH Inc., Palo Alto, CA) was probed with the mouse *Kv1.7*-specific 3′-noncoding region sequence. The *PstI/SacI Kv1.7* 3′-noncoding region was labeled by the random primer method (Boehringer Mannheim Random Primed DNA labeling kit). The RNA blot was hybridized at 60 °C for 18 h, washed at a final stringency of 0.2 × SSC and 0.1% SDS at 60 °C for 1 h, and exposed to x-ray film at −80 °C with an intensifying screen for 3 days.

In Situ Hybridization—cRNA probes labeled with α-^{35}S-labeled UTP (1300 Ci/mmol) were alkaline-denatured to an average size of 100 nucleotides and used for *in situ* hybridization on pancreatic frozen sections (6–10 μm thick) from *db/db* mice. Briefly, sections were hybridized overnight at 42 °C, RNase treated, washed five times in 0.5 × SSC at 65 °C, coated with Ilford K5 photographic emulsion, and exposed at 4 °C for varying times. After development, the sections were counterstained with hematoxylin and eosin Y and examined with a Leitz Aristoplan microscope equipped with reflected polarized light to visualize silver grains in dark field. The probes used for hybridization were as follows: *insulin*, 1.6-kb human insulin gene including the 5′- and 3′-flanking sequences (ATCC no. 57399); *hKv3.4*, 1.9-kb cDNA fragment spanning S1 through the 3′ end of the coding region (0.6 kb), and 1.3 kb of the 3′-noncoding region; *mKv1.7*, 540-bp *PstI/SacI* fragment containing 29 bp of C-terminal coding sequence and 511 bp of 3′-noncoding sequence.

Electrophysiological Studies—To make a *mKv1.7* expression construct we amplified a 588-bp fragment from mouse brain cDNA spanning the region encoded by the two Kv1.7 exons using reverse transcriptase PCR (5′-primer, 5′-TCTCCGTACTCGTCATCCTGG-3′; 3′-primer, 5′-AAATGGGTGTCCACCCGGTC-3′). Exon 1 (850-bp *BspHI/BinI* fragment), a 283-bp *BinI/BglII* fragment of our 588-bp PCR product, and exon 2 (747-bp *BglII/HindIII*), were ligated together at *BinI* and *BglII* sites to generate "fragment I" (1880 bp). Fragment I was blunt-ended at the 5′ end and cloned into the pBluescript vector at *SmaI/HindIII* sites. To remove the 5′-NCR from fragment I, and for the purpose of cloning this fragment into the pBSTA expression vector, we introduced a unique *BamHI* site just upstream of the initiator methionine using PCR: 5′-primer, 5′-ACAAAAGCTTCATATGACTACAAG-GAAAGCT-3′; and 3′-primer: 5′-AAGCGCAACCCGGCCACG-3′. The resulting PCR product (corresponding to the first 283 nucleotides of the coding region) was spliced to fragment I at the *NcoI* site, and the 1870-nucleotide fragment was ligated to the pBSTA vector.

mKv1.7 cRNA was transcribed *in vitro* (Ambion Kit, Austin, TX) and

diluted in a 0.1–0.5% fluorescein-dextran (M_r 10,000, Molecular Probes, Eugene, OR) in 100 mM KCl. Rat basophilic leukemic (RBL) cells were maintained in Dulbecco's modified Eagle's medium supplemented with 10% fetal calf serum (Hyclone, Logan, UT) and glutamine, and were plated onto glass coverslips one day prior to use for electrophysiological experiments. RBL cells were injected with cRNA using pre-pulled injection capillaries (Femtotip) in combination with an Eppendorf microinjection system (micromanipulator 5171 and transjector 5242; Madison, WI) as described previously (23). Four to six hours later, fluorescent cRNA-injected cells were evaluated electrophysiologically.

All membrane currents were recorded at room temperature (22–26 °C) with a LIST EPC-7 amplifier (Heka Elektronik, Germany). Series resistance compensation was employed if the current exceeded 2 nA, and the command input was controlled by a PDP 11/73 computer via a digital-to-analog converter. Capacitative and leak currents were subtracted using a P/8 procedure and the holding potential in all experiments was −80 mV. When membrane currents exceeded 2 nA 80% series resistance compensation was used.

RESULTS

The Protein-coding Region of mKv1.7 Contains an Intron Unlike Its Vertebrate Homologues

A restriction map of a 6.4-kb *EcoRI* DNA fragment containing the entire mouse *Kv1.7* coding region is shown in Fig. 1. The coding region is contained in two exons separated by a 1.9-kb intron. The upstream exon encodes the entire N terminus, S1, and part of the S1-S2 loop. The downstream exon contains the region extending from the S1-S2 loop to the C-terminal end of the protein. The intron-exon splice sites were determined by comparing the genomic sequence with cDNA sequences obtained from the hamster insulinoma cell line, HIT-T1S, and from mouse brain (Fig. 1).

The complete coding sequence of the *mKv1.7* is shown in Fig. 2. The mKv1.7 sequence is identical in the N terminus from bp 52 to 996 with the mouse EST sequence AA021711. Betsholtz *et al.* (24) amplified a short segment of Kv1.7 cDNA spanning the S5/S6 region from mouse (MK-6), rat (RK-6), and hamster (HaK-6) insulin-producing cells using PCR. Our sequence is identical to their MK-6 sequence, except for four nucleotide changes.

The deduced mKv1.7 protein consists of 532 amino acids and contains six putative membrane-spanning domains, S1–S6 (Fig. 2). The hydrophobic core of this protein shares considerable sequence similarity with other *Shaker* family channels, while the intracellular N and C termini and the external loops between S1/S2 and S3/S4 show little conservation. The protein contains conserved sites for post-translational modifications as indicated in Fig. 2. As do all other *Shaker*-related channels, mKv1.7 has a potential tyrosine kinase phosphorylation site (RPSFDAVLY) in its N-terminal region (2); the proline-rich stretch within the N terminus (see residues 29–42) may be a binding site for SH3 domains of tyrosine kinases. Two protein kinase C consensus sites (Ser/Thr-*X*-Arg/Lys) are present in the cytoplasmic loop between S4 and S5 of mKv1.7; at least one

```
                                ACTGTCACCCGGGCAATCCGAAGATGAGGCAGAGGATTGCCACAAGTTCGCGGTCAGCTTAAATGACAGGCTGAGGAGACTGTCTAAATAAC -141
AAACAAACAAATAAATAGCCATGATGCCATACGCCTGCAATCCCCAGCATTTGGGAGGTGGAGGCAGGAGGATCATAAATTCAAGGTCAGTTCAGCTACATAAGACCTCGGGTCATGAATCCAAAAGCCAAACAAATAAAATAG  -1

ATG ACT ACA AGG AAA GCT CAA GAG ATC CAC GGA AAA GCG CCG GGT GGC AGT GTT TCC ACA GGT GTG GGA ACG GCA GAG GGC GCC CCT AGC CCC GCG GGG GTA ACA CCG  108
Met Thr Thr Arg Lys Ala Gln Glu Ile His Gly Lys Ala Pro Gly Gly Ser Val Ser Thr Gly Val Gly Thr Ala Glu Gly Ala Pro Ser Pro Ala Gly Val Thr Pro   36

CCC CCT CCC CCG CGC CCT GGC CGG ACT TTC CAT GCT ATT TTT ACC CGC CGA CAC CGG ACA CCC GAC TGG GGT GGC TGC GGC GTC GGG GCC ACA CGT CCG TTC ACC GGT  216
Pro Pro Pro Pro Arg Pro Gly Arg Thr Phe His Ala Ile Phe Thr Arg Arg His Arg Thr Pro Asp Trp Gly Gly Cys Gly Val Gly Ala Thr Arg Pro Phe Thr Gly   72

CGC CCG GGC TGT GCG CGC CAT GGA GCC ACG GTG CCC GCC GCC CTG CGC TGC TGC GAG CGG CTG GTG CTC AAC GTG GCC GGG TTG CGC TTC GAG ACC CGC GCG CGC ACG  324
Arg Pro Gly Cys Ala Arg His Gly Ala Thr Val Pro Ala Ala Leu Arg Cys Cys Glu Arg Leu Val Leu Asn Val Ala Gly Leu Arg Phe Glu Thr Arg Ala Arg Thr  108

                                                                                             ┌───── TY-K ─────┐
CTC GGC CGC TTC CCG GAC ACG CTG CTG GGC GAC CCG GTG CGC CGC AGC CGC TTC TAC GAC GGC GCG CGC GCC GAG TAT TTC TTC GAC CGA CAC CGG CCC AGC TTC GAT  432
Leu Gly Arg Phe Pro Asp Thr Leu Leu Gly Asp Pro Val Arg Arg Ser Arg Phe Tyr Asp Gly Ala Arg Ala Glu Tyr Phe Phe Asp Arg His Arg Pro Ser Phe Asp  144

GCG GTG CTC TAC TAC TAC CAG TCG GGC GGC CGG CTG AGA CGG CCG GCG CAC GTG CCC CTC GAC GTC TTC CTG GAG GAG GTG TCC TTC TAC GGG CTG GGG CGG GGG CTG  540
Ala Val Leu Tyr Tyr Tyr Gln Ser Gly Gly Arg Leu Arg Arg Pro Ala His Val Pro Leu Asp Val Phe Leu Glu Glu Val Ser Phe Tyr Gly Leu Gly Arg Arg Leu  180

GCG CGG CTG CGG GAG GAC GAG GGC TGC GCG GTC GCC GAG CGG CCG CTG CCC CCG CCC TTT GCG CGT CAG CTC TGG CTG CTC TTC GAA TTT CCT GAG AGC TCG CAG GCT  648
Ala Arg Leu Arg Glu Asp Glu Gly Cys Ala Val Ala Glu Arg Pro Leu Pro Pro Pro Phe Ala Arg Gln Leu Trp Leu Leu Phe Glu Phe Pro Glu Ser Ser Gln Ala  216

                    ┌──────────────── S1 ────────────────────┐
GCG GCC GTG CTC GCC GTG GTC TCC GTC ATC CTG GTC TCC ATC GTG GTC TTT TGC CTC GAG ACA CTG CCA GAC TTC CGC GAC GAC CGC GAT GAC CCG GGG CTC  756
Ala Arg Val Leu Ala Val Val Ser Val Leu Val Ile Leu Val Ser Ile Val Val Phe Cys Leu Glu Thr Leu Pro Asp Phe Arg Asp Asp Arg Asp Asp Pro Gly Leu  252
                                                        ↓
GCG CCG GTA GCG GCT GCT ACT GGC TCG TTC CTC GCT CGG CTC AAT GGC TCC AGT CCC ATG CCA GGA GCC CCT CCC CGA CAG CCC TTC AAC GAT CCA TTC TTT GTG GTG  864
Ala Pro Val Ala Ala Ala Thr Gly Ser Phe Leu Ala Arg Leu Asn Gly Ser Ser Pro Met Pro Gly Ala Pro Pro Arg Gln Pro Phe Asn Asp Pro Phe Phe Val Val  288
        ┌──────── S2 ───────┐
GAG ACC CTG TGT ATC TGC TGG TTC TCC TTT GAG CTG CTG GTG CAT CTG GTG GCC TGC CCT AGC AAA GCT GTG TTC TTC AAG AAT CTC ATG AAC CTA ATT GAC TTC GTG  972
Glu Thr Leu Cys Ile Cys Trp Phe Ser Phe Glu Leu Leu Val His Leu Val Ala Cys Pro Ser Lys Ala Val Phe Phe Lys Asn Val Met Asn Leu Ile Asp Phe Val  324
    ┌──────── S3 ────────┐
GCC ATC CTG CCT TAC TTC GTG GCC CTG GGC ACG GAG TTA GCC CGG CAG CGG GGT GTG GGC CAG CCG GCT ATG TCC CTG GCC ATC CTA AGG GTC ATC CGA TTG GTG CGT 1080
Ala Ile Leu Pro Tyr Phe Val Ala Leu Gly Thr Glu Leu Ala Arg Gln Arg Gly Val Gly Pro Ala Met Ser Leu Ala Ile Leu Arg Val Ile Arg Leu Val Arg  360
          ┌──────── S4 ───────┐         ┌── PKC ──┐   ┌── PKC ──┐                            ┌─── S5 ──
GTC TTC CGC ATC TTC AAG CTC TCC AGG CAT TCG AAG GGT CTA CAG ATC TTG GGT CAG ACA CTG CGG GCT TCC ATG CGT GAG CTA GGT CTC CTC ATC TTC TTC CTC TTC 1188
Val Phe Arg Ile Phe Lys Leu Ser Arg His Ser Lys Gly Leu Gln Ile Leu Gly Gln Thr Leu Arg Ala Ser Met Arg Glu Leu Gly Leu Gly Leu Leu Ile Phe Phe Leu Phe  396
                                                                  ┌──────── P ─────
ATT GGC GTG GTC CTC TTT TCC AGC GCA GTC TAC TTT GCT GAA GTG GAC GGC GTG GAC ACC CAT TTC ACC AGC ATC CCG GAG TCC TTT TGG TGG GCA GTG GTC ACC ATG 129?
Ile Gly Val Val Leu Phe Ser Ser Ala Val Tyr Phe Ala Glu Val Asp Arg Val Asp Thr His Phe Thr Ser Ile Pro Glu Ser Phe Trp Trp Ala Val Val Thr Met  43?
                                                         ┌──────── S6 ═══
ACC ACG GTT GGC TAT GGG GAC ATG GCA CCC GTC ACC GTG GGT GGC AAG ATC GTG GGC TCT CTG TGT GCC ATT GCA GGT GTG CTC ACC ATC TCT CTG CCT GTG CCT GTC 1404
Thr Thr Val Gly Tyr Gly Asp Met Ala Pro Val Thr Val Gly Gly Lys Ile Val Gly Ser Leu Cys Ala Ile Ala Gly Val Leu Thr Ile Ser Leu Pro Val Pro Val  468

ATT GTC TCT AAC TTT AGC TAC TTT TAC CAC CGG GAG ACA GAG GGC GAA GAG GCA GGG ATG TAC AGC CAT GTG GAC ACA CAG CCC TGC GGT ACC CTG GAG GGC AAG GCT 1512
Ile Val Ser Asn Phe Ser Tyr Phe Tyr His Arg Glu Thr Glu Gly Glu Glu Ala Gly Met Tyr Ser His Val Asp Thr Gln Pro Cys Gly Thr Leu Glu Gly Lys Ala  504

AAT GGG GGG CTG GTG GAC TCT GAG GTG CCT GAA CTC CTC CCA CCA CTC TGG CCC CCT GCA GGG AAA CAC ATG GTG ACT GAC GTG TGA GGG TCA ACT GGG GTC TCC AGG 1620
Asn Gly Gly Leu Val Asp Ser Glu Val Pro Glu Leu Leu Pro Pro Leu Trp Pro Pro Ala Gly Lys His Met Val Thr Glu Val  *  532

GAGCAGTGGGGTGGGAGGGAGGAGGGAAGGCAGGTCAGGTGCTGGGTTAAGGACTAAGATGGTAACAAAATCTTAATCTGAAGGCATGTCACATGGTGGCGGGTACAGATTCCTAGGGGGACCTTATGTGACAGGAATTGCCA 1763
GGATTTGGGTTGTGTCCAGGGCTCCCCCCATTGATTGATGGCAGCTGGTAGAGCTGTGCAAATGTCCAGGGGCTCTAGGGGTAGCACTGTAAGAGACTTGGCCATAGATTGTGAGTTTCCTAGGTGTTCGTGGGGTCCCACTGG 1906
GGGCAAGTGTGGTCCCGTTAACACTTGATAGGTACTAATAGAACTTTGGGTCCTCTAGGGCCAAGTCGGCTCCTGTAGGTCTCTGGAGCACTGTTAAAGAGTGTGAGCTTGTGGCTACATGGTCACACACAGAGGTTATGTGG 2049
TGATACATAGCAGATTGTGTGGATTCATGTTTCTTCTAGGACTCAAGTTATTTTAGATTCTGTGAGCTCTGGAGGTCATGCAGACAGGATGTGATCACTCTGGGTCCTGATGGAAAAAGGGTTAGGGTATAAAAGATAGACAGA 2192
GGCAGAGACTCAGATAAAGGGACAGAGACACCCCCACACACACACACAACACACAATTCTCTGTGTTGTGCAGGGTTATAGGACTGGAATCATTTTAGGGCCATGCAAAGCTGAGATGGTGACCCCCATGTGTCTCCGAACAG 2335
TTGAGTCTGATGACTTCTACGGTCTCATGGGACTTGTGTTACTGTGAGTCCTGTGGAACTTTTGGTTGAATTTGACTGTATGTGAGGGCCATTTTAAACAGTAGATCAGGGTCACAGCACAGATAAAACTAACTACAAGGGAG 2478
CAAGCATGGGCACGTGGATGTGTGTGGCCCGTTGAACAAGTTTACTCAGGGTTATGCATTGTAGAGCTGGTAGTGTCTGTATCTCTGGGTCCCCCTGCCCCGAAGCACCTAGAAAGACGACTGGGAACTAGTAACCTGCCTGTCT 2621
TGCTCATGTGGGACCCATATTTCTATGTTGTCCCATGCTGTAGTACAAAGATTCAGAGGCTGGTTGGAGCCACAAGGAAAGAAAACACAGTAGGGCAAGAGTAGGTACTTGGGAAAAGATGTGGCAGGGGACAGAGATCTAGA 2764
AGAAAGAAAGATGGAGAAGGAGCAGGAGGAGCAGGGAGGGGGAAAGAGGCAAAGAGGGAGGAGAGCAGAGATGTGGGGGGGGGGGGAGAAGGACCTGGAGCCCAAGGGTCATCCTCTCT 2907
ATTCTCTGAGTCATAACAGACTCTAAGCTATGGCGTCAGCATCCCTTAGAGCCAAGGAAGGTCACCACACTCCTGGAGGTGCTCTGTGTTTCCTAGGACAGAAACCCAAGGCTGTAGTGTGCTGTGCTTCCTCAAGTTACCCA 3050
GCGGTCATAGACCAAGCTGGTGCCAGGTGGCCTGCCTGTGACACCCCCACAACTTCTGGTGTGCAGGTATTGCCTGAGGCCACTGGTCCTGTGTCCTTTGTTTATCCCTTAAAACAGGGTCCCTCTTTGTAGTGTTGGCTGTC 3193
CTGGAACTCACTACGTAGA 3212
```

FIG. 2. **Nucleotide sequence and deduced amino acid sequence of mouse Kv1.7.** The six putative membrane-spanning domains (S1 through S6) and pore-forming region (P) are indicated. The potential sites for phosphorylation by tyrosine kinase (TY-K) and protein kinase C (PKC) are shown. The position of the single intron between S1 and S2 is indicated by an *arrow*, and the critical residue for tetraethylammonium block (Ala-441, within the P region) is shown in bold and underlined.

of these sites is present in all members of the Kv1 family (2). mKv1.7, like Kv1.6, lacks an N-glycosylation site in the extracellular loop linking the S1 and S2 transmembrane segments; this consensus sequence is conserved in all other Kv1 family genes.

Fig. 3 shows a phylogenetic tree of the entire *Shaker* family of genes based on parsimony analysis of a nucleotide sequence alignment (generated from the amino acid sequence alignment) using the program PAUP (25). Our analysis places *mKv1.7* within the *Shaker* family of genes. The *mKv1.7* gene does not cluster with any of the known genes, and its position within the tree is not firmly established.

Kv1.7 Is Located on Mouse Chromosome 7 and Human Chromosome 19q13.3

The *mKv1.7/Kcna7* gene resides on mouse chromosome 7 (Fig. 4A), ~0.5 centimorgan telomeric to the *Shaw*-related K⁺ channel gene, *mKv3.3/Kcnc3*, and ~2.4 centimorgans centromeric of *MyoD1* (myoblast differentiation factor). The most centromeric marker in this study was *Gpi1* (glucose phosphate isomerase 1), which mapped ~6.1 centimorgans centromeric to *mKv3.3/Kcnc3*.

The interval on mouse chromosome 7 containing *mKv1.7/Kcna7* and *mKv3.3/Kcnc3* shares a region of homology with human chromosomes 19q13 and 11p15, and the human homologues of these K⁺ channel genes may therefore be expected to reside on one of these chromosomes. Confirming this predic-

FIG. 3. **Proposed phylogenetic relationship of *mKv1.7* and other *Shaker*-related Kv channel genes.** This tree is based on parsimony analysis of nucleotide sequence alignments using the program PAUP (25). Horizontal distance represents the number of nucleotide substitutions in each lineage, with the *scale bar* at the *upper left* representing 100 substitutions. *m*, mouse; *h*, human; *x*, *Xenopus*; *APLK*, *Aplysia*; *SHAKER*, *Drosophila Shaker*.

tion, we mapped both genes to human 19q13.3–13.4 using fluorescent *in situ* hybridization. The idiogram of human chromosome 19 shown in Fig. 4B, and a more detailed map shown in Fig. 4C, indicate that *hKv1.7/KCNA7* is located ~1.3 mb centromeric of *hKv3.3/KCNC3*. The genes for both muscle glycogen synthase (*GYS1*) and the histidine-rich calcium protein (*HRC*) also map to this region; Kv1.7/KCNA7 lies ~25 kb telomeric to GYS1 and ~200 kb centromeric to HRC (Fig. 4C).
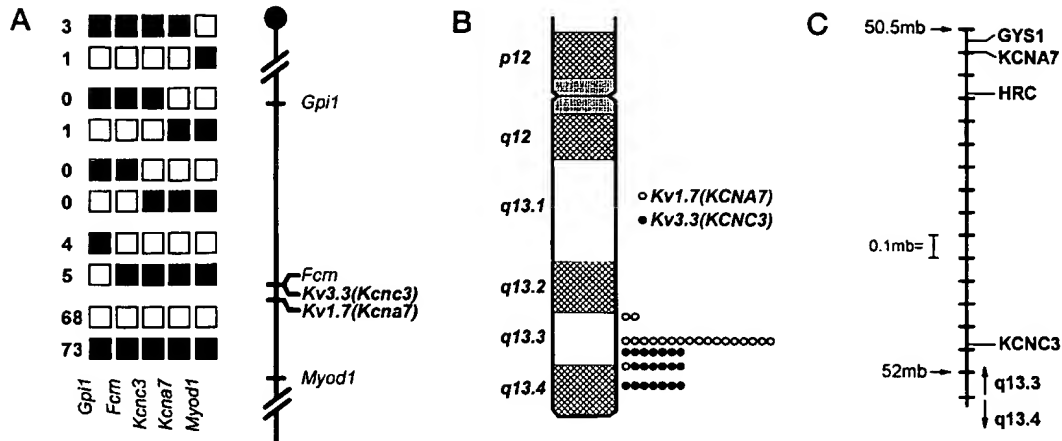
FIG. 4. **Chromosomal localization of the mouse and human *Kv1.7* genes.** *A*, mouse chromosome 7. (*Left*) results of segregation analysis in a (C57BL/6J × *M. spretus*)F₁ × C57BL/6J interspecific backcross. The genes indicated are as follows: *Gpi1*, glucose phosphate isomerase-1; *Fcrn*, Fc-receptor, neonatal form; *Myod1*, myoblast differentiation factor-1. The ratios of the total number of mice exhibiting recombinant chromosomes to the total number of mice analyzed for each pair of loci are *Gpi1* - 11/181 - *Fcrn* - 0/184 - *mKv3.3/Kcnc3* - 1/188 - *mKv1.7/Kcna7* - 4/167 - *Myod1*. The recombination frequencies expressed as genetic distances in centimorgans ± the S.E are: *Gpi1* - 6.1 ± 1.8 - [*Fcrn*, *mKv3.3*] - 0.5 ± 0.5 - *mKv1.7* - 2.4 ± 1.2 - *MyoD1*. *Filled boxes* indicate the presence of the C57Bl/6J allele, and *open boxes* the presence of the *M. spretus* allele. (*Right*) diagram showing the deduced order of *Kv1.7* and neighboring genes on mouse chromosome 7, with the centromere shown at the *top*. *B*, human chromosome 19. Diagram shows the deduced order of genes on human chromosome 19. A single *hKv1.7/KCNA7* cosmid was mapped to 19q13.3 by fluorescent *in situ* hybridization (FISH). Ten cells were scored for each cosmid used, and for each of two *hKv3.3/KCNC3* cosmids, signal was present on both chromatids in a position corresponding to 19q13.3-q13.4. The positions where signal was observed for the two probes are indicated as *open circles* (*hKv1.7/KCNA7*) and *solid circles* (*hKv3.3/KCNC3*). *C*, detailed map of the relevant region of human chromosome 19. The positions of *KCNA7*, *KCNC3*, *GYS1*, and *HRC* are shown, with each *cross-bar* indicating a distance of 100 kb. The positions corresponding to 50.5 and 52 mb of chromosome 19 (37) are indicated, as is the point of demarcation between chromosome bands q13.3 and q13.4.

Interestingly, a putative diabetes susceptibility gene has been suggested to be present at 19q13.3 (26, 27), especially in Finnish families with associated hypertension and difficulties in insulin-stimulated glucose storage. This region has also been suggested to contain a modifier locus for cystic fibrosis (28).

Biophysical and Pharmacological Characterization of Kv1.7 Channels

We carried out a detailed characterization of mKv1.7 channels expressed in RBL cells which express no native Kv currents (29, 30). The *mKv1.7* gene expressed in *Xenopus* oocytes produced currents (data not shown) similar to those obtained in RBL cells (Fig. 5).

Voltage Dependence—Patch clamp studies were performed in the whole-cell mode. Fig. 5A shows a family of outward currents elicited by a 200 ms depolarizing pulse from a holding potential of −80 mV in RBL cells injected with *mKv1.7* cRNA; no outward currents were detected in control cells (data not shown). The currents activate rapidly, and from the conductance-voltage curve shown in Fig. 5B we determined that the 1/2 activation potential (V₁/₂) is −20 mV.

Inactivation and Deactivation—Inactivation of mKv1.7 channels was rapid following a 200 ms depolarizing pulse from −80 to 40 mV (Fig. 5A). The rate of inactivation, measured by fitting the data to a single exponential function, yielded a time constant (τ_h) of 14 ± 2.1 ms (S.E., $n = 7$). As shown in Fig. 5C, the current became progressively smaller following repeated depolarizing pulses at 1-s intervals. This phenomenon, termed "cumulative inactivation," is due to the accumulation of channels in the inactivated state which are then unavailable for opening. The related channels, Kv1.3 (7) and Kv1.4 (31), also display this behavior.

The kinetics of channel closing (deactivation) was determined by first opening the channels with a 15 ms conditioning depolarizing pulse, and then forcing the channels to close by repolarizing to different potentials (Fig. 5D). The time constant, τ_{tail}, of the resulting "tail" current was 5.1 and 5.3 ms at −60 mV in two cells.

Single-channel Conductance—We measured single-channel currents in an outside-out patch by applying 450-ms voltage ramps from −90 to 80 mV every second (Fig. 5E). Single channel events were seen at potentials more positive than ∼−15 mV. The single-channel conductance of 21 pS was estimated from the slope of the current recorded during an opening (Fig. 5E).

Pharmacology—We determined the pharmacological sensitivity of the mKv1.7 channel using methods described previously (30, 32), IC₅₀ values in each case being determined when block reached steady-state. The channel was blocked by several non-peptide small molecule antagonists, 4-aminopyridine (IC₅₀ = 245 μM), capsaicin (25 μM), cromakalim (450 μM), tedisamil (18 μM), nifedipine (13 μM), diltiazem (65 μM), and resinifera-toxin (20 μM). Surprisingly, the dihydroquinoline compound, CP-339,818, that blocks rapidly inactivating Kv1 channels in the nanomolar range (30), had little effect on mKv1.7 (IC₅₀ = 10 μM). The channel was insensitive to externally applied tetraethylammonium (C₅₀ = 86 mM), probably because the residue at the tetraethylammonium-binding site, Ala-441 (Fig. 2), is hydrophobic.

The mKv1.7 channel is also potently blocked by a peptide (ShK toxin) obtained from sea anemone *Stichodactyla helianthus* (IC₅₀ = 13 nM), and by the scorpion toxins, noxiustoxin (IC₅₀ = 18 nM) and margatoxin (IC₅₀ = 116 nM). The channel was resistant to charybdotoxin (IC₅₀ >1000 nM) and kaliotoxin (IC₅₀ >1000 nM).

Expression of mKv1.7 Transcripts in Different Tissues

Northern blot assays using a mKv1.7-specific probe revealed strongly hybridizing 3-kb bands in heart and skeletal muscle; faint bands of similar size were visible in liver and lung (together with larger 7–8-kb bands), but none were seen in spleen, kidney, testis, or brain (Fig. 6) We were able to isolate *mKv1.7* transcripts from mouse brain by PCR (see Fig. 1). mKv1.7 is also expressed in placenta, since the mouse EST AA021711 was derived from this tissue.

PCR analysis demonstrated the presence of haKv1.7 mRNAs

FIG. 5. **Kv1.7 currents.** *A*, family of mKv1.7 currents. The holding potential was −80 mV and depolarizing pulses were applied every 30 s. The test potential was changed from −50 to 50 mV in 10-mV increments. *B*, peak K$^+$ conductance-voltage relation for currents shown in *A*. The line through the points was fitted with the Boltzmann equation: $g_k(E)$ = $g_{k(max)}/[1 + exp[(E_n − E)/k]]$, with parameter values $g_{k(max)}$ = 20 nS and k = −8 mV. *C*, cumulative inactivation of Kv1.7 currents. Currents were elicited by a train of six depolarizing voltage steps (200-ms duration) to 40 mV once every second from a holding potential of −80 mV. The current amplitude decreases significantly during this train of pulses from the largest (*first trace*) to the smallest (*last*). *D*, kinetics of deactivation of Kv1.7 currents. Tail currents were elicited by voltage steps from −100 to −40 mV after a 15-ms depolarizing prepulse to 40 mV. The tail current-decay time constants, τ_t, were measured by fitting single-exponential functions to the decay of the K$^+$ current during repolarization. *E*, single-channel currents of Kv1.7 in an outside-out patch. The *broken line* shows the slope conductance.
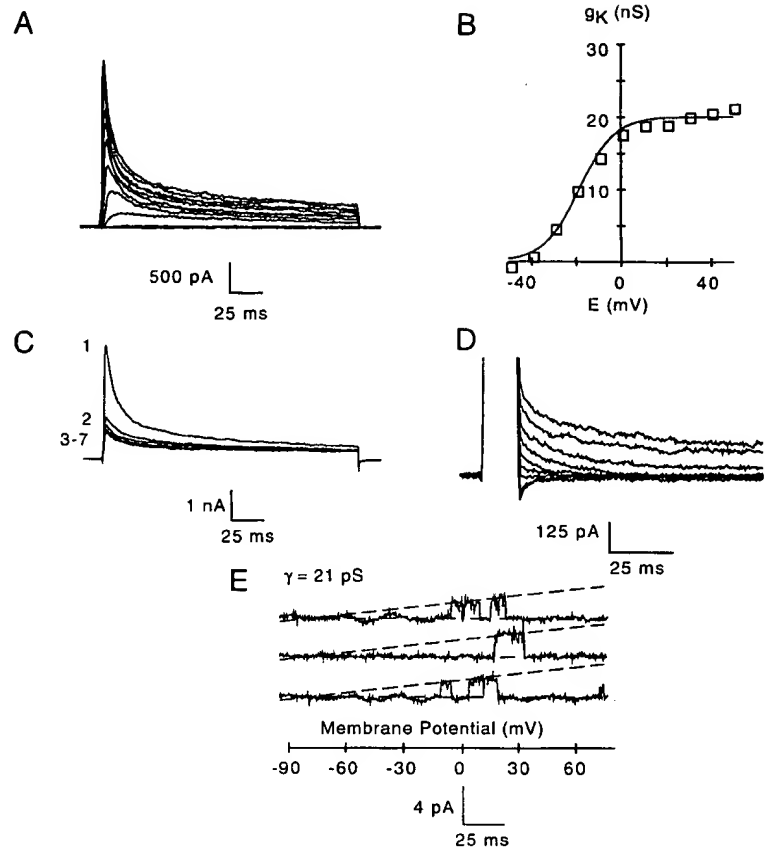
in hamster insulinoma cells (Fig. 1). We verified the presence of *mKv1.7* mRNA in pancreatic islet cells obtained from 9–16-week-old diabetic *db/db* mice by *in situ* hybridization (Fig. 7C) using a mKv1.7-specific antisense probe (12–14); *mKv1.7* mRNA was also present in islets from normal *db/+* mice (data not shown). Scattered acinar cells outside the islets also showed mKv1.7 hybridization (Fig. 7C). In contrast, *mKv3.4* mRNA was found in acinar cells surrounding islets, but not in islets, of both *db/db* (Fig. 7B) and *db/+* mice (data not shown). As a control, insulin mRNA was detected in both normal and diabetic islets, but not in acinar cells (Fig. 7A). A *Kv1.5*-specific probe did not show appreciable hybridization to islets (data not shown), despite a report of *Kv1.5* cDNA having been cloned from human insulinoma cells (33).

DISCUSSION

Unlike all other known mammalian *Shaker*-related genes (*Kv1.1–Kv1.6*) that have intronless coding regions (2, 9), the protein-coding region of *mKv1.7* is interrupted by a single 1.9-kb intron. The fly *Shaker* gene also contains an intron in the S1-S2 loop, raising the possibility that the intron in *Kv1.7* may be ancient, predating the divergence of flies and mammals. Both the mouse *Kv.1.7* and the fly *Shaker* intron are placed between codons, *i.e.* they are "phase 0" introns. While this is consistent with their having a common origin it may also be fortuitous, since there are only three possible "phases." Although we favor the idea that Kv introns were lost in the vertebrate lineage before their expansion by gene duplication (in which case the *Kv1.7* intron would represent a more recent insertion), the evolutionary history of this complex gene family remains to be elucidated.

Since *Kv1.7* mRNA is expressed in the mouse heart, we searched the literature for native cardiac A-type Kv currents
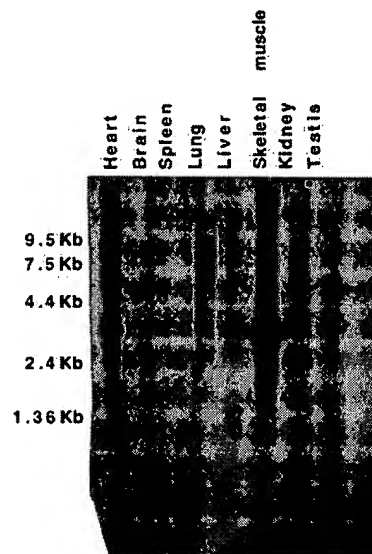
FIG. 6. **Expression of *Kv1.7* mRNA in tissues.** Northern blot assay.

with properties resembling those of Kv1.7. The Kv1.7 homotetramer shares many properties with the rapidly inactivating transient outward (I_{to}) current in cardiac Purkinje fibers, but not the I_{to} current in atrial and ventricular myocytes. Kv1.7 and the Purkinje I_{to} currents activate at negative potentials (∼−30 to −20 mV), inactivate rapidly (τ_h < 25 ms), exhibit cumulative inactivation, are blocked by micromolar concentrations of 4-aminopyridine, and are resistant to >20 mM tetra-

Kv1.7, a Novel Voltage-gated Potassium Channel Gene

Probes   A Insulin   B hKv3.4   C mKv1.7

Sense

Anti-sense
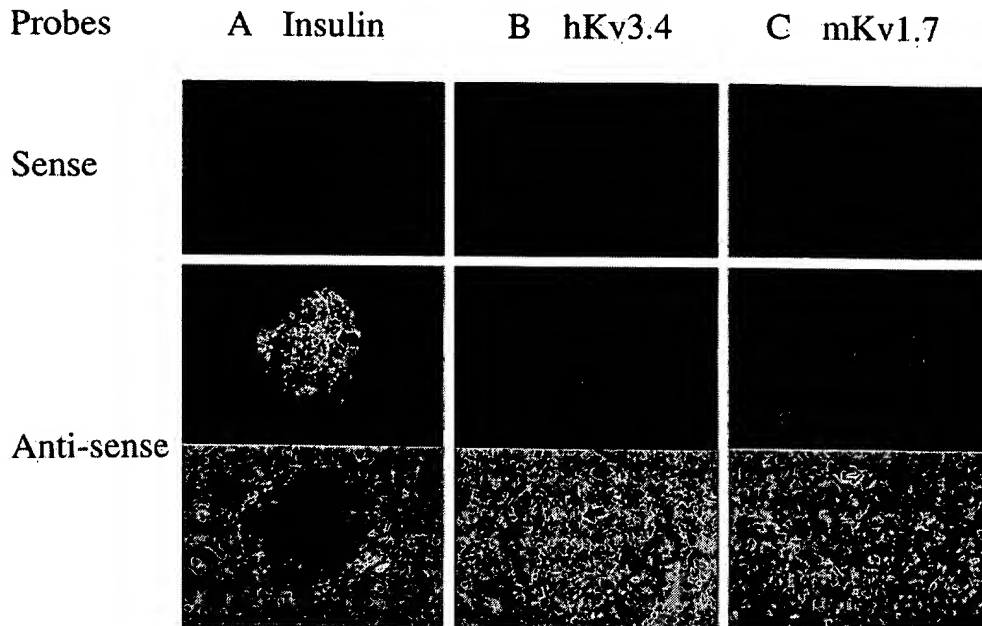
Fig. 7. *In situ* hybridization of mouse pancreas from diabetic *db/db* mice showing expression of *Kv1.7*, *Kv3.4*, and *insulin*. *A-C*, pancreatic sections from a *db/db* mouse hybridized with probes specific for insulin (*A*), Kv3.4 (*B*), or Kv1.7 (*C*). *Top*, sense probe, dark field; *middle*, antisense probe, dark field; *bottom*, antisense probe, bright field, showing the same field as the middle row. *Filled arrow*, pancreatic islet; *open arrow*, acinar cells that hybridized with *Kv1.7* antisense probe. *A*, sense and antisense probes, 0.1 ng/ml, 10 days of exposure; *B*, sense probe, 0.1 ng/μl, 10 days of exposure, and antisense probe, 0.5 ng/μl, 7 days of exposure; *C*, sense and antisense probes, 0.5 ng/μl, 1 month of exposure. Magnification: *A* and *B*, × 425; *C*, × 312.

ethylammonium (34–36) (this study). In contrast, the I_{to} current in atrial and ventricular muscle, a product of the *Kv4.3* gene, does not exhibit cumulative inactivation (36). These studies suggest that at least part of the Purkinje fiber I_{to} might be encoded by the *Kv1.7* gene, although more extensive biophysical and pharmacological studies are required to confirm the link, and the presence of *Kv1.7* mRNA and/or protein has yet to be demonstrated in these fibers. The abundant expression of *Kv1.7* mRNA in mouse heart suggests that this channel is also likely to be present in ventricular and/or atrial muscle where it may co-assemble with other Kv1 family channels to form heterotetramers.

Recent studies suggest an important role for Kv channels in regulating islet cell function, specifically in repolarizing the membrane potential following each action potential during the glucose-induced bursting phase associated with insulin secretion (3–6). Despite these interesting findings, the genes encoding Kv genes in β-cells have not been identified. Although the *Kv1.5* gene was isolated from human insulinoma cells (33), we did not detect *Kv1.5* mRNA in normal or diseased islets. We have, however, demonstrated the presence of *Kv1.7* mRNA in these cells. Unlike the noninactivating Kv channels in pancreatic β-cells (3, 4), the Kv1.7 homotetramer exhibits rapid C-type inactivation. Since *Kv1.7* mRNA is expressed in pancreatic islets, it is possible that heteromultimers composed of Kv1.7 and other Kv1 subunits constitute the native Kv channels in β-cells. Enhanced levels of such Kv channels would excessively hyperpolarize the membrane of β-cells and impair insulin secretion (5). The mapping of the *Kv1.7* gene to human chromosome 19q13.3, a region thought to contain a diabetic susceptibility gene (26, 27), also suggests that *Kv1.7* might contribute to the pathogenesis of type II diabetes mellitus in some humans.

In conclusion, we have described a novel *Kv1* family gene with a genomic organization distinct from all the other members of the family. The Kv1.7 channel produces a typical A-type

current, and transcripts are expressed in the heart, skeletal muscle, brain, placenta, and pancreatic β-cells. This channel is biophysically and pharmacologically similar to the Purkinje fiber I_{to} current, and the gene may contribute at least one subunit to heteromultimeric Kv channels in pancreatic β-cells.

REFERENCES

1. Hille, B. (1993) *Ionic Channels of Excitable Membranes*, 2nd Ed., Sinauer, Sunderland, MA
2. Chandy, K. G., and Gutman, G. A. (1995) in *Handbook of Receptors and Channels: Ligand and Voltage-gated Ion Channels* (North, A., ed) pp. 1–72, CRC Press, Boca Raton, FL
3. Smith, P. A., Bokvist, K., Arkhammar, P., Berggren, P. O., and Rorsman, P. (1990) *J. Gen. Physiol.* 95, 1041–1059
4. Smith, P. A., Ashcroft, F. M., and Rorsman, P. (1990) *FEBS Lett.* 261, 187–190
5. Philipson, L. H., Rosenberg, M., Kuznetsov, A., Lancaster, M. E., Worley, J. F., III, Roe, M. W., and Dukes I. D. (1994) *J. Biol. Chem.* 269, 27787–27790
6. Roe, M. W., Worley, J. F., 3rd, Mittal, A. A., Kuznetsov, A., DasGupta, S., Mertz, R. J., Witherspoon, S. M., 3rd, Blair, N., Lancaster, M. E., McIntyre, M. S., Shehee W. R., Dukes, I. D., and Philipson, L. H. (1996) *J. Biol. Chem.* 271, 32241–32246
7. Lewis, R. S., and Cahalan, M. D. (1995) *Annu. Rev. Immunol.* 13, 623–653
8. Pongs, O., Kecskemethy, N., Muller, R., Krah-Jentgens, I., Baumann, A., Kiltz, H. H., Canal, I., Llamazares, S., and Ferrsu, A. (1988) *EMBO J.* 7, 1087–1096
9. Schwarz, T. L., Papazian, D. M., Caretto, R. C., Jan, Y. N., and Jan, L. Y. (1988) *Nature* 331, 137–142
10. Chandy, K. G., Williams, C. B., Spencer, R. H., Aguilar, B. A., Ghanshani, S., Tempel, B. L., and Gutman, G. A. (1990) *Science* 247, 973–975
11. Ghanshani, S., Pak, M., McPherson, J. D., Strong, M., Dethlefs, B., Wasmuth, J. J., Salkoff, L., Gutman, G. A., and Chandy, K. G. (1992) *Genomics* 12, 190–196
12. deJong, P. J., Yokabata, K., Chen, C., Lohman, F., Pederson, L., McNinch, J., and van Dilla, M. (1990) *Cytogenet. Cell Genet.* 51, 985
13. Permutt, M. A., Koranyi, L., Keller, K., Lacy, P. E., Scharp, D. W., and Mueckler, M. (1989) *Proc. Natl. Acad. Sci. U. S. A.* 86, 8688–8692
14. Chen, H., Charlat, O., Tartaglia, L. A., Woolf, E. A., Weng, X., Ellis, S. J., Lakey, N. D., Culpepper, J., Moore, K. J., Breitbart, R. E., Duyk, G. M., Tepper, R., and Morgenstern, J. P. (1996) *Cell* 84, 491–495
15. Lee, G. H., Proenca, R., Montez, J. M., Carroll, K. M., Darvishzadeh, J. G., Lee, J. I., and Friedman, J. M. (1996) *Nature* 379, 632–635
16. Shafrir, E. (1992) *Diabetes Metab. Rev.* 8, 179–208

17. Green, E. L. (1981) in *Genetics and Probability in Animal Breeding Experiments*, pp 77–113, Oxford University Press, New York

18. Jenkins, N. A., Copeland, N. G., Taylor, B. A., and Lee, B. K. (1982) *J. Virol.* **43**, 26–36

19. Saunders, A. M., and Seldin, M. F. (1990) *Genomics* **8**, 525–535

20. Copeland, N. G., and Jenkins, N. A. (1991) *Trends Genet.* **7**, 113–118

21. Brandriff, B. F., Gordon, L. A., Tynan, K. T., Olsen, A. S., Mohrenweiser, H. W., Fertitta, A., Carrano, A. V., and Trask, B. J. (1992) *Genomics* **12**, 773–779

22. Trask, B., Fertitta, A., Christensen, M., Youngblom, J., Bergmann, A., Copeland, A., de Jong, P., Mohrenweiser, H., Olsen, A., Carrano, A., and Tynan, K. (1993) *Genomics* **15**, 133–145

23. Ikeda, S. R., Soler, F., Zuhlke, R. D., Lewis, D. L. (1992) *Pflueg. Arch. Eur. J. Physiol.* **422**, 201–203

24. Betsholtz, C., Baumann, A., Kenna, S., Ashcroft, F. M., Ashcroft, S. J., Berggren, P. O., Grupe, A., Pongs, O., Rorsman, P., Sandblom, J., and Welsh, M. (1990) *FEBS Lett.* **263**, 121–126

25. Swofford, D. L. (1993) PAUP: Phylogenetic analysis using parsimony. Version 3.1. Computer program distributed by the Illinois Natural History Survey, Champaign, IL

26. Groop, L. C., Kankuri, M., Schalin-Jantti, C., Ekstrand, A., Nikula-Ijas, P., Widen, E., Kuismanen, E., Eriksson, J., Franssila-Kallunki, A., Saloranta, C., and Koskimies, S. (1993) *N. Engl. J. Med.* **328**, 10–14

27. Elbein, S. C., Hoffman, M., Ridinger, D., Otterud, B., and Leppert, M. (1994) *Diabetes* **43**, 1061–1065

28. Estivill, X. (1996) *Nat. Genet.* **12**, 348–350

29. McCloskey, M., and Cahalan, M. D. (1990) *J. Gen. Physiol.* **95**, 208–222

30. Nguyen, QA, Kath, J., Hanson, D. C., Biggers, M. S., Canniff, P. C., Donovan, C. B., Mather, R. J., Bruns, M. J., Rauer, H., Aiyar, J., Lepple-Wienhues, A., Gutman, G. A., Grissmer, S., Cahalan, M. D., and Chandy, K. G. *Mol. Pharmacol.* **50**, 1672–1679, 1996

31. Wymore, R., Korenberg, J. R., Coyne, C. Chen, X-N, Hustad, C., Copeland, N. G., Gutman, G. A., Jenkins, N. A., Chandy, K. G. (1994) *Genomics* **20**, 191–202

32. Grissmer, S., Nguyen, A. N., Aiyar, J., Hanson, D. C., Mather, R. J., Gutman, G. A., Karmilowicz, M. J., Auperin, D. D., and Chandy, K. G. (1994) *Mol. Pharmacol.* **45**, 1227–1234

33. Philipson, L. H., Hice, R. E., Schaefer, K., LaMendola, J., Bell, G. I., Nelson, D. J., and Steiner, D. F. (1991) *Proc. Natl. Acad. Sci. U. S. A.* **88**, 53–57

34. Reder, R. F., Miura, D. S., Danilo, P., Jr., and Rosen, M. R. (1981) *Circ. Res.* **48**, 658–668

35. Gintant, G. A., Cohen, I. S., Datyner, N. B., and Kline, R. P. (1992) in *The Heart and Cardiovascular System* (Fozzard, H., ed) 2nd Ed., pp. 1122–1166, Raven Press, New York

36. Dixon, J. E., Shi, W., Wang, H. S., McDonald, C., Yu, H., Wymore, R. S., Cohen, I. S., and McKinnon, D. (1996) *Circ. Res.* **79**, 659–668

37. Ashworth, L. K., Batzer, M. A., Brandriff, B., Branscomb, E., de Jong, P., Garcia, E., Garnes, J. A., Gordon, L. A., Lamerdin, J. E., Lennon G., Mohrenweiser, H., Olsen, A. S., Slezak, T., and Carrano, A. V. (1995) *Nat. Genet.* **11**, 422–427

REVIEW ARTICLE

Molecular targets for autoimmune and genetic disorders of neuromuscular transmission

Angela Vincent, David Beeson and Bethan Lang

Institute of Molecular Medicine, John Radcliffe Hospital, Oxford, UK

The neuromuscular junction is the target of a variety of autoimmune, neurotoxic and genetic disorders, most of which result in muscle weakness. Most of the diseases, and many neurotoxins, target the ion channels that are essential for neuromuscular transmission. Myasthenia gravis is an acquired autoimmune disease caused in the majority of patients by antibodies to the acetylcholine receptor, a ligand-gated ion channel. The antibodies lead to loss of acetylcholine receptor, reduced efficiency of neuromuscular transmission and muscle weakness and fatigue. Placental transfer of these antibodies in women with myasthenia can cause fetal or neonatal weakness and occasionally severe deformities. Lambert Eaton myasthenic syndrome and acquired neuromyotonia are caused by antibodies to voltage-gated calcium or potassium channels, respectively. In the rare acquired neuromyotonia, reduced repolarization of the nerve terminal leads to spontaneous and repetitive muscle activity. In each of these disorders, the antibodies are detected by immunoprecipitation of the relevant ion channel labelled with radioactive neurotoxins. Genetic disorders of neuromuscular transmission are due mainly to mutations in the genes for the acetylcholine receptor. These conditions show recessive or dominant inheritance and result in either loss of receptors or altered kinetics of acetylcholine receptor channel properties. Study of these conditions has greatly increased our understanding of synaptic function and of disease aetiology.

Keywords: acetylcholine receptor; autoimmune; genetic; voltage-gated calcium channel; voltage-gated potassium channel.

NEUROMUSCULAR TRANSMISSION AND THE NEUROMUSCULAR JUNCTION

Neuromuscular transmission has long been considered to be a good model for synaptic transmission in general. The main features are illustrated schematically in Fig. 1. The nerve action potential, which is dependent on voltage-gated sodium channels, invades the motor nerve terminal leading to opening of voltage-gated calcium channels (VGCC) that are present on the presynaptic membrane. There is a very transient and localized increase in intracellular calcium which results in the exocytosis of packets (or quanta) of acetylcholine (ACh). ACh diffuses rapidly across the synaptic space and binds to the acetylcholine receptors (AChR) on the postsynaptic membrane. This results in opening of the AChR-channel, and an influx of sodium and other cations leading to depolarization of the motor endplate. This depolarization is called the endplate potential (EPP) and

Correspondence to A. Vincent, Neurosciences Group, Institute of
Molecular Medicine, John Radcliffe Hospital, Oxford OX3 9DS, UK.
Fax: + 44 1865 222402, Tel.: + 44 1865 222321,
E-mail: angela.vincent@imm.ox.ac.uk
Abbreviations: ACh, acetylcholine; AChE, acetylcholinesterase; AChR, acetylcholine receptor; AMC, arthrogryposis multiplex congenita; AZ, active zone; AZP, active zone particle; CMS, congenital myasthenic syndrome; CNS, central nervous system; EPP, endplate potential; MEPP, miniature endplate potential; MG, myasthenia gravis; MIR, main immunogenic region; LEMS, Lambert Eaton myasthenic syndrome; SCLC, small cell lung cancer; VGCC, voltage-gated calcium channel; VGKC, voltage gated potassium channel; VICE, very immunogenic cytoplasmic epitope.

can be measured using a microelectrode inserted into the muscle. As soon as the EPP exceeds a certain 'threshold', it opens the voltage-gated sodium channels that are located at the bottom of the synaptic folds. Opening these channels produces a regenerative action potential in the muscle membrane that propagates along the entire muscle surface and leads to activation of the contractile mechanism. Meanwhile voltage-gated potassium channels (VGKCs) in the motor nerve terminal open to restore the membrane potential to resting levels, and the Na^+/K^+ ATPase restores the chemical gradients. In the absence of motor nerve impulses, individual quanta of ACh are released spontaneously, and the resulting depolarization, the miniature EPP (MEPP), can also be measured by an intracellular electrode. The ratio between the EPP and MEPP amplitudes at an individual neuromuscular junction, after correction for nonlinear summation, is a measure of the number of quanta of ACh released per nerve impulse.

Only ≈ 50% of the ACh reaches the postsynaptic AChRs, the rest is destroyed by the enzyme acetylcholine esterase (AChE) that is anchored by a collagen tail, Col Q, in the basal lamina between the nerve terminal and the muscle surface. When ACh dissociates from the AChRs, it is rapidly destroyed by AChE, ensuring that, under normal conditions, each nerve action potential produces only one muscle action potential [1,2].

Structure of the neuromuscular junction

An understanding of the disorders that affect neuromuscular transmission, requires some further appreciation of the detailed structure of the neuromuscular junction [3]. In mammals, the neuromuscular junction, usually identified by staining for AChE,
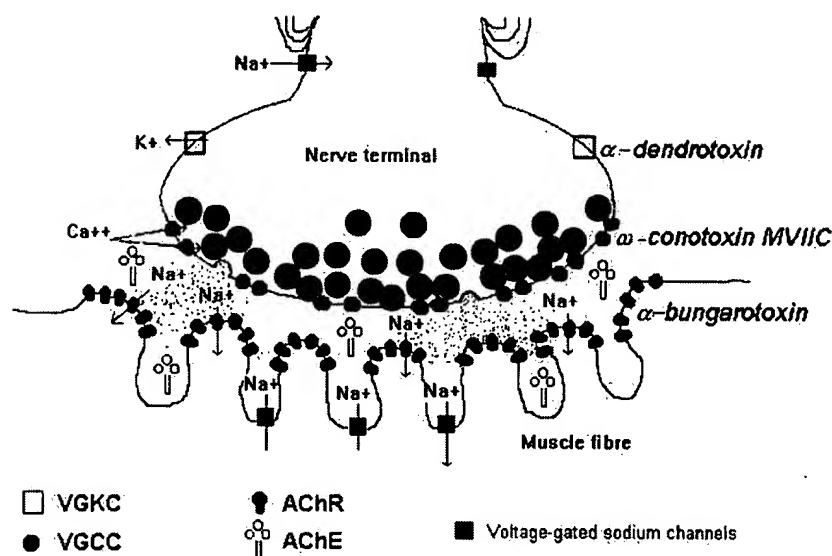
Fig. 1. The neuromuscular junction and its ion channels. A schematic representation of a nerve terminal bouton at the neuromuscular junction. Some of the main functional proteins involved in autoimmune and genetic disorders are represented. Neurotoxins that can be used to label the ion channels are indicated on the right. The transmitter, acetylcholine, is released from synaptic vesicles in the nerve terminal.

is oval in shape and ≈ 30–50 μm in its largest dimension which runs parallel to the length of the fibre. It consists of several discrete areas of contact between nerve and muscle, one of which is represented schematically in Fig. 1. The presynaptic nerve terminal contains mitochondria that provide energy for the synthesis and release of ACh and large numbers of small synaptic vesicles each thought to contain one quanta of ACh. These vesicles are particularly concentrated on the presynaptic face of the nerve terminal, directly opposite the postsynaptic junction folds, at areas of cytoplasmic densities called active zones (AZ). Using freeze–fracture electron microscopy, the AZs are seen to consist of ordered arrays of double parallel lines of active zone particles (AZPs). These particles are 10–12 nm in diameter, with a constant interparticle distance and are thought to be the morphological representation of the VGCCs. VGCCs are closely associated with several other proteins that are essential for the calcium-induced exocytosis of the neurotransmitter, such as syntaxin and neurexins [3].

The basal lamina between the nerve and the postsynaptic membrane, and within the postsynaptic folds, contains several synapse-specific proteins. AChE is tethered to the basal lamina at the neuromuscular junction by a covalent interaction with its collagen tail, Col Q, and follows the distribution of the basal lamina into the postsynaptic folds. The laminins are a family of collagen-like proteins that are important for cell–cell interactions. β2 laminin contributes to a protein, S-laminin, that is synapse specific and also anchored at the neuromuscular junction. Agrin and ARIA are proteins released by the motor nerve that bind to the basal lamina at the neuromuscular junction enabling them to interact with their postsynaptic receptors to regulate gene expression [3–5].

The AChRs are densely packed in the postsynaptic membrane at the tops of the folds, whereas voltage-gated sodium channels are located in the lower two-thirds of the postsynaptic folds [6]. At the tops of the folds, colocalizing with the AChRs, are several neuromuscular junction-specific cytoskeletal proteins. In particular, RAPsyn, a cytoplasmic protein of ≈ 400 amino acids is essential for the localization of AChRs and many other neuromuscular junction-specific proteins [7,8]. Utrophin shows extensive homology to dystrophin, which is found throughout the sarcoplasmic membrane, but is highly concentrated at the neuromuscular junction with a similar distribution

to the AChRs and RAPsyn [8]. α-Dystrobrevin 1 also colocalizes with AChRs, and utrophin is thought to link the AChR/α-dystrobrevin complex to actin filaments. Below the postsynaptic folds, within the cytoplasm of the myofibril, are several nuclei which, in contrast to those present extrasynaptically, are responsible for producing the proteins that are involved in postsynaptic structure and function [3,5].

Action of neurotoxins

As will become clear during this review, neurotoxins have been essential tools for dissecting the roles of different ion channels in neuromuscular transmission, labelling them for studies of their numbers and distribution, providing affinity labels for purification, and measuring autoantibodies directed against them. The different ion channels, their associated diseases and the neurotoxins used in their study are summarized in Table 1. Neurotoxins in general are reviewed by Harvey [9].

Immunological and molecular structure of the AChR

The most clinically important disorder that affects neuromuscular transmission is myasthenia gravis (MG) in which there is a reduction in the number or function of the AChR. Details of the structure and functional molecular anatomy of AChRs have been covered in many reviews [13–15] and only the relevant features are discussed here. The AChR is an oligomeric membrane protein which consists of five subunits arranged in a pseudosymmetrical fashion around a central ion channel. The two alpha subunits are separated by a gamma subunit in the fetal isoform and an epsilon subunit in the adult isoform. The binding sites for ACh appear to be formed at the interface between the alpha/gamma or alpha/epsilon and alpha/delta subunits [13]. A simple schematic is shown in Fig. 2.

Each AChR subunit is formed from a large extracellular domain of ≈ 210 amino acids, four transmembrane domains and a large cytoplasmic loop between transmembrane domains 3 and 4. Although much is now known about the transmembrane domains and the three-dimensional structure of the AChR, from many studies including the work of Unwin and his collaborators [15], little is known about how the extracellular sequences fold to make up the three-dimensional structure,

Table 1. Ion channels, diseases and neurotoxins at the neuromuscular junction.

Ion channel target	Tissue distribution of ion channel	Autoimmune disease association with ion channel	Genetic disease association with ion channel	Toxins active at the neuromuscular junction	Physiological effect of toxins	Reference
Acetylcholine receptor	Neuromuscular junction	Myasthenia gravis	Congenital myasthenic syndromes	α-Bungarotoxin and other α-Neurotoxins	Block neuromuscular transmission	[10]
Voltage-gated calcium channels (see Table 3 for details)	Many presynaptic nerve terminals in peripheral and central nervous systems	Lambert–Eaton myasthenic syndrome	Familial hemiplegic migraine Episodic ataxia II Subacute cerebellar ataxia type 6	ω-Conotoxins[a]	Block neuromuscular transmission	[11]
Voltage-gated potassium channels	Throughout the nervous system	Acquired neuromyotonia	Episodic ataxia and myotonia	Dendrotoxins and some scorpion toxins	Increase acetylcholine release; repetitive and spontaneous muscle activity	[12]

a Further details are given in Table 3.

apart from the presence of a disulfide bond between amino acids 128 and 142. However, one can make some predictions based on the sequences that are known to be involved in binding different toxins or antibodies. One sequence of the alpha subunit (amino acids 186–193) provides a substantial contribution to the binding affinity for α-bungarotoxin in most species studied [13], although in human AChR, this sequence does not bind α-bungarotoxin strongly and other interactions must contribute to the overall equally high affinity [16]. The glycosylation sites, one of which is conserved at alpha 141 on each subunit, must be exposed on the surface, and any site which binds autoantibodies must also be exposed. Unfortunately, the only site which has been consistently demonstrated to bind antibodies is amino acids 64–76 on the alpha subunit. This is the so called 'main immunogenic region' (MIR) which is the target for a high proportion of antibodies to AChR [17,18].

The fine structure of the cytoplasmic domains of each of the AChR subunits is also unclear. However, most of the subunits contain phosphorylation sites which must be available for serine, threonine and tyrosine phosphorylation in situ. Moreover, antibodies that are induced by immunization with either denatured AChR subunit, or by immunization against cyto-plasmic peptides, tend to bind well to the extracted native protein, or to tissue sections containing the native AChR, indicating that these cytoplasmic epitopes are easily accessible [19–21]. These antibodies target a region within the cyto-plasmic domain called the very immunogenic cytoplasmic epitope (VICE) which is not restricted conformationally because it is present in the native molecule and not destroyed by denaturation. It is surprising therefore that when animals are immunized against native solubilized AChR that has been carefully protected from degradation and denaturation during purification, antibodies are predominantly formed against the extracellular domain rather than the cytoplasmic domain [18].

DISORDERS OF NEUROMUSCULAR TRANSMISSION

Diseases that affect neuromuscular transmission typically cause weakness of voluntary muscle function that is described as myasthenic (my, muscle; aesthenia, weakness). For reasons that are not fully understood, myasthenic symptoms are frequently more pronounced in the ocular, facial and bulbar (swallowing and speech) muscles with relative sparing of trunk and limbs. However, proximal limb weakness can be a problem, and in severe cases weakness of respiratory muscles, including the diaphragm, can result in life-threatening respiratory insuffi-ciency. In most of the conditions discussed, the weakness can be improved transiently by use of short-acting AChE inhibitors, and longer acting inhibitors can give symptomatic relief. However, in some rare genetic myasthenic disorders, AChE inhibitors make the condition worse or have no effect (see slow channel syndrome and AChE deficiency). In addition to the myasthenic syndromes, there are conditions such as neuromyo-tonia in which spontaneous neuromuscular transmission leads to hyperactivity of the muscles with cramps and fasiculations. These disorders are reviewed by Newsom-Davis [22].

Neuromuscular transmission disorders can be due to toxins, genetic defects, or circulating autoantibodies that the patient acquires during life. Neurotoxins can target functional mole-cules of either the presynaptic or postsynaptic membrane gener-ally leading to muscle paralysis, and are a substantial cause of health problems in those countries in which venomous animals
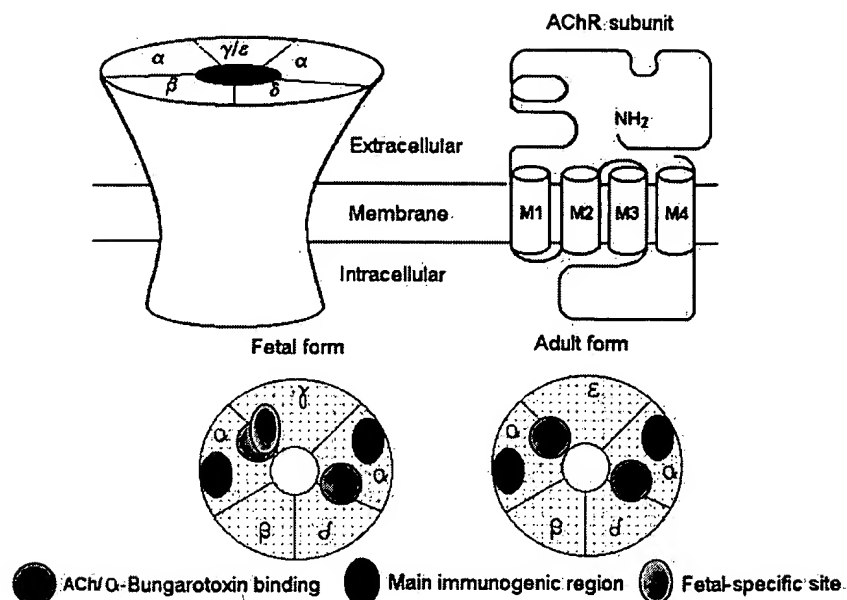
Fig. 2. The acetylcholine receptor. The AChR is an oligomer made up of five subunits. Each subunit is thought to contain a large extracellular domain, four transmembrane sequences (M1–M4) and a cytoplasmic loop. The adult and fetal isoforms differ by the substitution of the γ by the ε subunit. ACh and α-bungarotoxin bind to a site on the α subunits which lies at the interface between the α subunits and the adjacent γ/ε or δ subunits. Most of the antibodies in animals immunized against purified, native AChR bind to the main immunogenic regions on the α subunits. Mothers with high levels of antibodies to the fetal-specific site have babies born with severe joint contractures resulting from fetal paralysis.

are indigenous [23]. However, in nontropical countries the majority of patients with a defect in neuromuscular transmission have an autoantibody-mediated disease. A much smaller number have genetic defects in neuromuscular transmission, although these are relatively more frequent in countries where consanguinity is common. This review covers the genetic and antibody-mediated disorders only, but, as will become clear, their investigation has been greatly helped by the use of the many neurotoxins that target the neuromuscular junction (Table 1).

Myasthenia gravis

Myasthenia gravis (MG) is an acquired disease that can be present during adolescence or in young adults, but is also increasingly recognized in individuals first complaining of weakness over the age of 60 years. The weakness is improved by rest and by AChE inhibitors. The understanding of MG that has developed over the last 20 years is a classic convergence of basic science, serendipity and clinical application [24]. In the 1960s, Elmqvist and colleagues examined neuromuscular transmission in muscle biopsies from MG patients and showed that the MEPP amplitudes were extremely small [25]. This suggested that there was a reduction in ACh release or in AChR number, but at the time it was still unclear as to whether the AChR was a protein molecule. This problem was solved when Lee [10] demonstrated that α-bungarotoxin, purified from the venom of *Bungarus multicinctus*, the banded krait, blocked neuromuscular transmission, and that labelled ^{125}I-α-bungarotoxin bound very specifically to the neuromuscular junction of normal muscles. The binding of ^{125}I-α-bungarotoxin was prevented by ACh and curare, strongly suggesting that it bound to the AChRs. α-Bungarotoxin was then used to identify solubilized AChRs from electric organs of certain rays or from muscle leading to the purification [26], sequencing [27], cloning [28] and further study of AChR [13–15]. As regards the human diseases, the story developed in two ways. First, Fambrough *et al.* [29] found a marked reduction in the number of ^{125}I-α-bungarotoxin binding sites in muscle biopsies from

MG patients and secondly, Patrick & Lindstrom [26] induced a MG-like illness in rabbits by immunizing against AChRs that they had purified by affinity chromatography using neurotoxin–Sepharose columns. Impressively, as in human MG, the rabbits' symptoms improved with AChE inhibitors.

These observations suggested that MG might be caused by antibodies to AChR, confirming a hypothesis first proposed by Simpson in 1960 [30]. The presence of antibodies to the AChR in MG was confirmed by demonstrating that MG serum could bind to ^{125}I-α-bungarotoxin labelled AChRs solubilized in detergent from human muscle [31]. To prove that the antibodies were pathogenic, rather than secondary to tissue damage, several approaches were used. First, plasma exchange which removes circulating factors replacing them with a substitute solution, produced striking clinical benefit in MG [32]. Although the improvement was not permanent, the clinical benefit correlated with the reduction in serum anti-AChR antibodies over time. Secondly, the plasma or IgG purified from it, was able to transfer features of MG to mice [33]. Not all the mice became weak, but all showed reduction in MEPP amplitudes and reduced numbers of AChRs. Finally, human IgG, was detected at the neuromuscular junctions of MG muscles [34]. Together with the demonstration that immunization against AChRs consistently induced evidence of MG in experimental animals [26,35], these observations have established paradigms for the investigation of antibody-mediated disorders and are summarized in Table 2.

Table 2. Paradigms for establishing an antibody-mediated disorder

Loss of function associated with a specific membrane protein
Presence of an antibody against the specific membrane protein
Reduction in antibody levels by plasma exchange or immunosuppressive drugs leads to clinical improvement
IgG antibodies bound to the target molecule *in situ*
Injection of patient's IgG antibodies into mice leads to similar clinical syndrome (passive transfer)

Binding sites for antibodies in MG

Antibodies to the AChR in MG appear to be very similar to those induced in experimental animals immunized with purified, native, AChR [18,36]. Thus they bind to the extracellular domains of the AChR, mainly to the alpha subunits, and do not bind to the cytoplasmic domains including the VICE (Fig. 2). The extent to which they do or do not bind to the MIR (Fig. 2) is not so clear. Many MG antibodies compete with mAbs that are directed against the MIR [18,37], but many do not. In addition, some MG antibodies compete with mAbs that are now known to bind to the beta, gamma or delta [37,38]. Thus, although the majority of antibodies in many patients do seem to bind predominantly to the immunodominant alpha subunits, there is still considerable heterogeneity in antibodies and in their binding sites. This is also illustrated by the mechanisms by which these antibodies lead to AChR loss.

Antibody-mediated AChR loss

Antibodies to the AChR lead to loss of AChR from the neuromuscular junctions of MG patients. There are three mechanisms involved. Antibodies are divalent molecules and can cross-link AChRs in the muscle membrane or on the surface of cell lines in culture. Cross-linking results in an increase in the normal degradation rate leading to an overall loss of AChRs. In cultures the normal turnover has a half-life of ≈ 10–16 h and this may be decreased to ≈ 6 h by incubation in the presence of MG serum or IgG [39]. At the mature neuromuscular junction, in mice injected with IgG, the half-life is decreased from ≈ 10 days to ≈ 4 days [40]. This increase in turnover would lead to a loss of steady-state AChR to ≈ 60% normal values. This is not sufficient to explain the 80% loss of AChR in MG. Moreover, an increase in AChR synthesis has been shown both in culture, at the neuromuscular junction of mice injected with IgG [41], and in MG muscle biopsies [42]. A more important cause of AChR loss is probably complement-mediated lysis of the postsynaptic membrane. Complement components C3 and C9 and the membrane attack complex, which leads to cell lysis, have been identified in MG muscles [34], and their distribution colocalizes with AChRs and IgG. Moreover, strong membrane attack complex labelling was found at neuromuscular junctions that had very little remaining AChRs, implying that this mechanism can lead to substantial AChR loss [43]. In addition, recent evidence suggests that the loss of postsynaptic folds that follows complement-mediated lysis, probably contributes to the defect in neuromuscular transmission by reducing the number of sodium channels that initiate the action potential in the muscle [44].

Most antibodies in MG do not directly inhibit AChR function although in a few patients this mechanism may be important. An interesting and potentially important example of inhibitory antibodies are those that occur in mothers of babies with a rare, antibody-mediated, form of arthrogryposis multiplex congenita (AMC).

MG and pregnancy

A proportion of women with MG have babies who develop neonatal MG. Transient weakness occurs during the first days or weeks after birth, the condition responds to AChE inhibitors, and, if recognized, does not present major problems. It is not clear why only some babies develop neonatal MG, but the ability of the mother's serum antibodies to bind to the fetal isoform of the AChR may be a contributory factor [45].

AMC is a condition defined by multiple joint contractures occurring at birth or detected *in utero*. It can include other abnormalities such as lung hypoplasia and malformation of the facial bones. All of these defects are probably the result of lack of fetal movement and can be secondary to a wide variety of primary causes which include genetic disorders of the fetus, maternal uterine deformities, multiple pregnancies and maternal disease. An important indicator of the form caused by maternal antibodies is that every pregnancy is affected, clearly distinguishing this form from those caused by genetic disorders [46]. However, the mother herself is often mildly affected or may even show no symptoms of MG. The explanation lies in the two forms of AChR [47] (Fig. 2). In the mothers of AMC babies there are very high titres of antibodies that directly inhibit the function of the fetal form of AChR and, in all cases studied to date, have no effect on function of the adult isoform [46,48]. Thus these antibodies can cross the placenta and directly inhibit fetal AChR function from around 16 weeks gestation when IgG antibodies cross the placenta from the maternal circulation. At this stage, the neuromuscular junctions are formed but if the babies stop moving they develop fixed joint contractures. The condition is often fatal because of the lack of development of the lungs [49]. These observations suggest that other developmental abnormalities or neurodevelopmental conditions might also be caused by antibodies specific for fetal proteins. A mouse model has been developed which reproduces some of the changes of arthrogryposis in mice by injecting pregnant dams with serum from mothers of affected human babies [50].

Seronegative MG

Anti-AChR antibodies are present in > 80% of MG patients, but there are some who remain persistently negative by the immunoprecipitation assay that is used worldwide [51]. These patients clearly have an autoimmune disease (Table 2) because they respond to plasma exchange and immunosuppression and their plasma can transfer defects in neuromuscular transmission to mice [51]. Three pieces of evidence demonstrate that seronegative MG patients probably have antibodies that bind to another distinct muscle membrane target, closely associated with the AChRs at the neuromuscular junction. First, their sera inhibit AChR function in an acute, but transient, manner [52] and this inhibition is very similar to that found with addition of calcitonin gene related peptide and adrenergic agonists that act through G protein-coupled receptors [52,53] and lead to AChR desensitization [54]. This indicates that the antibodies can activate second messengers leading to AChR phosphorylation; phosphorylation of AChRs has been demonstrated in preliminary studies (P. Plested, T. Tang & A. Vincent, unpublished results). Secondly, IgG antibodies from seronegative MG patients bind to the surface of the fetal-muscle-like cell line, TE671, that expresses human fetal AChRs, but do not bind to the surface of HEK cells expressing human AChR [55]. Thirdly, seronegative MG IgG preparations up regulate AChR subunit genes but do not have any effect on surface AChR expression in TE671 cells [56]. Recent evidence suggests that the IgG antibodies bind specifically to MuSK (W. Hoch, J. McConville & A. Vincent, unpublished results), one of the muscle specific receptor tyrosine kinases present at the neuromuscular junction and involved in synaptic development [4,5].

Table 3. Subtypes of voltage-gated calcium channels and their associated neurotoxins [64]. DHP, dihydropyridines.

Subtype	Localization	Neurotoxin or other ligand specificity	α_1 subunit gene
L	Muscle (striated, cardiac, smooth)	DHP	α_{1C}
	Endocrine tissue		α_{1D}
			α_{1S}
N	Central nervous system	ω-conotoxin GVIA	α_{1B}
	Autonomic nervous system	ω-conotoxin MVIIC	
	Neuromuscular junction under some circumstances?		
P	Central nervous system	ω-agatoxin IVA	α_{1A}
	Neuromuscular junction	ω-conotoxin MVIIC	
	Autonomic nervous system		
Q	Central nervous system e.g. granular layer cells of the cerebellum	ω-agatoxin IVA	α_{1A}
		ω-conotoxin MVIIC	

LAMBERT EATON MYASTHENIC SYNDROME

Lambert Eaton myasthenic syndrome (LEMS) is a condition characterized by muscle weakness and fatigue but exhibiting some subtle differences from MG. Typically the weakness involves trunk and proximal limb muscles more commonly than in MG, and the bulbar or ocular muscles less frequently. Weakness is most pronounced on the initial contraction and improves briefly during repetitive activity or after sustained voluntary contraction. Approximately 60% of LEMS patients have an underlying tumour, a small cell lung carcinoma (SCLC), with the neurological symptoms preceding the detection of the tumour often by several months and in some cases years [57]. This interesting, and clinically important, association of LEMS with SCLC makes it one of a group of 'paraneoplastic' disorders that arise as a remote effect of cancer. In these conditions, the body mounts an immune response towards antigens expressed by the tumour which also happen to be present in neuronal tissue; the neurological disorder then occurs as a result of the immune response targeting the patients' neuronal antigens.

Muscle biopsies from LEMS patients show normal MEPP amplitudes [58] but a marked reduction in the EPP amplitudes indicating a reduction in the 'quantal content', i.e. the number of packets of ACh released. The physiological findings are very similar to those observed in the presence of raised Mg^{2+} levels, and can be overcome *in vitro* by raising extracellular calcium [59]. During repetitive stimulation, the intracellular calcium concentration accumulates, and any defect in calcium-evoked quantal release will be partially overcome, explaining the transient improvement that occurs after voluntary contraction. A major finding was a disturbance in the AZs observed in freeze–fracture preparations. The number of parallel arrays was reduced, and many were disrupted resulting in small aggregations of AZPs. Overall the number of AZPs was reduced [60].

LEMS fulfils the criteria for an antibody-mediated disease. Patients improve after plasma exchange and injection of LEMS IgG into experimental animals produced electrophysiological abnormalities similar to those found in the patients [61,62]. Moreover, the changes in AZPs found in patients, were reproduced in mice within 24 h of injection of LEMS IgG, but not if monovalent single Fabs were injected [62,63]. This strongly suggested that the main action of the LEMS IgGs were to cross-link the AZPs leading to their internalization. In contrast to the antibodies to AChRs in MG, complement-dependent mechanisms or direct block of function do not appear to be important. This apart, the analogies with MG implied that the patients had an autoimmune disease, caused by autoantibodies directed against the VGCCs present on the motor nerve terminal, but it was some time before it was possible to confirm this hypothesis by direct measurement of the antibodies.

VGCC subtypes

According to pharmacological and electrophysiological criteria there are at least six types of VGCC defined as T, L, N, P, Q and R. P-type and Q-type VGCCs were first identified on Purkinje cells and granular layer cells of the cerebellum, respectively [64] and have subtly different electrophysiological and pharmacological profiles with respect to their sensitivity to the spider toxin ω-agatoxin and cone snail toxin ω-conotoxin MVIIC (Table 3). P-type channels are more sensitive to ω-agatoxin than Q-type VGCCs, whereas ω-conotoxin MVIIC shows less selectivity between the two subtypes. Because of the difficulties in distinguishing them pharmacologically, the term P/Q-type VGCC is often used. The main VGCC involved in calcium-induced ACh release at the mammalian neuromuscular junction appears to be the P-type VGCC as both ω-conotoxin MVIIC and ω-agatoxin IVA reduce ACh release [65].
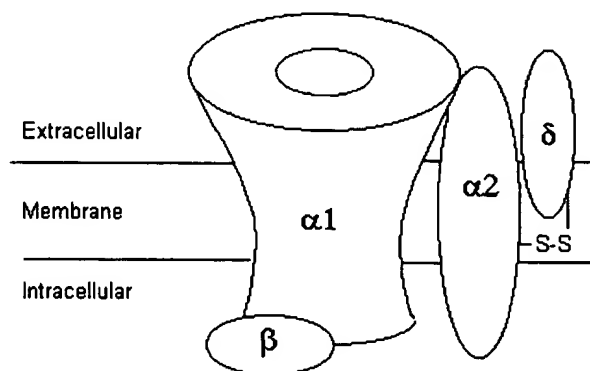

Fig. 3. The voltage-gated calcium channel. The VGCC is made up of four subunits, the α_2 and δ being covalently linked. The different forms of α_1 subunits are described in Table 3.

VGCC is an oligomeric protein with a main ion channel subunit (α_1). There are four accessory, regulatory subunits, including β, which is cytoplasmic, $\alpha_2\delta$ and γ (Fig. 3). The subtypes of VGCCs depend mainly on the α_1 subunit, but the electrophysiological and pharmacological characteristics of the VGCC can be modified by the other subunits [66]. Table 3 shows the main subtypes of relevance here. The L-type encoded by the α_{1C} subunit is involved mainly in neuroendocrine secretion from endocrine cells. The N-type VGCC, encoded by an α_{1B}, is blocked by ω-conotoxin GVIA. Neither L-type nor N-type VGCCs appear to be involved in calcium-induced ACh release at the normal neuromuscular junction because dihydropyridines and ω-conotoxin GVIA do not block neuromuscular transmission. However, during development or reinnervation, the pharmacological profile of the VGCCs at the neuromuscular junction is altered in favour of a role for both N-type and L-type VGCCs [65,67]. It is not yet clear to what extent they may be present, but inactive, under the *in vitro* conditions in which neuromuscular transmission is normally studied. Nor is it clear to what extent they may become up-regulated during an ongoing, autoimmune or other disease process [68].

VGCCs are the antigenic target in LEMS

VGCCs are present on many different cell types, mainly those involved in secretory activity. SCLC cells are derived from the neuroectoderm and secrete a variety of neuropeptides including serotonin and ACTH. The presence of VGCCs in SCLC was first indicated by electrophysiological measurements, and confirmed by showing that depolarization by high K^+ led to an increase in $^{45}Ca^{2+}$ uptake [69]. Incubation in IgG prepared from patients with LEMS, but not from controls, reduced the influx of $^{45}Ca^{2+}$ into these cells [69]. Further studies on other SCLC lines confirmed these findings and suggested that SCLC expresses a number of different VGCC subtypes [70,71], similar to the forms expressed at the neuromuscular junction. For instance, the MB cell line derived from a LEMS patient with SCLC, expresses VGCCs that are not blocked by L-type or N-type VGCC antagonists, but are strongly inhibited by P-/Q-type blockers ω-conotoxin MVIIC and ω-agatoxin IVA [72].

It has not proved easy to obtain radioactively labelled ω-agatoxin that binds specifically to extracted VGCCs, but both ω-conotoxins bind with high affinity to pharmacologically specific and saturable sites in brain tissue extracts. ^{125}I-ω-conotoxin-labelled extracts were therefore used as antigens for detection of antibodies to VGCCs in patients with LEMS. ^{125}I-ω-conotoxin GVIA was found to bind to a low number of sites in human and rabbit brain extracts (21 fmoles per mg protein, K_D 43 pM), but only $\approx 40\%$ of LEMS patients had serum antibodies that immunoprecipitated the binding sites [73]. In contrast, there was a higher concentration of ^{125}I-ω-conotoxin MVIIC binding sites in the cerebellar extracts (458 fmol per mg of protein, K_D 96 pM) and the binding sites were immunoprecipitated by $> 90\%$ of LEMS serum antibodies [73]. Thus, the main antigenic target for the antibodies in LEMS appears to be a P/Q-type VGCC and this assay is used now for diagnosis of LEMS [74,75].

Further dissection of the VGCC subtype has been achieved with human embryonic kidney cells transfected with the genes for the different VGCC subunits [76]. The cells were grown for 24 h in the presence of LEMS patients' IgG and the voltage-activated calcium influx measured by calcium photometry using the fluorescent dye FURA2 and compared with cells grown in control IgG. LEMS IgG only reduced calcium currents in HEK cells expressing α_{1A} subunits, and not in those that expressed α_{1B}, α_{1C} or α_{1E} subunits. The action of the LEMS antibodies on whole-cell calcium currents in cultured rat cerebellar Purkinje and granular layer cells was also studied. Interestingly, following overnight incubation in LEMS IgG, the voltage-activated calcium transients were not reduced substantially in amplitude in either cell type. To determine whether the expression of VGCC subtypes had changed during incubation with LEMS IgG, different VGCC blockers were applied. There was a significant loss of ω-agatoxin and ω-conotoxin MVIIC sensitive channels in both Purkinje and granular layer cells, and an increase in the R-type (resistant) VGCC subtype [76]. Thus these experiments illustrate that the α_{1A} subunit is present in both Purkinje cells and granular layer cells, and that the α_{1A} gene forms both P-type and Q-type VGCCs. Also, incubation in LEMS IgG causes a reduction in P-/Q-type VGCC, and a concomitant up-regulation of R-type VGCCs. A similar up-regulation of VGCCs, that do not bind LEMS IgG antibodies, at the neuromuscular junction may help limit the effects of the pathogenic antibodies.

One of the clinical features that can help to distinguish LEMS from MG is that LEMS patients frequently complain of autonomic symptoms such as dry mouth, constipation and, in males, sexual impotence. The profile of VGCC subtypes has been demonstrated in mouse smooth muscle tissues, such as the bladder and vas deferens, using the specific VGCC channel blockers. On this basis, transmitter release from both sympathetic and parasympathetic neurones appears to depend on calcium influx through N-type, P-type and Q-type channels. Using the mouse passive transfer model, animals injected with LEMS IgG showed a reduction in transmitter release subserved by P-type and Q-type VGCC, and to a lesser extent by N-type VGCCs [77]. These results help to explain the autonomic symptoms encountered by LEMS patients.

Anti-VGCC antibodies and cerebellar disturbance

Patients with SCLC have an increased chance of developing a range of neurological disorders including subacute sensory neuronopathy, limbic and brainstem encephalitis, and cerebellar ataxia. These paraneoplastic disorders are often associated with the presence of an antibody to a neuronal nuclear antigen called 'Hu'. The antibodies are not pathogenic because the antigen is intracellular, but their detection is important because it points to the presence of the SCLC [78].

Because LEMS is also associated with SCLC, it would not be surprising if some patients had antibodies to both Hu and VGCCs, and a range of symptoms involving both the central and peripheral nervous systems. Cerebellar ataxia is particularly distressing because it causes loss of co-ordination in gait, speech and swallowing. It is associated with progressive loss of Purkinje and other cerebellar cells (that express VGCCs as discussed above). Although probably present, the symptoms of LEMS may go unnoticed because of the cerebellar signs. The combination of LEMS and cerebellar ataxia with anti-VGCC antibodies suggests that in some situations circulating antibodies to neuronal antigens can cause central nervous system (CNS) disease [79].

NEUROMYOTONIA

The existence of two antibody-mediated diseases affecting ion channels at the neuromuscular junction has stimulated the search for other possible antibody-mediated 'channelopathies'. Acquired neuromyotonia, or Isaac's disease, is a condition in

which the patient complains of muscle twitching, painful cramps, difficulties in relaxing after muscle contraction (pseudo-myotonia), and often sweating and other signs of autonomic disturbance. The condition appears to be due to overactivity of the peripheral nerve, because the hyperactivity disappears if neuromuscular transmission is blocked with curare, but continues during sleep (which would abolish centrally driven hyperactivity) [80].

The role of autoantibodies in neuromyotonia was first demonstrated by showing that patients responded to plasma exchange, and that injection of their plasma IgG antibodies into mice produced an increase in ACh release [81]. The changes, which have not yet been studied successfully in patients' neuromuscular junctions, were similar to those found in the presence of low doses of the VGKC blocking drug, 3,4-diaminopyridine or dendrotoxins [82]. VGKCs are even more heterogenous in their genetic make up than VGCCs, and the targets for the antibodies are not yet clear. However, at least 50% of patients have antibodies that bind to ^{125}I-dendrotoxin labelled VGKCs, and this toxin binds to VGKCs KV1.1, KV1.2 and KV1.6 [82]. Whether there are antibodies to other VGKCs that are not labelled by dendrotoxin, to calcium-activated, inward rectifying potassium channels, or to other neuronal targets remains to be seen.

In a few reported cases, neuromyotonia has been described in association with sleep disorders, anxiety, confusion and memory loss, suggesting a central component (called Morvan's syndrome). Antibodies to VGKCs have also been detected in patients with Morvan's syndrome, and in a few cases with similar CNS system symptoms but without neuromyotonia (R. Liquori and A. Vincent, unpublished results). It seems likely, therefore, that the antibodies can enter the CNS under certain circumstances, but the extent to which the antibodies cause observable symptoms, in the periphery or centrally, might depend on the ability of the neuronal tissue to up-regulate other forms of potassium channels (compare LEMS above).

GENETIC DISORDERS

As it began to be clear that MG was caused by autoantibodies to the AChR, it also became evident that there was a group of patients with typical myasthenic symptoms whose disease was likely to be inherited rather than autoimmune. Their symptoms started at or shortly after birth rather than in later childhood, adolescence or adulthood as is generally the case for MG. The patients did not have antibodies to the AChR, and plasma exchange induced no improvement in clinical symptoms [83]. Muscle biopsies were studied from five patients. All had small MEPP amplitudes, very similar to those found in MG, but interestingly only four of the five had reduced numbers of AChRs at the neuromuscular junctions as determined by ^{125}I-α-bungarotoxin binding. Thus, even in these initial studies it became clear that congenital myasthenia was likely to be heterogeneous in its genetic origins [84].

Acetylcholine receptor deficiency

This condition usually presents soon after birth with weakness and delayed development of motor functions such as sitting, walking or climbing stairs. Weakness is quite variable and can be relatively mild and the disease may improve slowly with age. A common finding is a history of consanguinity in the parents, and the incidence among siblings is consistent with
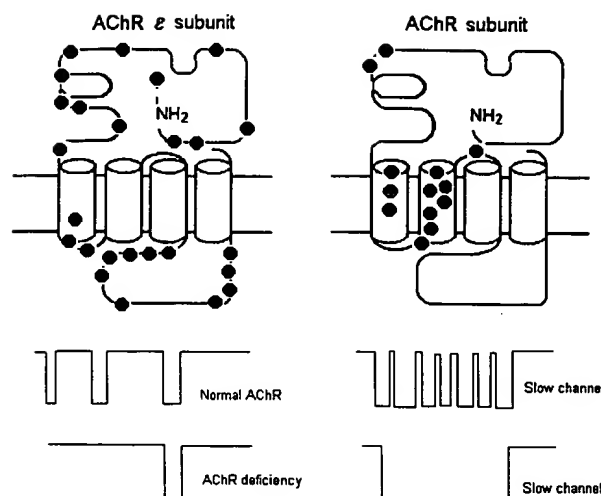
Fig. 4. Mutations in the acetylcholine receptor genes. Mutations in the AChR ε subunit cause AChR deficiency (left). They can be anywhere within the coding sequence or in the promoter region and mostly lead to premature truncation and reduced expression of functional AChR. The main effect is a reduced number of AChR channel openings (bottom left). Persistence of the γ subunit may provide a compensatory mechanism, and in some cases alternatively spliced forms can rescue ε subunit expression. Mutations that cause the slow channel syndrome (right) are found in all the AChR subunits and are generally in extracellular regions involved in ACh binding, or in the transmembrane domains M1 and M2. In general, ACh binding site mutations cause prolonged bursts of channel openings due to increased affinity for ACh (see below right), whereas mutations in the M2 domain cause prolonged single channel openings (bottom right). M1 domain mutations may affect both affinity and channel gating.

recessive inheritance. Investigation of muscle biopsies from these patients shows a marked reduction in the amplitude of MEPPs and in the number of AChRs. The findings are similar to those in acquired MG, but no immunoglobulins are detected at the neuromuscular junction. In the last 5 years it has become clear that most cases of AChR deficiency are due to mutations affecting the AChR epsilon subunit (Fig. 4). These may be insertions, deletions, missense or splice-site mutations. However, the majority cause a shift in the codon reading frame and result in epsilon subunit peptides that are prematurely truncated [84,85].

A particularly interesting mutation is one that has now been identified in many independent families, probably with its origin in the eastern Mediterranean. This mutation, epsilon 1267delG, leads to premature truncation of the epsilon subunit prior to the M4 transmembrane domain. In the homozygous condition, this would mean an absence of functional epsilon subunits and lack of adult AChR at the neuromuscular junction. The survival of affected individuals may reflect the expression of the gamma subunit which can persist at the neuromuscular junction and lead to functional transmission. However, there is another explanation. It appears that intron 11 is frequently retained within the epsilon subunit mRNA transcripts in both normal and affected individuals. When the 1267delG mutation is expressed with this alternatively spliced epsilon transcript, the reading frame is restored, the fourth transmembrane domain is present, and in HEK293 cells there is some surface expression of this mutant AChR. Surprisingly, when expressed in *Xenopus* oocytes, all four permutations of the epsilon subunit that are present in an individual heterozygous for the 1267delG

mutation can form functional AChR channels, although surface expression of each of the mutant forms is severely reduced. Thus this naturally occurring human mutant raises questions about the need for the fourth transmembrane domain in AChR ion channel function [85].

Another type of mutation that leads to the same phenotype as those in the promoter region of the epsilon subunit of the AChR. These mutations result in reduced expression of the adult isoform [86].

Slow channel syndromes

These conditions present at birth, during adolescence or even during adult life, making them initially difficult to distinguish from MG. However, the distribution of weakness is different with much more involvement of shoulder and hand muscles, and commonly thinning of the muscles [87]; they often deteriorate when given AChE inhibitors. They do not respond to immunological treatments.

It was a major breakthrough when Engel and his colleagues identified the first AChR mutation in a family with the slow channel syndromes, which he had described 10 years previously [88]. This mutation and many others that have been studied by expression in HEK cells or *Xenopus* oocytes, causes AChR channels to remain open for too long [88,89]. This results in prolonged action of ACh and prolonged decay phases of the MEPPs and EPPs. There are two main types of slow channel syndrome mutations. In some cases the mutation appears to increase the affinity of the AChR for ACh. Thus ACh does not dissociate quickly when the AChR channel closes, the channel reopens and the AChR oscillates between the open and closed states until ACh finally dissociates [88]. The other type of mutation appears to directly affect the gating of the ion channel and individual channel openings are prolonged (Fig. 4). In either case, the overall effect is to increase the time for which the AChR channel is open and thus lead to an increase in the number of ions that flow through the AChRs. The location of mutations that cause the slow channel syndrome phenotypes, and the type of AChR ion channel openings that result, are illustrated in Fig. 4.

The cause of muscle weakness in this syndrome is unclear. It is hypothesized that the prolonged ACh-induced postsynaptic currents lead to increased influx of calcium through the receptors, and its accumulation in the postsynaptic cytoplasm [87]. This could lead to activation of intracellular enzymes resulting in 'myopathic' changes. Alternatively, or perhaps in addition, the prolonged AChR openings might lead to depolarization-block of the voltage-gated sodium channels. Finally, the slow channel syndrome mutations appear to increase the rate at which AChRs undergo desensitization, which might itself contribute to defects in transmission. There is little evidence at present to distinguish between these theories *in vitro* or to assess how they might contribute to the defects *in vivo*.

Fast channel syndrome

One of the first cases of congenital myasthenic syndromes studied had very small MEPP amplitudes with normal α-bungarotoxin binding sites [83], suggesting either a reduction in the amount of ACh released in each packet or a kinetic defect in the AChR itself. Three different mutations have been identified in which the AChR channel open times are reduced substantially [84]. The disease is not easy to distinguish from AChR deficiency, although there tends to be less ocular muscle involvement.

AChE deficiency

Only a few patients have been described with deficiency of AChE. The clinical features are often very severe with considerable thinning of the muscles and consequent truncal deformities. There is little that can be done clinically; the patients do not, as expected, show any response to AChE inhibitors or immunosuppressive drugs. All of the patients described to date have mutations in the ColQ gene that encodes the collagen-like tail of AChE [89].

Other targets for genetic disorders at the neuromuscular junction

In the large number of cases studied by Engel and his associates at the Mayo Clinic, and also by Beeson and his colleagues in Oxford, a primary defect in the AChR has been identified in at least 60% of patients with well-defined congenital myasthenic syndromes. Thus, defects in the other functional or structural proteins at the neuromuscular junction must be relatively rare. However, there are many potential targets, for example, missense mutations or heterozygous mutations in RAPsyn or utrophin, or in the equally important molecules that are responsible for development of the neuromuscular junction, e.g. agrins, ARIA and their receptors. It may be that mutations in these proteins are lethal and lead to severe intrauterine paralysis with fatal consequences, but some may be involved in genetic forms of AMC and/or in the less severe neuromuscular junction disorders [90]. In addition, although VGCC mutations have been detected in patients with CNS disorders [91], it would be surprising if these mutations did not sometimes cause neuromuscular junction failure. Moreover, mutations in VGKC have been identified in patients with a genetic form of ataxia with neuromyotonia (Table 1) [92] indicating that these genes may also be involved.

ACKNOWLEDGEMENTS

REFERENCES

1. Aidley, D.J. (1999) *The Physiology of Excitable Cells.* Cambridge University Press, Cambridge, UK.

2. Vincent, A. & Wray, D., eds. (1992) *Neuromuscular Transmission: Basic and Applied Aspects.* Pergamon Press, Oxford, UK.

3. Hall, Z.W. & Sanes, J.R. (1993) Synaptic structure and development. The neuromuscular junction. *Cell* 72, 99–121.

4. Hoch, W. (1999) Formation of the neuromuscular junction. Agrin and its unusual receptors. *Eur. J. Biochem.* 265, 1–10.

5. Sanes, J.R. & Lichtman, J.W. (1999) Development of the vertebrate neuromuscular junction. *Ann. Rev. Neurosci.* 22, 389–442.

6. Wood, S.J. & Slater, C.R. (1998) Beta-spectrin is colocalized with both voltage-gated sodium channels and ankyrin G at the adult rat neuromuscular junction. *J. Cell Biol.* 140, 675–684.

7. Froehner, S.C., Luetje, C.W., Scotland, P.B. & Patrick, J. (1990) The postsynaptic 43 K protein clusters muscle nicotinic acetylcholine receptors in *Xenopus* oocytes. *Neuron* 4, 403–410.

8. Bewick, G.S., Young, C. & Slater, C.R. (1996) Spatial relationships of utrophin, dystrophin, b-dystroglycan and b-spectrin to acetylcholine receptor clusters during postnatal maturation of the rat neuromuscular junction. *J. Neurocytol.* 25, 267–279.

9. Harvey, A.L., ed. (1993) *Natural and Synthetic Neurotoxins. Neuroscience Perspectives.* Academic Press, London, UK.

10. Lee, C.Y. (1979) Recent advances in chemistry and pharmacology of snake toxins. *Adu Cytopharmacol.* **3**, 1–16.

11. Olivera, B.M., Miljanich, G.P., Ramachandran, J. & Adams, M.E. (1994) Calcium channel diversity and neurotransmitter release: the ω-conotoxins and ω-agatoxins. *Annu. Rev. Biochem.* **63**, 823–867.

12. Anderson, A.J. & Harvey, A. (1988) Effects of the potassium channel blocking dendrotoxins on acetylcholine release and motor nerve terminal activity. *Br. J. Pharmacol.* **93**, 215–221.

13. Karlin, A. & Akabas, M.H. (1995) Toward a structural basis for the function of nicotinic acetylcholine receptors and their cousins. *Neuron* **15**, 1231–1244.

14. Hucho, F., Tsetlin, V.I. & Machold, J. (1996) The emerging three-dimensional structure of a receptor. The nicotinic acetylcholine receptor. *Eur. J. Biochem.* **239**, 539–557.

15. Miyazawa, A., Fujiyoshi, Y., Stowell, M. & Unwin, N. (1999) Nicotinic acetylcholine receptor at 4.6 Å resolution: transverse funnels in the channel wall. *J. Mol. Biol.* **288**, 765–786.

16. Vincent, A., Jacobson, L. & Curran, L. (1998) Alpha-bungarotoxin binding to human acetylcholine receptor; measurement of affinity, delineation of AChR subunit residues critical to binding, and protection of AChR function by synthetic peptides. *Neurochem. Int.* **32**, 427–433.

17. Tzartos, S.J. & Lindstrom, J.M. (1980) Monoclonal antibodies used to probe acetylcholine receptor structure: localization of the main immunogenic region and detection of similarities between subunits. *Proc. Natl Acad. Sci. USA* **77**, 755–759.

18. Tzartos, S.J., Barkas, T., Cung, M.T., Mamalaki, A., Marraud, M., Orlewski, P., Papanastasiou, D., Sakarellos, C., Sakarellos-Daitsiotis, M., Tsantili, P. & Tsikaris, V. (1998) Anatomy of the antigenic structure of a large membrane autoantigen, the muscle-type nicotinic acetylcholine receptor. *Immunol. Rev.* **163**, 89–120.

19. Ratnam, M., Sargent, P.B., Sarin, V., Fox, J.L., Nguyen, D.L., Rivier, J., Criado, M. & Lindstrom, J. (1986) Location of antigenic determinants on primary sequences of subunits of nicotinic acetylcholine receptor by peptide mapping. *Biochemistry* **25**, 2621–2632.

20. Tzartos, S.J. & Remoundos, M.S. (1992) Precise epitope mapping of monoclonal antibodies to the cytoplasmic side of the acetylcholine receptor alpha subunit. Dissecting a potentially myasthenogenic epitope. *Eur. J. Biochem.* **207**, 915–922.

21. Palace, A., Vincent, A., Beeson, D. & Newsom-Davis, J. (1994) Immunogenicity of human recombinant acetylcholine receptor α subunit. Cytoplasmic epitopes dominate the antibody response in four mouse strains. *Autoimmunity* **18**, 113–119.

22. Newsom-Davis, J. (1997) Autoantibody-mediated channelopathies at the neuromuscular junction. *Neuroscientist* **3**, 337–346.

23. Warrell, D.A. (1993) Venomous bites and stings in the tropical world. *Med. J. Aust.* **159**, 773–779.

24. Drachman, D.B. (1994) Myasthenia gravis. *N. Engl. J. Med.* **330**, 1797–1810.

25. Elmqvist, D., Hofmann, W.W., Kugelberg, J. & Quastel, D.M.J. (1964) An electrophysiological investigation of neuromuscular transmission in myasthenia gravis. *J. Physiol. (Lond.)* **174**, 417–434.

26. Patrick, J. & Lindstrom, J. (1973) Autoimmune response to acetylcholine receptor. *Science* **180**, 871–872.

27. Raftery, M.A., Hunkapiller, M.W., Strader, C.D. & Hood, L.E. (1980) Acetylcholine receptor: complex of homologous subunits. *Science* **208**, 1454–1456.

28. Numa, S., Noda, M., Takahashi, H., Tanabe, T., Toyosato, M., Furutani, Y. & Kikyotani, S. (1983) Molecular structure of the nicotinic acetylcholine receptor. *Cold Spring Harbor Symp. Quat. Biol.* **48**, 57–69.

29. Fambrough, D.M., Drachman, D.B. & Satyamurti, S. (1973) Neuromuscular junction in myasthenia gravis. Decreased acetylcholine receptors. *Science* **182**, 293–295.

30. Simpson, J.A. (1960) Myasthenia gravis: a new hypothesis. *Scot. Med. J.* **5**, 419–439.

31. Lindstrom, J.M., Seybold, M.E., Lennon, V.A., Whittingham, S. &

32. Newsom-Davis, J., Pinching, A.J., Vincent, A. & Wilson, S.G. (1978) Function of circulating antibody to acetylcholine receptor in myasthenia gravis. Investigation by plasma exchange. *Neurology* **28**, 266–272.

33. Toyka, K.V., Drachman, D.B., Griffin, D.E., Pestronk, A., Winkelstein, J.A., Fischbeck, K.H. & Kao, I. (1977) Myasthenia gravis. Study of humoral immune mechanisms by passive transfer to mice. *N. Engl. J. Med.* **296**, 125–131.

34. Engel, A.G. (1984) Myasthenia gravis and myasthenic syndromes. *Ann. Neurol.* **16**, 519–534.

35. Vincent, A. (1994) Experimental autoimmune myasthenia gravis. In *Autoimmune Disease Models* (Cohen, I.R. & Miller, A., eds) pp 83–106. Academic Press, New York, USA.

36. Vincent, A., Willcox, N., Hill, M., Curnow, J., MacLennan, C. & Beeson, D. (1998) Determinant spreading and immune responses to acetylcholine receptors in myasthenia gravis. *Immunol. Rev.* **164**, 157–168.

37. Vincent, A., Whiting, P.J., Schluep, M., Heidenreich, F., Lang, B., Roberts, A., Willcox, N. & Newsom-Davis, J. (1987) Antibody heterogeneity and specificity in myasthenia gravis. *Ann. N.Y. Acad. Sci.* **505**, 106–120.

38. Jacobson, L., Beeson, D., Tzartos, S. & Vincent, A. (1999) Monoclonal antibodies raised against human acetylcholine receptor bind to all five subunits of the fetal isoform. *J. Neuroimmunol.* **98**, 112–120.

39. Drachman, D.B., Angus, D.W., Adams, R.N., Michelson, J.D. & Hoffman, G.J. (1978) Myasthenia antibodies cross-link acetylcholine receptors to accelerate degradation. *N. Engl. J. Med.* **198**, 1116–1122.

40. Stanley, E.F. & Drachman, D.B. (1978) Effect of myasthenic immunoglobulin on acetylcholine receptors of intact mammalian neuromuscular junctions. *Science* **200**, 1285–1287.

41. Wilson, S., Vincent, A. & Newsom-Davis, J. (1983) Acetylcholine receptor turnover in mice with passively transferred myasthenia gravis. II. Receptor synthesis. *J. Neurol. Neurosurg. Psychiatry* **46**, 383–387.

42. Guyon, T., Lavasseru, P., Truffault, F., Cottin, C., Gaud, C. & Berrih Aknin, S. (1994) Regulation of acetylcholine receptor alpha subunit variants in human myasthenia gravis: quantification of steady-state levels of messenger RNA in muscle biopsy using the polymerase chain reaction. *J. Clin. Invest.* **94**, 16–24.

43. Engel, A.G. & Arahata, K. (1987) The membrane attack complex of complement at the endplate in myasthenia gravis. *Ann. N.Y. Acad. Sci.* **505**, 326–332.

44. Ruff, R.L. & Lennon, V.A. (1998) End-plate voltage-gated sodium channels are lost in clinical and experimental myasthenia gravis. *Ann. Neurol.* **43**, 370–379.

45. Vernet Der Garabedian, B., Lacokova, M., Eymard, B., Morel, E., Faltin, M., Zajac, J., Sadovsky, O., Dommergues, M., Tripon, P. & Bach, J.-F. (1994) Association of neonatal myasthenia gravis with antibodies against the fetal acetylcholine receptor. *J. Clin. Invest.* **94**, 555–559.

46. Vincent, A., Newland, C., Brueton, L., Beeson, D., Riemersma, S., Huson, S.M. & Newsom-Davis, J. (1995) Arthrogryposis multiplex congenita with maternal autoantibodies specific for a fetal antigen. *Lancet* **346**, 24–25.

47. Missias, A.C., Chu, G.C., Klocke, B., Sanes, J.R. & Merlie, J.P. (1986) Maturation of the acetylcholine receptor in developing skeletal muscle: regulation of the AChR g to e switch. *Dev. Biol.* **179**, 223–238.

48. Riemersma, S., Vincent, A., Beeson, D., Newland, C. & Hawke, S., Vernet-der Garabedian, B., Eymard, B. & Newsom-Davis, J. (1996) Association of arthrogryposis multiplex congenita with maternal antibodied inhibiting fetal acetylcholine receptor function. *J. Clin. Invest.* **98**, 2358–2363.

49. Brueton, L.A., Huson, S.M., Cox, P.M., Shirley, L., Thompson, E.M.,

Barnes, P.R.J., Price, J., Newsom-Davis, J. & Vincent, A. (2000) Asymptomatic maternal myasthenia as a cause of Pena-Shokeir phenotype. *Am. J. Med. Genet.* 92, 1–6.

50. Jacobson, L., Polizzi, A., Morriss-Kay, G. & Vincent, A. (1999) Plasma from human mothers of fetuses with severe arthrogyrposis multiplex congenita causes deformities in mice. *J. Clin. Invest.* 103, 1031–1938.

51. Mossman, S., Vincent, A. & Newsom-Davis, J. (1986) Myasthenia gravis without acetylcholine receptor antibody: a distinct disease entity. *Lancet* 1, 116–119.

52. Yamamoto, T., Vincent, A., Ciulla, T.A., Lang, B., Johnston, I. & Newsom-Davis, J. (1991) Seronegative myasthenia gravis: a plasma factor inhibiting agonist-induced acetylcholine receptor function copurifies with IgM. *Ann. Neurol.* 30, 550–557.

53. Vincent, A., Li, Z., Hart, A., Barrett-Jolley, R., Yamamoto, T., Burges, J., Wray, D., Byrne, N., Molenaar, P. & Newsom-Davis, J. (1993) Seronegative myasthenia gravis. Evidence for plasma factor(s) interfering with acetylcholine receptor function. *Ann. N.Y. Acad. Sci.* 681, 529–538.

54. Mulle, C., Benoit, P., Pinset, C., Roa, M. & Changeux, J.-P. (1988) Calcitonin gene-related peptide enhances the rate of desensitisation of the nicotinic acetylcholine receptor in cultured mouse muscle cells. *Proc. Natl Acad. Sci. USA* 85, 5728–5732.

55. Blaes, F., Beeson, D., Plested, P., Lang, B. & Vincent, A. (2000) IgG from 'seronegative' myasthenia gravis patients binds to a muscle cell line, TE671, but not human acetylcholine receptor. *Ann. Neurol.* 47, 504–510.

56. Poea, S., Guyon, T., Bruand, C., Mouly, V. & Berrih-Aknin, S. (2000) Modulation of acetylcholine receptor expression in seronegative myasthenia gravis. *Ann. Neurol.* in press.

57. O'Neill, J.H., Murray, N.M. & Newsom-Davis, J. (1988) The Lambert–Eaton myasthenic syndrome. A review of 50 cases. *Brain* 111, 577–596.

58. Elmqvist, D. & Lambert, E.H. (1968) Detailed analysis of neuromuscular transmission in a patient with the myasthenic syndrome sometimes associated with bronchogenic carcinoma. *Mayo Clin. Proc.* 43, 689–713.

59. Lambert, E.H. & Elmqvist, D. (1971) Quantal components of end-plate potentials in the myasthenic syndrome. *Ann. N.Y. Acad. Sci.* 183, 183–199.

60. Fukunaga, H., Engel, A.G., Osame, M. & Lambert, E.H. (1982) Paucity and disorganisation of presynaptic membrane active zones in the Lambert–Eaton myasthenic syndrome. *Muscle Nerve* 5, 686–697.

61. Lang, B., Newsom-Davis, J., Wray, D., Vincent, A. & Murray, N.M.F. (1981) Autoimmune aetiology for myasthenic (Eaton–Lambert) syndrome. *Lancet* 2, 224–226.

62. Lang, B., Newsom-Davis, J., Prior, C. & Wray, D. (1983) Antibodies to motor nerve terminals: an electrophysiological study of a human myasthenic syndrome transferred to mouse. *J. Physiol. (Lond.)* 344, 335–345.

63. Fukuoka, T., Engel, A.G., Lang, B., Newsom-Davis, J. & Vincent, A. (1987) Lambert–Eaton myasthenic syndrome: II. Immunoelectron microscopy localization of IgG at the mouse motor end-plate. *Ann. Neurol.* 22, 200–211.

64. Llinas, R., Sugimori, M., Hillman, D.E. & Cherksey, B. (1992) Distribution and functional significance of the P-type, voltage-dependent Ca^{2+} channels in the mammalian central nervous system. *Trends Neurosci.* 15, 351–355.

65. Protti, D.A., Reisin, R., Mackinley, T.A. & Uchitel, O.D. (1996) Calcium channel blockers and transmitter release at the normal human neuromuscular junction. *Neurology* 46, 1391–1396.

66. De Waard, M., Gurnett, C.A. & Campbell, K.P. (1996) Structural and functional diversity of voltage-activated calcium currents. *Ion Channels* 4, 41–83.

67. Smith, D.O., Conklin, M.W., Jensen, P.H. & Atchison, W.D. (1995) Decreased calcium currents in motor nerve terminals of mice with Lambert Eaton myasthenic syndrome. *J. Physiol.* 487, 115–123.

68. Katz, E., Ferro, P.A., Weisz, G. & Uchitel, O.D. (1996) Calcium

channels involved in synaptic transmission at the mature and regenerating mouse neuromuscular junction. *J. Physiol.* 497, 687–697.

69. Roberts, A., Perera, S., Lang, B., Vincent, A. & Newsom-Davis, J. (1985) Paraneoplastic myasthenic syndrome IgG inhibits $^{45}Ca^{2+}$ flux in a human small cell carcinoma line. *Nature* 317, 737–739.

70. De Aizpurua, H.J., Lambert, E.H., Griesmann, G.E., Olivera, B.O. & Lennon, V.A. (1988) Antagonism of voltage-gated calcium channels in small cell carcinomas of patients with and without Lambert–Eaton myasthenic syndrome by autoantibodies, W-conotoxin and adenosine. *Cancer Res.* 48, 4719–4724.

71. Johnston, I., Lang, B., Leys, K. & Newsom-Davis, J. (1994) Heterogeneity of calcium channel autoantibodies detected using a small cell lung cancer line derived from a Lambert–Eaton syndrome patient. *Neurology* 44, 334–338.

72. Lang, B., Waterman, S., Pinto, A., Jones, D., Moss, F., Boot, J., Brust, P., Williams, M., Stauderman, K., Harpold, M., Motomura, M., Moll, J.W., Vincent, A. & Newsom-Davis, J. (1998) The role of autoantibodies in Lambert–Eaton myasthenic syndrome. *Ann. N.Y. Acad. Sci.* 841, 598–605.

73. Motomura, M., Lang, B., Johnston, I., Palace, J., Vincent, A. & Newsom-Davis, J. (1997) Incidence of serum anti-P/Q-type and anti-N-type calcium channel autoantibodies in the Lambert Eaton myasthenic syndrome. *J. Neurol. Sci.* 147, 35–42.

74. Motomura, M., Johnston, I., Lang, B., Vincent, A. & Newsom-Davis, J. (1995) An improved diagnostic assay for Lambert–Eaton myasthenic syndrome. *J. Neurol. Neurosurg. Psychiatry* 58, 85–87.

75. Lennon, V.A., Kryzer, T.J., Griesmann, G.E., O'Suilleabhain, P.E., Windebank, A.J., Woppmann, A., Miljanich, G.P. & Lambert, E.H. (1995) Calcium channel antibodies in the Lambert Eaton myasthenic syndrome and other paraneoplastic syndromes. *N. Engl. J. Med.* 332, 1467–1474.

76. Pinto, A., Gillard, S., Moss, F., Whyte, K., Brust, P., Williams, M., Stauderman, K., Harpold, M., Lang, B., Newsom-Davis, J., Bleakman, D., Lodge, D. & Boot, J. (1998) Human autoantibodies specific for the a1A calcium channel subunit reduce both P-type and Q-type calcium currents in cerebellar neurons. *Proc. Natl Acad. Sci. USA* 95, 8328–8333.

77. Waterman, S.A., Lang, B. & Newsom-Davis, J. (1997) Effect of Lambert Eaton myasthenic syndrome antibodies on autonomic neurons in the mouse. *Ann. Neurol.* 42, 147–156.

78. Dalmau, J., Gultekin, H.S. & Posner, J.B. (1999) Paraneoplastic neurologic syndromes: pathogenesis and physiopathology. *Brain Pathol.* 9, 275–284.

79. Trivedi, R., Mundanthanam, G., Amyes, E., Lang, B. & Vincent, A. Screening for autoantibodies in cerebellar ataxia. *Lancet* 356, 565–566.

80. Newsom-Davis, J. & Mills, K.R. (1993) Immunological associations of acquired neuromyotonia (Isaacs' syndrome). Report of five cases and literature review. *Brain* 116, 453–469.

81. Sinha, S., Newsom-Davis, J., Mills, K., Byrne, N., Lang, B. & Vincent, A. (1991) Autoimmune aetiology for acquired neuromyotonia. *Lancet* 338, 75–77.

82. Shillito Hart, I., Waters, C., Vincent, A., Newland, C., Beeson, D., Pongs, O., Morris, C. & Newsom-Davis, J. (1997) Autoantibodies detected to expressed K^+ channels are implicated in neuromyotonia. *Ann. Neurol.* 41, 238–246.

83. Vincent, A., Cull-Candy, S.G., Newsom-Davis, J., Trautmann, A., Molenaar, P.C. & Polak, R.L. (1981) Congenital myasthenia: end-plate acetylcholine receptors and electrophysiology in five cases. *Muscle Nerve* 4, 306–318.

84. Engel, A.G., Ohno, K. & Sine, S.M. (1999) Congenital myasthenic syndromes. *Rec. Adv. Arch. Neurol.* 56, 163–167.

85. Croxen, R., Newland, C., Berry, M., Vincent, A., Newsom-Davis, J. & Beeson, D. (1999) Novel functional e-subunit polypeptide generated by a single nucleotide deletion in acetylcholine receptor deficiency congenital myasthenic syndrome. *Ann. Neurol.* 46, 639–647.

86. Nichols, P., Croxen, R., Vincent, A., Rutter, R., Hutchinson, M., Newsom-Davis, J. & Beeson, D. (1999) Mutation of the acetylcholine

receptor ε-subunit promoter in congenital myasthenic syndrome. *Ann. Neurol.* **45**, 439–443.

87. Engel, A.G., Lambert, E.H., Mulder, D.M., Torres, C.F., Sahashi, K., Bertorini, T.E. & Whitaker, J.N. (1982) A newly recognized congenital myasthenic syndrome attributed to a prolonged open time of the acetylcholine-induced ion channel. *Ann. Neurol.* **11**, 553–569.

88. Sine, S.M., Ohno, K., Bouzat, C., Auerbach, A., Milone, M., Pruitt, J.N. & Engel, A.G. (1995) Mutation of the acetylcholine receptor alpha subunit causes a slow-channel myasthenic syndrome by enhancing agonist binding affinity. *Neuron* **15**, 229–239.

89. Croxen, R., Newland, C., Beeson, D., Vincent, A. & Newsom-Davis, J. (1997) Mutations in different functional domains of the human muscle acetylcholine receptor α subunits in patients with the slow-channel congenital myasthenic syndrome. *Hum. Mol. Genet.* **5**, 767–774.

90. Ohno, K., Engel, A.G., Brengman, J.M., Shen, X.-M., Heidenreich, F.R., Vincent, A., Milone, M., Tan, E., Anlar, B., Walsh, P., Nakano, S. & Akiguchi, I. (2000) The spectrum of mutations causing endplate acetylcholinesterase deficiency. *Ann. Neurol.* **47**, 162–170.

91. Ophoff, R.A., Terwindt, G.M., Vergouwe, M.N. et al. (1996) Familial hemiplegic migraine and episodic ataxia type-2 are caused by mutations in the calcium channel gene, *CACNL1A4*. *Cell* **87**, 543–552.

92. Lehmann-Horn, F. & Jurkat-Rott, K. (1999) Voltage-gated ion channels and hereditary disease. *Physiol. Rev.* **79**, 1317–1372.

Sequence and functional expression in *Xenopus* oocytes of a human insulinoma and islet potassium channel

(cDNA/gene/insulin secretion/Shaker/delayed rectifier)

Louis H. Philipson*, Rita E. Hice*, Kristen Schaefer*, Joseph LaMendola[†], Graeme I. Bell*[†][‡],
Deborah J. Nelson*[§][¶], and Donald F. Steiner*[†][‡][‖]

Departments of *Medicine, [†]The Howard Hughes Medical Institute, [‡]Departments of Biochemistry and Molecular Biology, [§]Neurology, and [¶]the Committee on Cell Physiology, The University of Chicago, 5841 S. Maryland Ave., Box 23, Chicago, IL 60637

ABSTRACT Regulation of insulin secretion involves the coordinated control of ion channels in the β-cell membrane. We have isolated and characterized cDNA and genomic clones encoding a voltage-dependent K^+ channel isoform expressed in human islets and in a human insulinoma. This K^+ channel isoform, designated hPCN1, with a deduced amino acid sequence of 613 residues ($M_r = 67,097$), is related to the Shaker family of *Drosophila* K^+ channels. hPCN1 is homologous to two other human K^+ channel isoforms we have isolated, hPCN2 and hPCN3, with 55% and 65% amino acid sequence identity, respectively. The electrophysiological characteristics of hPCN1 were determined after microinjection of synthetic RNA into *Xenopus* oocytes. Two-microelectrode voltage-clamp recordings of oocytes injected with hPCN1 RNA revealed a voltage-dependent outward K^+ current that inactivated slowly with time. Outward currents were inhibited by 4-aminopyridine with a K_i less than 0.10 mM and were relatively insensitive to tetraethylammonium ion or Ba^{2+}. A delayed rectifier K^+ channel such as hPCN1 could restore the resting membrane potential of β cells after depolarization and thereby contribute to the regulation of insulin secretion.

K^+ channels have been implicated in the regulation of the electrical activity of β cells in response to glucose as well as to the sulfonylurea oral hypoglycemic agents (1–6). The initial β-cell response to glucose metabolism or sulfonylureas is closure of ATP-sensitive K^+ channels. This results in depolarization of the membrane potential, thereby opening voltage-sensitive Na^+ and Ca^{2+} channels giving rise to action potentials. The resting membrane potential is then restored by K^+ channels, which open in response to both the change in membrane potential and Ca^{2+} influx (3–6). The time course of activation and inactivation of K^+ channels serves to entrain the frequency and modulate the duration of Ca^{2+}-dependent action potentials and thus regulate insulin release (3–6).

An extended family of four voltage-gated K^+ channel genes has been described in *Drosophila*: Shaker (*Sh*), Shab, Shaw, and Shal (7–11). Alternative splicing of the Shaker and Shab genes has been shown to be a mechanism for generating further channel diversity (10–12). By using homology screening, expression cloning, or the polymerase chain reaction (PCR), cDNAs and genes encoding a family of K^+ channels related to each of the *Drosophila* K^+ channel genes have been identified in mammalian tissues and cell lines (10–20). The data suggest that K^+ channel diversity in mammalian tissues is a consequence of the presence of multiple genes that lack introns and hence are not subject to alternative splicing as a mechanism for generating multiple isoforms (7, 17, 18, 23).

Additional diversity may be achieved by formation of heteromultimers between the products of these different mammalian genes (21–23).

As a first step in characterizing the ion channels expressed in β cells, we screened a human insulinoma cDNA library for voltage-gated K^+ channels by low-stringency cross-hybridization with a probe encoding the highly conserved membrane-spanning S4–H5 region of a rat brain K^+ channel isoform (13). The cDNA clones obtained did not contain all of the protein coding region, and the remainder was determined by isolating and sequencing the gene, designated hPCN1** (see Fig. 1).

The hPCN1 gene is most closely related to the Shaker gene in *Drosophila*. Comparison of the sequences of hPCN1 and other K^+ channels suggests that hPCN1 may be the human homolog of a rat K^+ channel, the partial sequence of which was obtained by PCR of rat islet and rat insulinoma RNA (20); the complete sequence of this rat protein, kv1, was recently described (17). Amplification of hPCN1 mRNA in human islet RNA indicated that it is also present in this tissue. Expression of hPCN1 in *Xenopus* oocytes indicated that it has characteristics of delayed rectifier-type channels. The pharmacological properties of hPCN1 are similar to the rat brain K^+ channel kv1 (17) but are distinct from other mammalian K^+ channels.

MATERIALS AND METHODS

General Methods. Standard procedures were as described (24). A 263-base-pair (bp) probe, pKC6, was generated from rat brain RNA corresponding to nucleotides 874–1137 of the MBK1 (mouse brain K^+ channel) cDNA sequence (13) by PCR and was used to screen a human insulinoma cDNA library (25). One clone was identified, λhKC-1, under low-stringency conditions (26), and the insert from this clone was used to rescreen the cDNA library and a genomic library (27).

Amplification of hPCN1 mRNA in Human Tissues. To detect the presence of the specific hPCN1 transcript in a malignant human β-cell tumor (provided by K. M. Pinnamaneni, A. O'Connor, and B. D. Ragsdale, Mesa, AZ) and normal human islets (RNA provided by S. Seino, University of Chicago, Chicago, IL), oligonucleotide primers were designed to amplify the 3' untranslated region in two steps. First-strand cDNA was primed with a $(dT)_{17}$-adapter as described (28, 29) and then amplified by using sense oligonucleotides from the H6 membrane-spanning region of

hPCN1 (see Fig. 1) (TGTGCCATCGCCGGGGTCCT) and the adapter in the antisense direction (29). An aliquot was removed and reamplified with an internal primer pair (sense, GCAGACTGGTGGCAGTGG; antisense, ACAGGAAACA-GAACAGCC). Positive (hKC-1 cDNA) and negative (water) controls were run with each sample.

Xenopus **Expression Vector.** *Bam*HI linkers were added to a *Sac* II/*Eco*RV genomic fragment encoding hPCN1 and ligated into the *Bgl* II cloning site of pSP64T (30). This plasmid was linearized with *Eco*RI or *Sal* I, and SP6 transcripts were prepared with kits from Promega and Stratagene. The transcripts include 89 bp of 5′ and 141 bp of 3′ untranslated regions of *Xenopus* β-globin mRNA as well as the hPCN1 sequence.

Oocyte Injection. Adult female *X. laevis* (Xenopus I, Ann Arbor, MI) were maintained, and oocytes were harvested by published methods (31). Defolliculated oocytes were microinjected with ≈50 nl of solution containing 0.1–2 ng of *in vitro* transcribed RNA or water and incubated at 19°C in OR-2 medium (31).

Current Recording and Data Analysis. Current recordings using a two-microelectrode voltage clamp were made with a commercially available amplifier (Warner Instruments, Hamden, CT) from oocytes 8 hr to 8 days after RNA injection. Microelectrodes filled with 3 M KCl had resistances of 0.3–0.6 MOhm. OR-2 medium without pyruvate or gentamicin was used as the standard recording solution. Current decays were analyzed as a sum of exponentials by a Fourier method (32) that determined the number, amplitudes, and time constants of the components. Where three or more experiments were performed, values were reported as either the mean ± SEM or as the range with the number of experiments in parentheses.

RESULTS

Isolation and Sequence of Human K⁺ Channel Clones. Screening of a human insulinoma cDNA library by hybridization under low-stringency conditions with a 263-bp rat brain K⁺ channel cDNA probe identified a single positive clone, λhKC-1, having a 1.8-kilobase (kb) *Eco*RI insert. The sequence of this clone revealed that it encoded part of a protein homologous to rodent brain K⁺ channels (13). As the murine genes encoding K⁺ channels expressed in brain do not

contain introns (18), we isolated a human genomic clone, λhPCN1, to obtain the complete sequence of this human K⁺ channel isoform, designated hPCN1. The insert in this genomic clone contained *Eco*RI fragments of 3, 4, and 9 kb; the 9-kb fragment hybridized to the insert from the cDNA clone λhKC-1. The composite sequence of hPCN1 was obtained from the sequences of the cDNA and genomic clones.

The hPCN1 sequence contains an open reading frame of 1839 bp that was predicted to encode a 613-amino acid protein (M_r = 67,097); there are translation termination codons in all three frames upstream of the predicted initiating ATG (33). The deduced amino acid sequence of hPCN1 has 50–87% identity and 65–93% similarity with previously described rodent K⁺ channel isoforms. hPCN1 is also related to two other human K⁺ channel isoforms we have recently characterized. The amino acid sequence identity between hPCN1 and hPCN2 is 55% and between hPCN1 and hPCN3 is 67% (Fig. 1). The sequences are highly conserved in the membrane-spanning domains (H1, H2, H3, S4, H4, H5, and H6), including the presence of the Shaker-type (Arg or Lys-Xaa-Xaa)₇ repeat in S4. A putative leucine zipper sequence is also conserved in the S4–H4 region (34). The amino terminus of hPCN1 is divergent from other members of the family until residue 121, just prior to the first putative N-linked glycosylation site [Asn-Xaa-(Ser or Thr)], which also is conserved in the Shaker and Shal families (10, 11, 13). A putative calcium/calmodulin protein kinase II phosphorylation site [Arg-Xaa-Xaa-(Ser or Thr)] is conserved in hPCN1 at threonine-133 as well as similar locations in Shaker, Shal, Shab, and Shaw (35). A consensus protein kinase A phosphorylation site [(Arg or Lys)-(Arg or Lys)-Xaa-(Xaa)-(Ser or Thr); refs. 36 and 37] at hPCN1 serine-557 is conserved in Shaker and Shab; a second such site is found at serine-580. An additional feature of hPCN1 is an almost perfect direct repeat from residues 61–82, which contains a proline-rich region with homology to a similar region in the recently reported rat brain K⁺ channel RKShIIIA, related to the Shaw family (16).

hPCN1 most closely resembles the rat brain K⁺ channel kv1 (17) among K⁺ channel sequences described to date. The nucleotide sequence identity in the protein coding regions of hPCN1 and kv1 is 84%; the 5′ and 3′ untranslated regions are more divergent, having 71% and 69% identity, respectively. Amino acid sequence identity between these two proteins is 88%, with 94% similarity. While it is likely that kv1 is the rat

hPCN1	MEIALVPLENGGAHTVRGGDEARAGCCGATGGELQCPPTAGLSDGPKEPAPKGRGAGRDADSGVRPLPPLPDPGVRPLPPLPEELPRPRRPPPEDEEEEGD	101
hPCN2	MEVAMVSAESSGCNSHMPVGYAAQARARERERLAHSRRAAARAVAAATAAVEGSGGSGGGSHHHHQSRGACTSHDPQGSRGSREEEATRTEKKKAHYRQSS	101
hPCN3	MTVVPGDHLLEPEV...............................ADGGGGPPQGGCCGGGCCDRYEPVPPSLP..............................	42
hPCN1	PGLGTV..EDQALGTASLHH.QKVHIHISGLRFETQLGTLAQP?	142
hPCN2	FPHCSDLMPSGSEEKILRELSEEEEDEEEEEEEEEEEGRFYYSEDDHGDECSYTDLLPQDEGGGGYSSVRY...SDCC.ERVVINVSGLRFETQMKTLAQP?	198
hPCN3	....AAGEQDCCGEKVVINISGLRFETQLKTLCQP?	74
hPCN1	NTLLGDPAKRLPYFDPLRNEYFFDRNRPSFDGIIYYTQSGGRLRRPVNVSLDVFADEIRFYQLGDEAMERFREDEGFIKEEE.KPLPRNEFQRQVVLIFEY	242
hPCN2	CPLLGDPEKETQYFDPLRNEYFFDRNRPSFDAILYYTQSGGRLRRPVNVPFDIFTEEVKFYQLGEEALLKFREDEGFVREEEDRALPENEFKKQIWLLFEY	299
hPCN3	ETLLGDPKRRMRYFDPVRNEYFFDRNRPSFDAILYYTQSGGRIRRPVNVPIDIFSEEIRFYQLGELAMEKFREDEGFLREEE.RPLPRRDFQRQVVLLFEY	174
	---------H1----------		---------H2--------	
hPCN1	PESSGSARAIAIVSVLVILISIITFCLETLPEFRDERELLRHPPAPHQPPAPAPGANGSGVMAPPSGPTVAPLLPRTLADPFFIVETTCVIWFTFELLVRF	343
hPCN2	PESSDPARGIAIVSVLVILISIVIFCLETLPEFRDDRDLVHALSAGGHGGLLNDTSAPHLEN.........SGHTIFNDPFFIVETVCIVWFSFEFVVRC	390
hPCN3	PESSGPARGIAIVSVLVILISIVIFCLETLPEFRDEKDYPASTSQDSFEAAGNSTSGSR............AGASSFSDPFFVVETLCIIWFSFELLVRF	262
	--	----------H3----------		----------S4----------		----H4--	
hPCN1	FACPSKAGFSRNDMNIIDVVAIFPYFITLGTELAEQQPGGGGGGQNGQQAMSLAILAVIRLVRVFRIFKLSRHSKGLQILGKTLQASMRELGLLIFFLFIG	444
hPCN2	FACPSQALFFKNDMNIIDIVSILPYFITLGTDLAQQQGGGN..GQQ.QQAMSFAILRIIRLVRVFRIFKLSRHSKGLQILGHTLRASMRELGLLIFFLFIG	488
hPCN3	FACPSKATFSRNDMNLIDIVAIIPYFITLGTELAERQ..GN..G...QQAMSLAILAVIRLVRVFRIFKLSRHSKGLQILGQSLKASMRELGLLIFFLFIG	356
	---H4------		--------H5-------		-----------H6--------	
hPCN1	VILFSSAVYFAEADNQGTHFSSIPDAFWWAVVTMTTVGYGDMRPITVGGKIVGSLCAIAGVLTIALPVPVIVSNFNYFYHRETDHEEPAVLKEEQGTQSQG	545
hPCN2	VILFSSAVYFAEADEPTTHFQSIPDAFWWAVVTMTTVGYGDMKPITVGGKIVGVLCAIAGVLTIALPVPVIVSNFNYFYHRETENEEQTQLTQNAVSCPYL	589
hPCN3	VILFSSAVYFAEADOPTSGFSSIPDAFWWAVVTMTTVGYGDMHPVTIGGKIVGSLCAIAGVLSIALPVPVIVSNFNYFYHRETEGEEQSQYMHVGSCQHLS	457
hPCN1	QGPGLDRGVQRKVSGSRGSFCKAGGTLENADSARRGSCPLEKCNVKAKSNVDLRRSLYAL..CLDTSR.ETDL	613
hPCN2	YLPSNLL...KKFRSSTSSSLGDKSEYLEMEEGVKESLCAKEEKCQAKGDDSETDKNN....CSNAKAVETDV	653
hPCN3	LSSSAEEL..RKARSNSTLS...KSEYMVIEEGGMNHTAFPQTPFKTGNSTATCTTHNNPNSCVNIKKIFTDV	519

FIG. 1.   Predicted amino acid sequences of three human K⁺ channels. The human proteins are named P (potassium) CN (channel) 1, 2, and 3 by analogy to human sodium channels (hSCN). Cloning of hPCN1 is described in the text. The sequence of hPCN2 (45) was deduced from the sequence of a cDNA clone isolated from a human fetal skeletal muscle library. The sequence of hPCN3 was deduced from the sequence of a genomic clone obtained from the same genomic library as hPCN1 (ref. 27; L.H.P., J.L., and D.F.S., unpublished results). Amino acids are indicated by their single-letter abbreviations. Gaps introduced to generate this alignment are represented by periods. Potential membrane-spanning domains (13) are noted by dashed lines. Residues that are identical in the three human proteins are indicated by bold type.

isoform of hPCN1, there are several interesting sequence differences of possible function significance: two additional putative protein kinase A phosphorylation sites in kv1 and the absence of the direct repeat (hPCN1 residues 61–82) in kv1 (17). By PCR analysis of this region of the rat and human genes, we have confirmed that the repeat is present in the human gene but lacking in the rat (data not shown). In contrast, other human/rat homologous isoforms share greater amino acid sequence identity: 97% between hPCN2 and RCK4 and 97% between hPCN3 and RCK3 (Fig. 1) (14).

Tissue Distribution of PCN1 mRNA. Northern blotting with 10 μg of total RNA prepared from various adult human tissues and several solid tumor cell lines revealed hybridization to a single faint transcript of about 4 kb in a human insulinoma (different from those that were combined to construct the insulinoma cDNA library) (data not shown). The transcript was more clearly evident with 5 μg of poly(A)$^+$ RNA from this human insulinoma. Transcripts of similar size were also obtained from RIN 5FS and HIT m2.2 cell RNA (data not shown). No hybridization was seen to total cellular RNA from human brain, skeletal muscle, liver, kidney, skin fibroblasts, or HepG2 cells, indicating that if hPCN1 is expressed in these tissues, the abundance of its RNA is less than in the insulinoma. Using RNA amplification of the 3' untranslated region, we have been able to show that hPCN1 RNA is also present in normal human islets (data not shown).

Expression of hPCN1 in *Xenopus laevis* Oocytes. K$^+$ channels expressed after injection of hPCN1 RNA into *Xenopus* oocytes were characterized by using a two-microelectrode voltage clamp. Outward currents in noninjected control oocytes were typically less than 250 nA during steps to +100 mV from a holding potential (V_h) of −80 mV (data not shown). Slowly inactivating outward K$^+$ currents were elicited by depolarizing voltage steps positive to −30 mV in RNA-injected oocytes (Fig. 2 *Upper left*). At the higher RNA concentrations used ($\approx$2 ng per oocyte), outward currents greater than 1 μA were recorded at 8 or more hr after RNA injection (Fig. 2 *Lower left*).

The threshold for hPCN1 activation was −25 mV. The time course of current activation decreased with increasing depo-
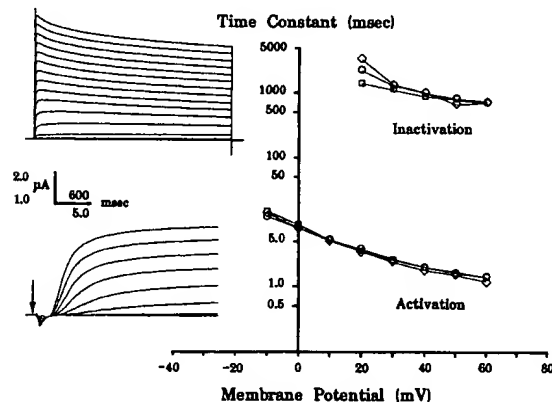

FIG. 2. (*Right*) Activation and inactivation time courses of hPCN1 K$^+$ currents (n = 3). Sampling rate/filter cutoff values were 5 kHz/2.5 kHz for activation and 2 kHz/1 kHz for inactivation. Current inactivation was fitted from peak current to the end of 1-sec depolarizations to the potentials indicated. (*Upper Left*) Currents obtained during 3.2-sec depolarizing steps from −70 to 60 mV in 10-mV increments; V_h = −80 mV. Currents are shown unsubtracted for leak or capacity transients. (*Lower Left*) Onset of currents evoked during steps from −30 to 40 mV in 10 mV increments in an oocyte 18 hr after RNA injection; V_h = −40 mV, subtracted with equal but opposite polarity steps. The arrow marks the start of depolarization; inward deflection is a subtraction artifact.

larization and could be fit with two exponentials (Fig. 2 *Right*). The ratio of the amplitudes of the two time constants describing the activation process increased with increasing depolarization (in three experiments, $A_{\tau 1}/A_{\tau 2}$ was 2.18 $\pm$ 0.1 and 4.73 $\pm$ 0.40 at −10 and 60 mV, respectively). The mean time constant of current activation for the three cells in Fig. 2 *Right* was 8.33 $\pm$ 0.36 msec at 0 mV and 1.35 $\pm$ 0.06 msec at 60 mV. The activation kinetics of hPCN1 and kv1 appear similar when expressed in *Xenopus* oocytes.

The expressed hPCN1 K$^+$ currents inactivated slowly with time during steps to positive voltages (Fig. 2 *Right*) most closely resembling RCK1 among the rat brain K$^+$ channels described by Stühmer and co-workers (14). The time constants of inactivation as determined from single exponential fits to the current data are plotted as a function of voltage in Fig. 2. Inactivation of the K$^+$ current was relatively voltage independent. The mean time constant of current inactivation for the three cells in Fig. 2 was 1155 $\pm$ 54 msec at 30 mV and 690 $\pm$ 17 msec at 60 mV.

Representative steady-state inactivation and conductance–voltage relationships of hPCN1 expressed in oocytes are given in Fig. 3. Steady-state inactivation of the hPCN1 currents became apparent at holding potentials more positive than −50 mV, and the delayed outward currents were completely blocked by holding potentials more positive than −10 mV. For eight oocytes the mean midpoint of the steady-state inactivation curve obtained from similar fits to the data was −25.3 $\pm$ 0.4 mV with a slope factor of 3.5 $\pm$ 0.2 mV. At depolarizations greater than 30 mV, the current–voltage relationship for hPCN1 expressed in *Xenopus* oocytes was linear. The conductance–voltage relationship was determined from deactivating steady-state currents at −40 mV (Fig. 3). An envelope of tails (data not shown) was constructed to confirm the validity of this method (38, 39). Half-maximal current activation, $V_{1/2}$, was −6.0 $\pm$ 0.6 mV with a slope (k) of −6.4 $\pm$ 0.5 mV (n = 5).

The selectivity of the current was determined from tail-current experiments in which the K$^+$ concentration in the external solution was varied between 2.5 and 75 mM (Fig. 4, A and B). Tail currents reversed polarity at −35 mV and −4 mV with external K$^+$ concentrations of 25 (n = 5) and 75 mM (n = 2), respectively (Fig. 4A). The 31-mV shift in reversal potential was close to the expected shift of 28 mV for a K$^+$ selective current (Fig. 4B).

The pharmacology of the hPCN1 currents expressed in *Xenopus* oocytes was examined by using K$^+$ channel blockers 4-aminopyridine (4-AP), tetraethylammonium ion (Et$_4$N$^+$), and Ba^{2+}. hPCN1 K$^+$ currents were blocked by 4-AP (Fig. 4C); however, the block was dependent on current activation and enhanced by repetitive stimulation. Repetitive stimulation in the presence of 50 μM 4-AP resulted in 30–38% block of the outward current (n = 6) and 54–62% block with 100 μM 4-AP (n = 5). Outward currents remaining in the presence of 10 mM 4-AP were comparable to endogenous current levels (n = 3). The presence of 20 mM Et$_4$N$^+$ in the external medium had no significant effect on hPCN1 currents (n = 2). In comparison, both RCK1 (14) and kv1 are blocked by low concentrations of 4-AP [K_i = 1.0 mM and K_i < 0.5 mM, respectively (hPCN1 K_i < 0.1 mM)] but differ in their sensitivity to Et$_4$N$^+$ [K_i = 0.6 mM for RCK1 (14) versus K_i > 40 mM for kv1 (17) (hPCN1 K_i > 20 mM)]. Ba^{2+} (10 mM) partially blocked hPCN1 currents. Currents measured 25 msec after onset of steps to 40 mV were reduced by 53% (n = 2), and the percentage block decreased during the voltage step (Fig. 4D). No shift was observed in the current–voltage relationship in medium containing 10 mM Mg^{2+}. Increasing Ca^{2+} from 1 to 10 mM in the external solution, substitution of Mg^{2+} for Ca^{2+}, or addition of 100 μM Cd^{2+} to the external medium had no effect on hPCN1 currents.
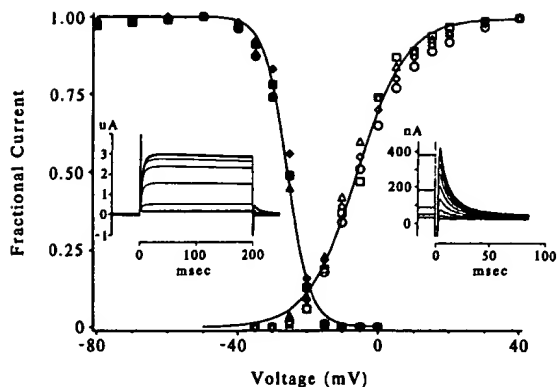
FIG. 3. Steady-state inactivation and conductance–voltage relationships. Steady-state inactivation (filled symbols) of hKCl currents in four oocytes is shown as a function of membrane potential. The steady-state parameters of activation and inactivation, $V_{1/2}$, k and $g_{K,max}$, were determined from conductance–voltage and steady-state inactivation curves fitted with a single Boltzmann isotherm of the form:

$$g_{K,(V)} = g_{K,max}/\{1 + \exp\{(V - V_{1/2})/k\}\}, \qquad [1]$$

where $V_{1/2}$ is the voltage at the midpoint of the activation or inactivation curve and k is the steepness of the voltage dependence. A solid line represents the fitted curve ($n = 4$); the $V_{1/2}$ (−25.6 mV) and k (3.41 mV) values for the single curve were not significantly different from the fitted curves for each cell. The holding potential was varied from −80 to 0 mV (10-mV increments from −80 to −40 mV, 5-mV increments thereafter) for a period of 1 min prior to recording the K^+ current at a constant test potential of 40 mV. Currents elicited from holding potentials of −10, −5, and 0 mV showed no kinetic component and were averaged for subtraction from peak currents evoked from more negative holding potentials. (*Left Inset*) Effect of holding potential on currents elicited in one oocyte with the voltage protocol described. The conductance versus voltage relationships (open symbols) are shown for a second set of oocytes ($n = 4$). Conductance (g) was measured from deactivating steady-state currents using exponential fits to determine the amplitude of the instantaneous K^+ tail current. Conductances were normalized according to the relationship

$$g = I_{K,tail}/I_{K,tail,max}, \qquad [2]$$

where $I_{K,tail,max}$ is the amplitude of the instantaneous current following a depolarization to 40 mV. The solid line represents the fitted curve for the four cells; the slope (−6.9) and midpoint (−5.7) for the single curve were not significantly different from the fitted curves for each cell. (*Right Inset*) Deactivating outward currents following depolarizing steps from −35 to 20 mV in 5-mV increments and steps to 30 and 40 mV. Outward currents during the activating steps are shown truncated and off scale. Instantaneous tail-current amplitudes were normalized to the value obtained following depolarizations to 40 mV.

DISCUSSION

In our initial studies of β-cell ion channels, we have characterized a K^+ channel, hPCN1, isolated from a human insulinoma cDNA library. The sequence of hPCN1 shows that it is related to the Shaker family of *Drosophila* K^+ channel genes. It is most similar to the rat brain K^+ channel isoform kv1 (17) but differs primarily by the presence of a proline-rich direct repeat in the amino-terminal cytoplasmic domain. RNA amplification by PCR has demonstrated the presence of hPCN1 RNA in normal human islets, suggesting that this K^+ channel may also participate in normal islet function. Expression of hPCN1 in *Xenopus* oocytes indicates that it is a K^+ channel with delayed rectifier kinetics.

Overexpression of a delayed rectifier such as hPCN1 would cause stabilization of the membrane resting potential. The presence of high levels of hPCN1 RNA in a malignant
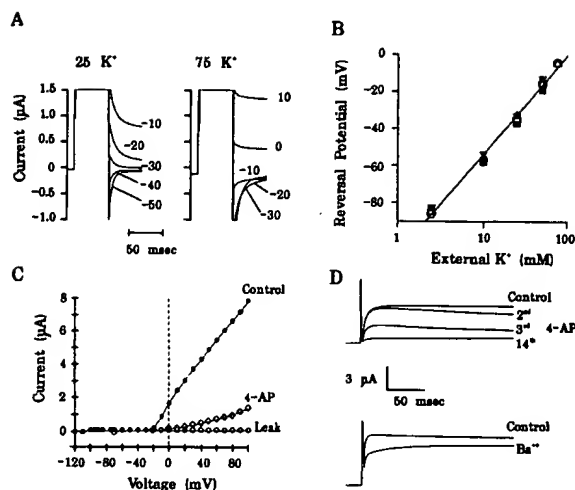

FIG. 4. Selectivity and pharmacology of hPCN1 K^+ currents. (*A*) Tail current reversal potentials shown for an oocyte in medium containing 25 mM and 75 mM K^+. Outward currents during the prepulses to 40 mV are shown. Test potentials are indicated for each tail current shown. (*B*) Plot of tail-current reversal potentials versus external K^+ concentration. Data are shown for five oocytes. The line through the data points represents the linear least-squares regression fit to the logarithmic transform of the data and has a slope of 54 mV per decade in external K^+ concentration. (*C*) Current–voltage relationship for an oocyte in OR-2 medium (control, ●) and in 1 mM 4-AP (◇); V_h = −80 mV. Current–voltage relationship in 4-AP was obtained after repetitive stimulation to maximize the 4-AP block (see *D*). Current values plotted are not leak-subtracted. Leakage current in OR-2 medium estimated from steps from −70 to −40 mV is also shown (○). Currents during hypolarizing steps are shown only for OR-2. (*D*) Block of hPCN1 K^+ currents by 4-AP and Ba^{2+}. (*D Upper*) Records showing the onset of block of 4-AP (1 mM) with the same cell as in C. The uppermost trace shows the current evoked during the step to 40 mV in OR-2 (control). The lower three traces are the second, third, and fourteenth step to 40 mV after addition of 1 mM 4-AP to the bath. The apparent shift in kinetics during steps 2 and 3 is due to use-dependence of the 4-AP block. The interpulse interval was 15 sec. (*D Lower*) Records showing currents evoked in OR-2 medium (control) and in 10 mM Ba^{2+}-containing medium during steps to 100 mV; V_h = −80 mV for both records.

human insulinoma may therefore account for the reduced glucose-responsiveness of insulin secretion in some insulinomas as compared with normal β cells (40). This expression in some tumors may also reflect differences in gene regulation between fetal and adult islets. Fetal β cells secrete insulin poorly in response to glucose (41–43). Cell-attached patch recordings of these cells are dominated by a small conductance K^+ channel, consistent with a delayed rectifier (43). K^+ currents through channels of this type could stabilize the membrane potential of fetal β cells below the threshold required for action potential initiation. Thus, the cells could remain quiescent even upon glucose-induced closure of the ATP-sensitive K^+ channels. This would explain the failure of tolbutamide, a sulfonylurea, to induce action potentials in the majority of such cells (43). Although alternative mechanisms have been proposed (40, 43), the possibility thus exists that both fetal β cells and some insulinomas are less responsive to glucose-induced insulin release than normal β cells in part because of increased expression of voltage-sensitive K^+ channels.

Voltage-sensitive K^+ channels in normal islets are critical in the restoration of the cell membrane to a hyperpolarized state after a calcium action potential (3, 5, 6, 44). The mouse β-cell voltage-sensitive K^+ channel was found to be sensitive to 4-AP and Et_4N^+ (3, 5); hPCN1 was sensitive to 4-AP but

Neurobiology: Philipson *et al.*

Proc. Natl. Acad. Sci. USA 88 (1991)   57

resistant to Et_4N^+. However, the delayed rectifier currents seen in β cells may actually be produced by heteromultimeric K^+ channels, as RNA amplification of *ob/ob* mouse islets and rat and hamster insulinomas indicates that two to six different K^+ channel genes may be expressed in these cells (ref. 20; L.H.P. and D.F.S., unpublished results). Furthermore, when two rat K^+ channel isoforms with differing Et_4N^+ sensitivities were coexpressed in *Xenopus* oocytes, the Et_4N^+ sensitivity of the resulting current was intermediate to that of either isoform expressed alone (22, 23). Therefore, hPCN1 could play an important role in regulating membrane potential and the secretion of insulin in normal islets.

1. Peterson, O. H. & Findlay, I. (1987) *Physiol. Rev.* **67**, 1054–1116.
2. Ashcroft, F. M. (1988) *Annu. Rev. Neurosci.* **11**, 97–118.
3. Satin, L. S., Hopkins, W. F., Fatherazi, S. & Cook, D. L. (1989) *J. Membr. Biol.* **112**, 213–222.
4. Boyd, A. E. (1988) *Diabetes* **37**, 847–50.
5. Bokvist, K., Rorsman, P. & Smith, P. A. (1990) *J. Physiol.* **423**, 311–325.
6. Smith, P. A., Bokvist, K., Arkhammar, P., Berggren, P. O. & Rorsman, P. (1990) *J. Gen. Physiol.* **95**, 1041–1059.
7. Baumann, A., Krah-Jentgens, I., Muller, R., Muller-Holtkamp, F., Seidel, R., Kecskemethy, N., Casal, J., Ferrus, A. & Pongs, O. (1987) *EMBO J.* **6**, 3419–3429.
8. Papazian, D. M., Scwarz, T. L., Tempel, B., Jan, Y. N. & Jan, L. Y. (1987) *Science* **237**, 749–753.
9. Kamb, A., Iverson, L. & Tanouye, M. A. (1987) *Cell* **50**, 405–413.
10. Butler, A., Wei, A., Baker, K. & Salkoff, L. (1989) *Science* **243**, 943–947.
11. Wei, A., Covarrubias, M., Butler, A., Baker, K., Pak, M. & Salkoff, L. (1990) *Science* **248**, 599–603.
12. Schwarz, T. L., Tempel, B., Papazian, D. M., Jan, Y. N. & Jan, L. Y. (1988) *Nature (London)* **331**, 137–142.
13. Tempel, B., Jan, Y. N. & Jan, L. Y. (1988) *Nature (London)* **332**, 837–839.
14. Stühmer, W., Ruppersberg, J. P., Schroter, K. H., Sakmann, B., Stocker, M., Giese, K. P., Perschke, A., Baumann, A. & Pongs, O. (1989) *EMBO J.* **8**, 3235–3244.
15. Frech, G. C., VanDongen, A. M., Schuster, G., Brown, A. M. & Joho, P. (1989) *Nature (London)* **340**, 642–645.
16. McCormack, T., Vega-Saenz de Miera, E. C., Rudy, B. (1990) *Proc. Natl. Acad. Sci. USA* **87**, 5227–5231.
17. Swanson, R., Marshall, J., Smith, J. S., Williams, J. B., Boyle, M. B., Folander, K., Luneau, C. J., Antanavage, J., Olivia, C.,
18. Buhrow, S. A., Bennet, C., Stein, R. B. & Kaczmarek, L. K. (1990) *Neuron* **4**, 929–939.
19. Chandy, K. G., Williams, C. B., Spencer, R. H., Aguilar, B. A., Ghanshani, S., Tempel, B. L. & Gutman, G. A. (1990) *Science* **247**, 973–975.
20. Kamb, A., Weir, M., Rudy, B., Varmus, H. & Kenyon, C. (1989) *Proc. Natl. Acad. Sci. USA* **86**, 4372–4376.
21. Betsholtz, C., Baumann, A., Kenna, S., Ashcroft, F. M., Ashcroft, S. J. H., Berggren, P., Grupe, A., Pongs, O., Rorsman, P., Sandblom, J. & Welsh, M. (1990) *FEBS Lett.* **263**, 121–126.
22. Isacoff, E. Y., Jan, Y. N. & Jan, L. Y. (1990) *Nature (London)* **345**, 530–534.
23. Ruppersberg, J. P., Schroter, K. H., Sakmann, B., Stocker, M., Sewing, S. & Pongs, O. (1990) *Nature (London)* **345**, 535–537.
24. Christie, M. J., North, P. A., Osborne, P. B., Douglass, J. & Adelman, J. P. (1990) *Neuron* **2**, 405–411.
25. Maniatis, T., Fritsch, E. F. & Sambrook, J. (1982) *Molecular Cloning: A Laboratory Manual* (Cold Spring Harbor Lab., Cold Spring Harbor, NY).
26. Sanke, T., Bell, G. I., Sample, C., Rubenstein, A. H. & Steiner, D. F. (1988) *J. Biol. Chem.* **263**, 17243–17246.
27. Kayano, T., Fukumoto, H., Eddy, R. L., Fan, Y.-S., Byers, M. G., Shows, T. B. & Bell, G. I. (1988) *J. Biol. Chem.* **263**, 15245–15248.
28. Lawn, R. M., Fritsch, E. F., Parker, R. C., Blake, G. & Maniatis, T. (1978) *Cell* **15**, 1157–1174.
29. Saiki, R. K., Scharf, S., Faloona, F., Mullis, K. B., Horn, G. T., Erlich, H. A. & Arnheim, N. (1985) *Science* **230**, 1350–1354.
30. Frohman, M. A., Dush, M. K. & Martin, G. R. (1988) *Proc. Natl. Acad. Sci. USA* **85**, 8998–9002.
31. Krieg, P. A. & Melton, D. A. (1987) *Proc. Natl. Acad. Sci. USA* **84**, 2331–2335.
32. Marcus-Sekura, C. J. & Hitchcock, M. J. M. (1987) *Methods Enzymol.* **152**, 284–287.
33. Provencher, S. W. (1976) *Biophys. J.* **16**, 21–41.
34. Kozak, M. (1989) *J. Cell Biol.* **108**, 229–241.
35. McCormack, K., Campanelli, J. T., Ramaswami, M., Mathew, M. K., Tanouye, M. A., Iverson, L. E. & Bernardo, R. (1989) *Nature (London)* **340**, 103.
36. Blackshear, P. J., Nairn, A. C. & Kuo, J. F. (1988) *FASEB J.* **2**, 2957–2962.
37. Glass, D. B. & Krebs, E. G. (1982) *J. Biol. Chem.* **262**, 772–775.
38. House, C. & Kemp, B. E. (1987) *Science* **238**, 1726–1728.
39. Giles, W. R. & Shibata, E. F. (1985) *J. Physiol.* **368**, 265–292.
40. Hodgkin, A. L. & Huxley, A. F. (1952) *J. Physiol.* **116**, 473–496.
41. Flatt, P. R. (1990) *Biochem. Soc. Trans.* **18**, 124–127.
42. Espinosa, M. M. A., Driscoll, S. G. & Steinke, J. (1970) *Science* **168**, 1111–1112.
43. Asplund, K. & Freinkel, N. (1978) *Diabetes* **27**, 611–619.
44. Rorsman, P., Arkhammar, P., Bokvist, K., Hellerstrom, C., Nilsson, T., Welsh, M., Welsh, N. & Berggren, P. (1989) *Proc. Natl. Acad. Sci. USA* **86**, 4505–4509.
45. Bokvist, K., Rorsman, P. & Smith, P. A. (1900b) *J. Physiol.* **423**, 327–342.
46. Philipson, L. H., Schaefer, K., LaMendola, J., Bell, G. I. & Steiner, D. F. *Nucleic Acids Res.*, in press.